Double-Hinged Di-1,2,4-Triazoles for Synthesis of Breathing MOFs

A Dissertation Presented for the

Doctor of Philosophy

Degree

The University of Tennessee, Knoxville

Christopher Ray Murdock

May 2014

Copyright © 2014 by Christopher Ray Murdock.

All rights reserved.

DEDICATION

I dedicate my dissertation research to my parents, the people who have motivated me and supported me the most throughout my educational career. Without their support and encouragement, I would not be where I am today and would not have strived for the goals I have achieved. The ability for someone to push and motivate so hard has led to my desire to succeed in hopes that I can one day repay their passion and do the same for others.

ACKNOWLEDGEMENTS

I would like to acknowledge Dr. David M. Jenkins for his support during my graduate career. During my time as a graduate student, he has allowed me to grow as an individual and discover what problem solving in chemistry really entails. Pushing me to critically think as an individual, while at the same time providing guidance and motivation, has allowed for my personal growth during my career.

Additionally, I would like to acknowledge current and past group members who have contributed to my knowledge and experience as a graduate student, whether inside or outside of school: Dr. Heather M. Bass, S. Alan Cramer, Brianna C. Hughes, Dr. Zheng Lu, Preeti Chandrachud, and Dr. Chi-Linh Do-Thanh. In particular, Dr. Zheng Lu contributed vastly to my knowledge as a graduate student. Dr. Lu constantly provided in-depth discussions and assistance with research, and allowed me to develop into the chemist I am today.

ABSTRACT

Employing semi-rigid di-1,2,4-triazoles as ligands has led to the formation of a plethora of Metal-Organic Framework (MOF) architectures. The ability for the ligands to exhibit multiple conformations through a “hinge” effect allows for the formation of a multitude of MOF topologies and dimensionalities. Employment of a di-triazole containing a central *trans*-butene moiety was initially studied and led to the formation of two three-dimensional copper MOFs. The frameworks can be synthesized independently, but a reaction occurs in water wherein the kinetic product is used as a reagent to synthesize the topologically distinct thermodynamic product.

Additional testing of reaction conditions with the butene-containing di-triazole led to the formation of a three-dimensional breathing framework by utilizing a mixed anion system. The framework structure flexes reversibly upon removal or addition of water to form semi-hydrated and dehydrated MOFs. Single crystal X-ray analysis demonstrated the 2-butene subunit of the ligand rotates between positions, causing changes in the solvent accessible volume. This double hinge within the ligand is a built-in breathing mechanism and suggests a general synthesis for breathing MOFs.

Replacing the central butene moiety with a xylene moiety resulted in the di-triazole adopting a *syn* conformation between copper chains, forming two-dimensional MOFs that resemble fused 1D metal-organic nanotubes (MONTs). The 2D sheet layers can expand or contract, or, more remarkably, the phenyl

ring can rotate between positions as a function of solvation. The transformations were followed by powder X-ray diffraction and solid state NMR. Additionally, frameworks which contain extended naphthyl and biphenyl linkers have been synthesized and characterized.

The *syn* conformation adopted by the di-triazoles was further exploited for the formation of a series of 1D MONTs. The di-triazole ligands bridge rigid metal chains while appropriate anion choice provides a “capping” of the metal fragments, leading to nanotube formation instead of 2D sheets. The pore size of the MONTs can be adjusted by changing the central portion of the double-hinged ligand, allowing for a general synthesis of MONTs. Adsorption studies of MONTs revealed selective uptake of carbon dioxide and methane with copper MONTs exhibiting the highest uptake.

TABLE OF CONTENTS

Chapter 1 Introduction 1

Chapter 2 Three-dimensional MOFs as reagents 6

Abstract 7

Introduction 7

Results and Discussion 9

Conclusion 16

Experimental 16

Chapter 3 Three-dimensional breathing MOFs 23

Abstract 24

Introduction 24

Results and Discussion 28

Conclusion 39

Experimental 40

Chapter 4 Two-dimensional MOFs 45

Abstract 46

Introduction for Gate Switching Breathing: Rotating Phenyl Rings 47

Results and Discussion for Gate Switching Breathing: Rotating Phenyl Rings 51

Conclusion for Gate Switching Breathing: Rotating Phenyl Rings 71

Experimental for Gate Switching Breathing: Rotating Phenyl Rings 72

Introduction for Isoreticular Synthesis 80

Results and Discussion for Isoreticular Synthesis 83
Conclusion for Isoreticular Synthesis 88
Experimental for Isoreticular Synthesis 89
Chapter 5 One-dimensional MOFs 96
Abstract 97
Introduction 97
Results and Discussion 100
Conclusion 112
Experimental 113
Chapter 6 By-Products of MOF Synthesis 121
Abstract 122
Introduction 122
Results and Discussion 122
Conclusion 131
Experimental 131
Chapter 7 Conclusion 137
References 142
VITA 165

LIST OF TABLES

Table 6.1. Potentially porous MOFs. 129

Table 6.2. Non-porous MOFs. 130

LIST OF FIGURES

Figure 1.1. Illustration of the three classes of breathing MOFs. 3

Figure 1.2. Illustration of the points of flexibility in breathing MOFs. 4

Figure 2.1. PXRD pattern for $[Cu_4(\mathbf{L})_4(SO_4)_4]\bullet 4[Cu(H_2O)_6(SO_4)]$: experimental (red) and simulated (black). 11

Figure 2.2. PXRD pattern for $[Cu_6(\mathbf{L})_3(SO_4)_5(OH)_2(H_2O)_6]\bullet 13H_2O$: experimental (red) and simulated (black). 11

Figure 2.3. X-ray structure of $[Cu_4(\mathbf{L})_4(SO_4)_4]\bullet 4[Cu(H_2O)_6(SO_4)]$.....12

Figure 2.4. X-ray structure of $Cu_6(\mathbf{L})_3(SO_4)_5(OH)_2(H_2O)_6\bullet 13H_2O$. 14

Figure 2.5. Powder pattern X-ray diffraction measurements taken as a function of time. 15

Figure 3.1. Illustration of three classes of 3D breathing materials. 26

Figure 3.2. X-ray structure of $[Cu_2(\mathbf{L})_2(SO_4)(Br)_2] \bullet xH_2O$. 29

Figure 3.3. Powder pattern X-ray diffraction measurements taken of samples showing effects of solvation. 31

Figure 3.4. TGA measurements for all Copper MOFs. 31

Figure 3.5. X-ray structure of $[Cu_2(\mathbf{L})_2(SO_4)(Br)_2] \bullet 4H_2O$. 32

Figure 3.6. Comparison of X-ray structures. 34

Figure 3.7. PXRD pattern for $[Cu_2(\mathbf{L})_2(SO_4)(Br)_2]\bullet xH_2O$: experimental (red) and simulated (black). 37

Figure 3.8. PXRD pattern for $[Cu_2(\mathbf{L})_2(SO_4)(Br)_2] \bullet 4H_2O$: experimental (red) and simulated (black). 37

Figure 3.9. CO_2 (squares) and CH_4 (triangles) depict adsorption isotherms for $[Cu_2(\mathbf{L})_2(SO_4)(Br)_2]\bullet xH_2O$ (blue) and $[Cu_2(\mathbf{L})_2(SO_4)(Br)_2]\bullet 0H_2O$ (red) at 298 K. 39

Figure 4.1. Graphical depiction of methods in which the "kneecap" is placed solely on the ligand. 49

Figure 4.2. X-ray structure of $[Cu(\mathbf{L})(ClO_4)] \bullet DMF \bullet H_2O$. 54

Figure 4.3. Crystal structure of $[Cu_2(\mathbf{L})_2(ClO_4)_2] \bullet 4DMF \bullet H_2O$ viewed orthogonal to the y-axis showing the fused-tube topology. 55

Figure 4.4. X-ray structure of $[Cu(\mathbf{L})(ClO_4)] \bullet DMA \bullet H_2O$. 57

Figure 4.5. Crystal structure of $[Cu(\mathbf{L})(ClO_4)] \bullet NMP \bullet H_2O$ viewed orthogonal to the y-axis showing the fused-tube topology. 58

Figure 4.6. Crystal structure of $[Cu(\mathbf{L})(ClO_4)] \bullet 3NMP$ viewed orthogonal to the x-axis showing the fused-tube topology. 59

Figure 4.7. Powder pattern X-ray diffraction measurements taken for a sample of $[Cu_2(\mathbf{L})_2(ClO_4)_2] \bullet 4DMF \bullet H_2O$ and after exposure to water for 1 h. 61

Figure 4.8. Powder pattern X-ray diffraction measurements taken for a sample of $[Cu(\mathbf{L})(ClO_4)] \bullet 3NMP$ after exposure to water and NMP for 1 h, and resolvation with NMP for 8 h at 85 °C. 62

Figure 4.9. HSQC in DMSO-d_6. 64

Figure 4.10. HMBC in DMSO-d_6. 64

Figure 4.11. ^{13}C CP MAS NMR of ligand. 65

Figure 4.12. ^{13}C CP MAS NMR of $[Cu(\mathbf{L})(ClO_4)] \bullet DMF \bullet H_2O$. 66

Figure 4.13. ^{13}C CP MAS NMR of $[Cu_2(\mathbf{L})_2(ClO_4)_2] \bullet 4DMF \bullet H_2O$. 67

Figure 4.14. ^{13}C CP MAS NMR of $[Cu(\mathbf{L})(ClO_4)] \bullet NMP \bullet H_2O$. 68

Figure 4.15. ^{13}C CP MAS NMR of $[Cu(\mathbf{L})(ClO_4)] \bullet 3NMP$. 69

Figure 4.16. ^{13}C CP MAS NMR following the dynamic transition of $[Cu_2(\mathbf{L})_2(ClO_4)_2] \bullet 4DMF \bullet H_2O$ to $[Cu(\mathbf{L})(ClO_4)] \bullet DMF \bullet H_2O$ upon hydration. 70

Figure 4.17. ^{13}C CP MAS NMR spectrum of $[Cu(\mathbf{L})(ClO_4)] \bullet 3NMP$ after exposure to water for 1 h, and resolvation with NMP for 8 h at 85 °C. 71

Figure 4.18. X-ray structure of $[Cu(\mathbf{L})(ClO_4)] \bullet DMF \bullet H_2O$. 83

Figure 4.19. X-ray structure of $[Cu(\mathbf{L2})(ClO_4)] \bullet DMA \bullet H_2O$. 86

Figure 4.20. X-ray structure of $[Cu(\mathbf{L3})(ClO_4)] \bullet DEF$. 87

Figure 5.1. Pictorial representation of the three classes of MONTs: helical chains formed by a curling up mechanism (left), 4-column pillars (center), and 2-column pillars (right). 99

Figure 5.2. X-ray structures of $[Cu_2(\mathbf{2a})(Br)_2] \bullet DMF$ and $[Cu_2(\mathbf{2b})(Br)_2] \bullet DMF$. 103

Figure 5.3. X-ray structures of $[Ag_2(\mathbf{2a})(NO_3)_2] \bullet NMP$ and $[Ag_2(\mathbf{2c})(NO_3)_2] \bullet NMP$. 106

Figure 5.4. X-ray crystal structure of $[Cu_2(\mathbf{2a})(SO_4)(OH)_2(H_2O)_2] \bullet H_2O$. 108

Figure 5.5. CO_2 (squares) and CH_4 (triangles) depict adsorption isotherms for MONTs $[Cu_2(\mathbf{2a})(Br)_2] \bullet DMF$ (red) and $[Cu_2(\mathbf{2a})(SO_4)(OH)_2(H_2O)_2] \bullet H_2O$ (blue).....111

Figure 5.6. CO_2 (squares) and CH_4 (triangles) depict adsorption isotherms for MONTs [Ag_2(**2a**)$(NO3)_2$] • NMP (green) and [Ag_2(**2c**)$(NO3)_2$] • NMP (purple). 112

Figure 6.1. X-ray structure of [Co(**1**)(SO_4)] • [$Co(H_2O)_6(SO_4)$] • $3H_2O$. 124

Figure 6.2. X-ray structure of [Cu_2(**2**)$_2(SO_4)$] • 2DMF • $3H_2O$. 125

Figure 6.3. X-ray structure of [Cu(**2**)(NO_3)] • NMP • H_2O. 126

Figure 6.4. X-ray structure of [Cu(**2**)(SO_3CF_3)] • DMF. 127

Figure 6.5. X-ray structure of [Cu(**2**)(SO_3CF_3)] • DMA. 128

Figure 6.6. X-ray structure of [Cu(**2**)$(ClO_4)_2$] • NMP. 129

LIST OF SCHEMES

Scheme 2.1. Synthesis of di-triazole ligand.....9

Scheme 2.2. Synthesis of copper MOFs designated $[Cu_4(\mathbf{L})_4(SO_4)_4]$ • $4[Cu(H_2O)_6(SO_4)]$ and $[Cu_6(\mathbf{L})_3(SO_4)_5(OH)_2(H_2O)_6]$ • $13H_2O$.....10

Scheme 3.1. Synthesis of copper MOFs. 29

Scheme 4.1. Di-triazole ligand synthesis.....52

Scheme 4.2. Synthesis of copper frameworks utilizing various solvents and metal to ligand ratios.....53

Scheme 4.3. Conversion between framework states as a function of solvent. ...60

Scheme 4.4. General synthesis of di-triazole ligands.....84

Scheme 5.1. Synthesis of di-triazole ligands for MONT formation. 101

Scheme 5.2. Synthesis of frameworks utilizing various metals, solvents, and metal to ligand ratios.....101

Scheme 6.1. Di-triazoles for MOF synthesis. 123

Scheme 6.2. Synthesis of frameworks that are structurally analogous to published examples. 124

Chapter 1

Introduction

Metal-Organic Frameworks (MOFs), being comprised of metal centers bridged through organic linkers to form frameworks of multiple dimensionalities, are a rigorously studied class of porous materials.[1] MOFs are under continuous investigation as their elegant structures, yet elementary design principles, allow for the fine-tuning of their internal cavities.[1b, 2] Through the use of advanced organic synthesis, frameworks are designed for applications in gas storage and separation, sensing, catalysis, and luminescence.[3]

Synthesis of MOFs generally involves the use of rigid organic linkers to bridge metal centers in a manner that will produce a robust, permanently porous framework.[1a-c, 4] The ability to predict framework structures stems from the formation of discrete secondary building units (SBUs) or geometric shapes upon MOF formation. The employment of chelating ligands, most commonly dicarboxylate ligands, leads to formation of metal-ligand clusters forming a cubic topology. Formation of known metal-ligand clusters then allows for the synthesis of isoreticular frameworks via the use of linkers of various sizes, leading to fine-tuning of the storage and transport properties of the framework.[2, 5]

While most MOF structures are synthesized as static frameworks with the goal of maintaining their robustness for adsorption applications, a third generation of MOFs labeled breathing frameworks that possess multiple stable states has been pioneered by Kitagawa and Férey.[6] The ability to synthesize

frameworks which possess a highly ordered network yet the ability to transform states while maintaining porosity has led to properties unattainable in rigid, static MOFs.[6a, 6b, 7] A gate-opening phenomenon results in the selective adsorption of guests that favor the pore opening process, resulting in applications that value the ability to control pore size as a function of both pressure and concentration. This characteristic gate-opening occurs upon sorption of small molecules, ranging from CO_2 and CH_4 to small molecules for drug delivery, and results in a "step" in the adsorption isotherm.[3b, 3h, 6b, 7a, 8]

Kitagawa arranged breathing MOFs into three classes (Figure 1.1) which include 2D coordination polymer layers connected via a flexible ligand, 1D coordination polymers which form a rhombus in the remaining dimensions, or interpenetrating 3D networks.[7b] While all three approaches have led to frameworks with intriguing properties, the ability to design additional examples has proved a challenge as the guidelines for static systems do not involve the topologies necessary for breathing.[2d] Most examples of breathing MOFs today therefore rely on the isoreticular synthesis of a few known examples such as MIL-53 and cannot be viewed as design since original syntheses were unpredictable.[6d, 9] With emerging classes of MOFs such as breathing MOFs straying from the traditional secondary building units (SBUs), additional reticular synthesis techniques are in dire need.

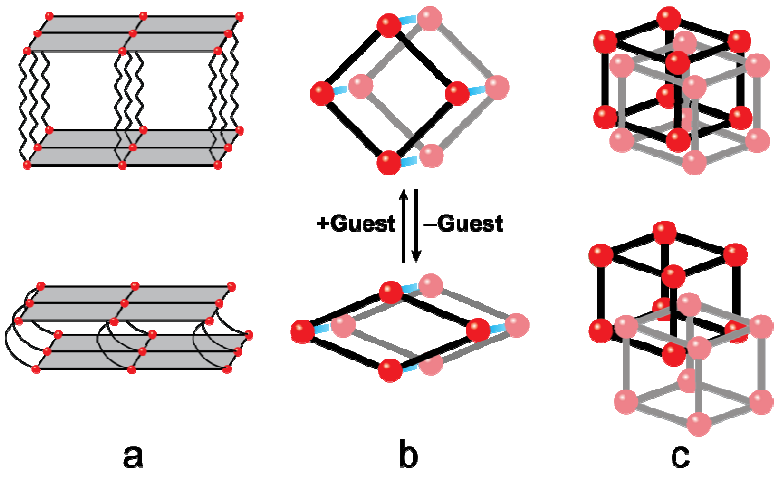


Figure 1.1. Illustration of the three classes of breathing MOFs. (a) 2D coordination polymers connected via a flexible ligand; (b) 1D coordination polymers which form a rhombus in the remaining dimensions; (c) interpenetrating 3D networks.

To advance the synthesis and application of breathing MOFs, as well as develop methods for reticular synthesis, appropriate mechanisms in which framework flexing or bending occurs must first be identified. The most thoroughly studied breathing MOFs consist of a single dimension which remains rigid, resulting in a facial rhombohedral topology in the orthogonal two dimensions.[6b, 7c, 10] The point of flexibility or the "kneecap" in which the framework undergoes dynamic changes is largely focused on transformations at the rigid metal-ligand interface which results in a change in pore size or rhombus dimensions (Figure 1.2, top). Flexing at the metal-ligand interface reduces the number of available topologies and is the reason for limiting breathing MOFs to the isoreticular synthesis of a few known examples.[6b, 7c, 7e]

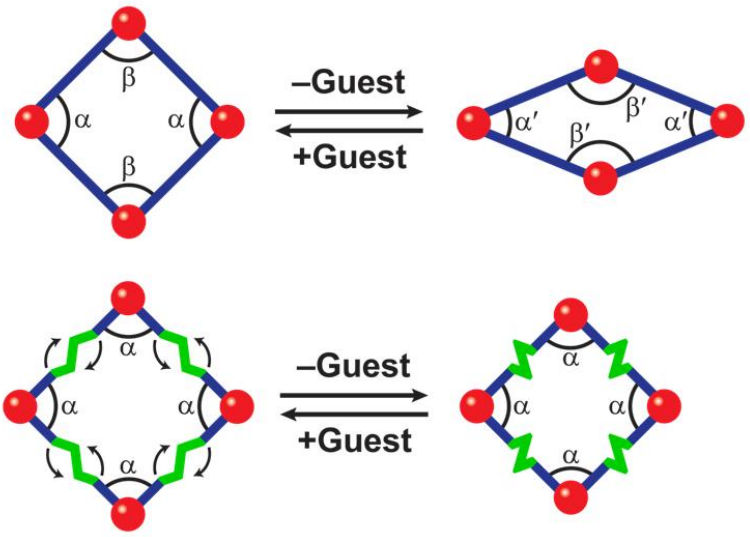


Figure 1.2. Illustration of the points of flexibility in breathing MOFs. Breathing can occur through changes at the metal-ligand interface (top) or changes within the ligand itself (bottom).

An alternative method to breathing is to move the point of breathing or "kneecap" *away* from the metal-ligand interface through the employment of semi-rigid ligands (Figure 1.2, bottom).[10-11] Placing the "kneecap" solely on the ligand allows for a method in which breathing is not restricted by the SBU and can be incorporated in a pre-synthetic manner through judicious choice of flexible ligand.[10-11] Breathing through changes at the ligand allows for a change in rhombus dimensions as seen in Figure 1.2 through a "screw-like" effect, contracting and expanding the 1D chains, but interactions at the SBU remain constant.[10, 11b]

We have turned our attention to the synthesis and employment of semi-rigid di-1,2,4-triazoles as a method to move the point of flexibility away from the

rigid metal interface.[10, 11b, 11c, 12] The semi-rigid ligands synthesized contain symmetric moieties with two points of rotation, leading to formation of a double-hinge motif. Keeping the periphery of the ligand constant allows for a fine tuning of the core of the ligand, leading to a plethora of possible di-triazoles to be synthesized.[11b, 11c, 12] As only the central core of the semi-rigid ligand is modified, the possibility of synthesizing frameworks in an isoreticular manner becomes plausible. Keeping the SBU constant while utilizing di-triazoles of varying composition allows for studies on breathing behavior which have as of yet not been performed due to a lack of reticular design. In addition, the presence of two points of rotation not only allows for built-in flexibility through a double-hinge effect but also leads to the formation of framework architectures which have not been explored.[11b, 11c]

Chapter 2

Three-dimensional MOFs as reagents

A version of this chapter was originally published by Christopher R. Murdock, Zheng Lu, and David M. Jenkins:

Murdock, Christopher R.; Lu, Zheng; Jenkins, David M. "Utilizing a Copper MOF as a Reagent in a Solvent Mediated Reaction to Form a Topologically Distinct MOF." *Dalton Trans.* **2012**, *41*, 7839-7841.

All work presented herein is the work of Chris Murdock with assistance in crystallography by Zheng Lu.

Abstract

Employing a semi-rigid di-1,2,4-triazole ligand leads to the formation of new MOFs $[Cu_4(L)_4(SO_4)_4]\bullet 4[Cu(H_2O)_6(SO_4)]$ (**3**) and $[Cu_6(L)_3(SO_4)_5(OH)_2(H_2O)_6]\bullet 13H_2O$ (**4**). The frameworks can be synthesized independently, but a reaction occurs in water wherein kinetic product **3** is used as a reagent to synthesize the topologically distinct thermodynamic product **4**.

Introduction

Due to their large surface area and ability to adsorb guests within their host framework, MOFs are being considered for a wide range of practical applications, from gas storage to heterogeneous catalysis.[1e, 3e, 13] While the size and shape of the MOF's pores are critical for many applications, the ability to change these properties on already synthesized MOFs through postsynthetic modification is of particular benefit to applications such as chemical sensing and

gas separation.[1d, 3f, 3h, 14] The ability to tune the pores of the crystalline material may, therefore, allow a single MOF to be selective for different guests as a function of its postsynthetic modification.[15]

Postsynthetically modified MOFs can have their properties tailored after the initial crystalline material has been synthesized and, as such, are being vigorously pursued.[16] These MOFs can be modified by a variety of techniques including altering the organic linkers,[17] exchanging anions,[18] removing interstitial solvent,[19] or photochemical reactions.[20] Some techniques modify the linkers or the material in the pores while keeping the general topology intact,[17a, 17c, 17e, 18a, 20d] while others change the topology of the MOF.[19c, 21]

The ability to change the topology of a MOF, and therefore its properties, without additional reagents is quite valuable. While MOF-to-MOF transformations have been observed in the solid state, these examples are quite limited.[19a, 19b, 19d] If a method could be devised wherein MOFs with different topologies can be converted between each other in a solvent with no additional reagents, then this new method may be a very powerful technique to tune the properties of MOFs.

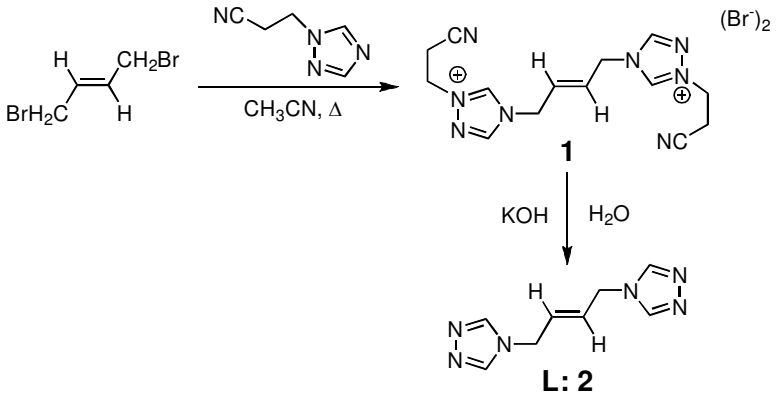
A demonstration of this method can be shown with a reaction which yields both kinetic and thermodynamic products. To our knowledge, very few pairs of MOFs have been synthesized which fit the description of a kinetic and thermodynamic product pair.[22] However, it is unclear from previous examples whether additional reagents in solution facilitate the conversion from the kinetic to

the thermodynamic product. In neither case has the kinetic product been isolated and utilized as the sole reagent to form the thermodynamic product in a solvent. This communication presents a pair of MOFs in which the kinetic product is isolated, reintroduced into a solvent, and used as the only reagent to form the thermodynamic product.

Results and Discussion

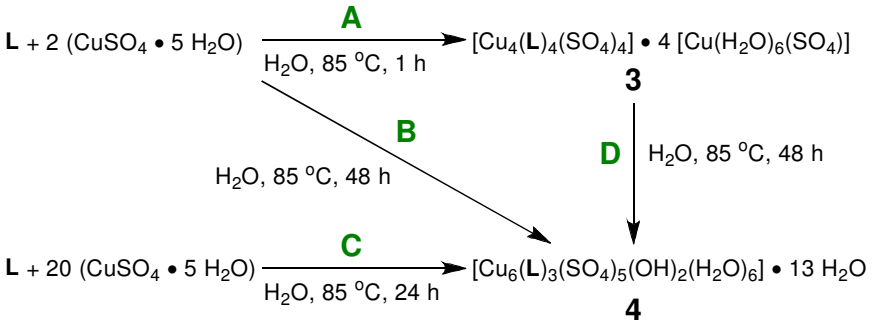
We have prepared a semi-rigid di-1,2,4-triazole for the production of MOFs using a two-step synthesis. Using the method of Horváth,[23] the addition of 1,2,4-triazole-1-propanenitrile to the dielectrophile *trans*-1,4-dibromo-2-butene gives **1** in 90% yield (Scheme 2.1). The addition of excess potassium hydroxide cleaves the propanenitrile group leaving 1,4-di(1,2,4-triazole)-*trans*-2-butene (**L: 2**) in 89% crude yield. Ligand **2** can be purified by Soxhlet extraction with chloroform to give the analytically pure product.

Scheme 2.1. Synthesis of di-triazole ligand.



Two structurally distinct MOFs can be prepared under a single set of reaction conditions simply by varying the time of the reaction. Mixing two equivalents of copper sulphate with **L** yields $[Cu_4(\mathbf{L})_4(SO_4)_4]$•4$[Cu(H_2O)_6(SO_4)]$ (**3**) as blue needle-shaped crystals in water after 1 h at 85° C (Scheme 2.2, Reaction **A**). If the reaction is allowed to proceed for 48 h under the same conditions $[Cu_6(\mathbf{L})_3(SO_4)_5(OH)_2(H_2O)_6]$•$13H_2O$ **(4)** is formed as large blue block crystals during which time **3** appears and then subsequently recedes (Scheme 2.2, Reaction **B**). MOF **4** can be independently synthesized by changing the metal to ligand ratio (Scheme 2.2, Reaction **C**) and **3** is not observed under these conditions. Both MOFs **3** and **4** have distinct PXRD patterns as observed in Figures 2.1 and 2.2.

Scheme 2.2. Synthesis of copper MOFs designated $[Cu_4(\mathbf{L})_4(SO_4)_4]$ • 4$[Cu(H_2O)_6(SO_4)]$ (**3**) and $[Cu_6(\mathbf{L})_3(SO_4)_5(OH)_2(H_2O)_6]$ • $13H_2O$ (**4**).



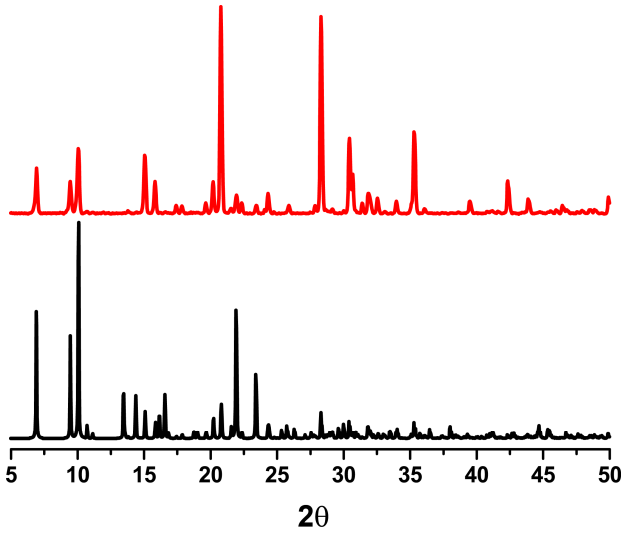


Figure 2.1. PXRD pattern for $[Cu_4(\mathbf{L})_4(SO_4)_4]\bullet 4[Cu(H_2O)_6(SO_4)]$ (**3**): experimental (red) and simulated (black).

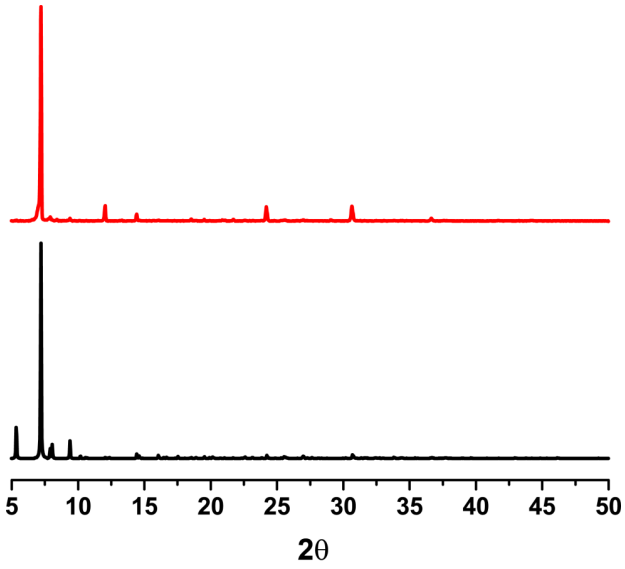


Figure 2.2. PXRD pattern for $[Cu_6(\mathbf{L})_3(SO_4)_5(OH)_2(H_2O)_6]\bullet 13H_2O$ (**4**): experimental (red) and simulated (black).

To establish the binding mode for the di-1,2,4-triazole ligand (**2**) to the copper ions, single crystal X-ray studies were performed on both MOFs **3** and **4**. Compound **3** crystallizes as bright blue needles (Figure 2.3) in the orthorhombic system with $P2_12_12_1$ space group. Each octahedral copper centre is coordinated to four triazole ligands which form an equatorial plane and two oxygen atoms from the sulphate ligands in the axial positions. Adjacent copper atoms along the y-axis are bridged by two triazole fragments using the N1 and N2 atoms on each

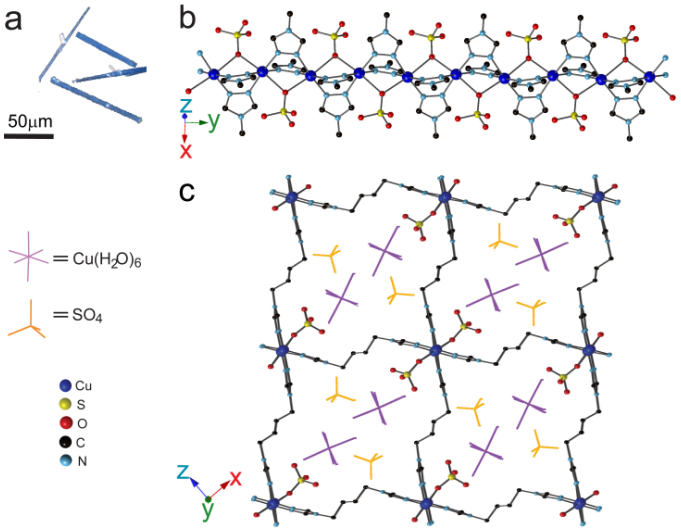


Figure 2.3. X-ray structure of $[Cu_4(\mathbf{L})_4(SO_4)_4]\bullet 4[Cu(H_2O)_6(SO_4)]$, **3**. (a) Photograph of crystals of **3**; (b) X-ray structure of **3** showing copper chains formed along y-axis; (c) X-ray structure of **3** showing links between copper chains viewed along the xz-plane**.**

triazole and a bridging oxygen atom from a sulphate anion to form a linear chain (Figure 2.3b). These chains are linked in the other two dimensions by the second triazole moiety of the ligand, forming the three dimensional network (Figure 2.3c). This neutral MOF **3** co-crystallizes with guest molecules of copper sulphate hexahydrate that occupy the pores of the MOF, which makes **3** non-porous.

Compound **4** crystallizes as large blue blocks (Figure 2.4a) in orthorhombic system with *Pnna* space group. The asymmetrical unit contains a pair of triangular trinuclear copper cores along the z-axis. These trinuclear cores are alternatively bridged by three triazole fragments and a centre hydroxyl ligand. Two of the three di-1,2,4-triazole linkers link to another triangular unit with two of its copper atoms; the third di-1,2,4-triazole linker connects the next triangular trinuclear copper core to form a wavy chain (Figure 2.4b). The tricopper core is capped by a sulphate anion through three of the four oxygen atoms. One of these three oxygen atoms is shared with another copper from an adjacent chain. Finally, another second distinct sulphate anion bridges two copper atoms from two chains through the use of two of the four oxygen atoms. These bridging sulphate anions form the three-dimensional structure for **4** (Figure 2c).

Since 1,2,4-triazoles have many different binding modes in MOFs/coordination polymers,[24] it is not surprising that different MOFs can be formed with the same ligand. What is noteworthy is that the ratio of copper to ligand to sulphate is almost identical for **3** (M:**L**:A = 6:3:6) and **4** (6:3:5) if the

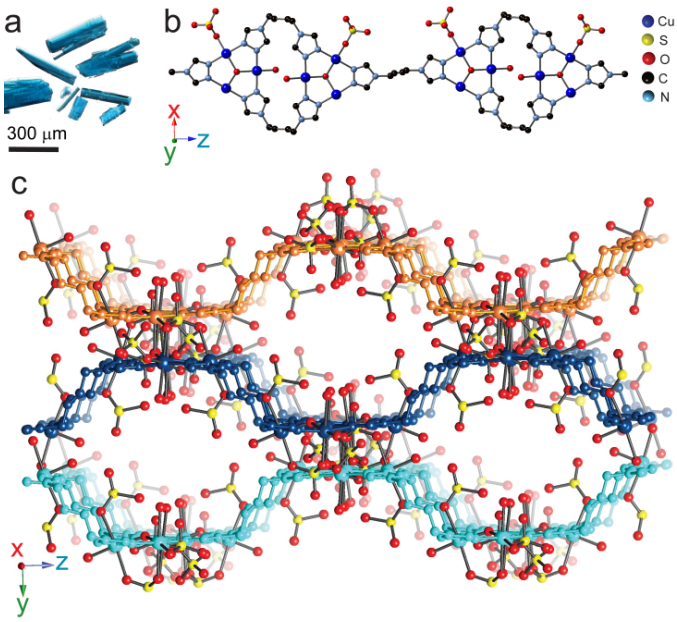


Figure 2.4. X-ray structure of $Cu_6(\mathbf{L})_3(SO_4)_5(OH)_2(H_2O)_6 \bullet 13H_2O$, **4**. (a) Photograph of crystals of **4**; (b) X-ray structure of **4** showing trinuclear copper cores and their connectivity along the z-axis; (c) X-ray structure of **4** showing links between trinuclear copper cores viewed along the yz-plane.

guests are included in the ratios. These comparable M:**L**:A ratios, combined with the fact that both **3** and **4** can be prepared under the same reaction conditions, suggest that neither the mother liquor nor additional reagents are required to from **4** from **3**, only the presence of water.

To test this hypothesis, isolated crystals of **3** were reintroduced to heated water. At 85 ℃, **4** was isolated in 33% yield after 48 h (Scheme 2.2, Reaction **D**). Notably, **3** was heated to 85 ℃ as a crystalline solid without any water present, but the reaction to give **4** did not occur under these conditions.

Because the reaction is sufficiently fast and can be followed by PXRD,[25] we performed time dependent measurements on this reaction. Parallel small scale reactions of **3** to **4** were set-up and stopped at time intervals between 1 h and 48 h followed by collection of PXRD patterns (Figure 2.5). The green lines show the disappearance of peaks associated with **3** and the red lines show the growth of peaks associated with **4**.

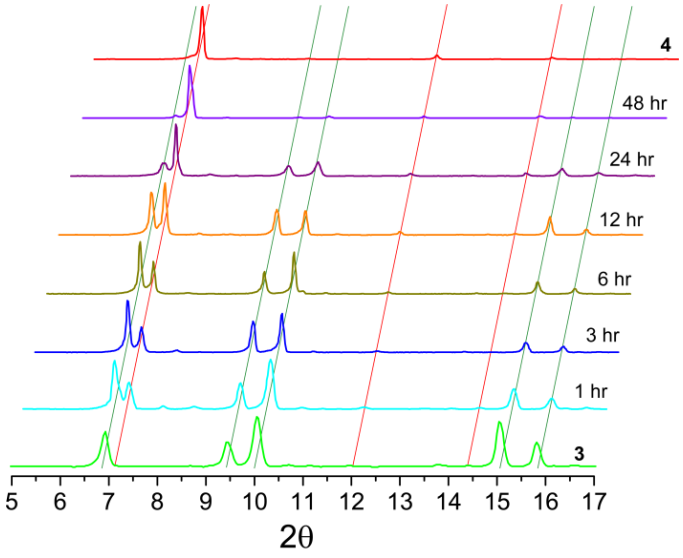


Figure 2.5. Powder pattern X-ray diffraction measurements taken as a function of time. The green cascading lines represent the peaks that are associated with **3** whereas the red cascading lines represent peaks that are associated with **4**. PXRD patterns for independently prepared **3** and **4** are shown on the bottom and top, respectively.

Conclusion

In conclusion, two three-dimensional copper MOFs were synthesized from a new semi-rigid di-1,2,4-triazole ligand. These frameworks can be synthesized separately under identical conditions by only varying the time of the reaction. However, an alternative route to synthesize **4** is to use **3** as a single source precursor. This results in an irreversible transformation to yield an entirely different framework. This solvent mediated conversion expands the possibility of creating MOFs in which the distinct characteristics of both topologies can be altered solely as a function of the time of reaction.

Experimental

The compound 1,2,4-triazole-1-propanenitrile[23] was prepared as described previously. All other reagents were purchased from commercial vendors and used without purification. ^{1}H and $^{13}C\{^{1}H\}$ NMR spectra were recorded at ambient temperature on a Varian Mercury 300 MHz or a Varian VNMRS 500 MHz narrow-bore broadband system. ^{1}H and ^{13}C NMR chemical shifts were referenced to the residual solvent. All mass spectrometry analyses were conducted at the Mass Spectrometry Center located in the Department of Chemistry at the University of Tennessee. The ESI/MS analyses were performed using a QSTAR Elite quadrupole time-of-flight (QTOF) mass spectrometer with an electrospray ionization source from AB Sciex (Concord, Ontario, Canada). Infrared spectra were collected on a Thermo Scientific Nicolet

iS10 with a Smart iTR accessory for attenuated total reflectance. Thermogravametric analysis data were collected on a TA Instruments TGA Q50 under N_2. Carbon, hydrogen, and nitrogen analyses were obtained from Atlantic Microlab, Norcross, GA.

Synthesis of 4,4'-(1,4-(*trans*-2-butene)diyl)bis-(1-(2-cyanoethyl)-1,2,4-triazolium) dibromide, 1. *Trans*-1,4-dibromo-2-butene (8.97 g, 0.0419 mol) was added to a 250 mL round bottom flask which had 1,2,4-triazole-1-propanenitrile (10.2 g, 0.0840 mol) and the mixture was diluted with acetonitrile (30 mL). The reaction was heated to reflux until a white precipitate had formed after 30 min. The reaction was cooled to rt and the precipitate was washed with diethyl ether (10 mL), and then dried under reduced pressure. The crude white solid was then washed with acetonitrile (3 x 30 mL) and dried under reduced pressure to yield the pure product (18.2 g, 89.8% yield). ^{1}H NMR (DMSO-d_6, 300.1 MHz): δ 10.47 (s, 2H), 9.41 (s, 2H), 6.17 (s, 2H), 5.07 (d, J = 3.0 Hz, 4H), 4.76 (t, J = 6.3 Hz, 4H), 3.28 (t, J = 6.3 Hz, 4H). ^{13}C{^{1}H} NMR (DMSO-d_6, 125.66 MHz): δ 144.93, 143.43, 128.94, 117.65, 48.29, 47.19, 17.35. IR (neat): 3418, 3117, 2957, 2942, 2253, 1726, 1581, 1532, 1443, 1409, 1386, 1359, 1340, 1275, 1185, 1157, 1070, 1018, 915, 878, 857, 816, 762, 670 cm^{-1}. ESI/MS (*m/z*): [M-Br]$^+$ 377.05, [M-2Br]$^{2+}$ 149.07. Anal. Calcd for $C_{14}H_{18}Br_2N_8$: C, 36.70; H, 3.96; N, 24.46. Found: C, 36.80; H, 3.98; N, 24.60.

Synthesis of 4,4'-(1,4-(*trans*-2-butene)diyl)bis-(1,2,4-triazole), L, 2. Potassium hydroxide (4.37 g, 0.0780 mol) and 4,4'-(1,4-(*trans*-2-butene)diyl)bis-

(1-(2-cyanoethyl)-1,2,4-triazolium) dibromide (9.55 g, 0.0195 mol) were added to a 250 mL Erlenmeyer flask containing 80 mL of water and stirred for 24 h. The solution was extracted with a 1:1 ethanol:chloroform solution (5 x 100 mL) and the organic layer was subsequently evaporated under reduced pressure. The resulting white solid was washed with acetonitrile (3 x 30 mL) and dried under reduced pressure to yield the crude product (3.32 g, 89.4% yield). Soxhlet extraction using chloroform yielded 0.233 g of the analytically pure product after 6 d. Further Soxhlet extraction allows for additional product to be obtained as needed. ^{1}H NMR (DMSO-d_6, 300.1 MHz): δ 8.50 (s, 4H), 5.77 (tt, J_1 = 3.0 Hz, J_2 = 1.5 Hz, 2H), 4.70 (dd, J_1 = 3.0 Hz, J_2 = 1.4 Hz, 4H). ^{13}C{^{1}H} NMR (DMSO-d_6, 125.66 MHz): δ 143.08, 128.88, 45.05. IR (neat): 3368, 3103, 2940, 2253, 1660, 1590, 1530, 1510, 1453, 1436, 1382, 1337, 1277, 1176, 1080, 1066, 995, 970, 948, 873, 833, 743, 682 cm^{-1}. DART/MS (*m/z*): 191.1 $[M+H]^+$. Anal. Calcd for $C_8H_{10}N_6$: C, 50.52; H, 5.30; N, 44.18. Found: C, 49.93; H, 5.22; N, 43.70.

Synthesis of $[Cu_4(L)_4(SO_4)_4]$•4$[Cu(H_2O)_6(SO_4)]$, 3. Copper(II) sulphate pentahydrate (0.0367 g, 0.147 mmol) and **2** (0.0140 g, 0.0735 mmol) were added to separate 4 mL scintillation vials and dissolved with 1 mL and 2 mL of water, respectively. The vials were heated to 85 °C for 30 min in an aluminum heating block. The solutions were mixed and heated for an additional 1 h until large blue crystalline needles had formed. The needles were collected using a Buchner funnel and filter paper and the crystals were washed with water (2 x 5 mL) and ether (3 x 5 mL) (0.0216 g, 47.5% yield). IR (neat): 3114, 1636, 1566, 1450,

1402, 1377, 1215, 1048, 974, 891, 746 cm^{-1}. Anal. Calcd for $C_{32}H_{88}Cu_8N_{24}O_{56}S_8$: C, 15.56; H, 3.59; N, 13.61. Found: C, 15.94; H, 3.59; N, 13.53.

Synthesis of $[Cu_6(L)_3(SO_4)_5(OH)_2(H_2O)_6]\cdot 13H_2O$, 4. Copper(II) sulphate pentahydrate (0.0918 g, 0.367 mmol) and **2** (0.0035 g, 0.018 mmol) were added to separate 4 mL scintillation vials and dissolved with 1 mL and 2 mL of water, respectively. The vials were heated to 85 °C for 30 min in an aluminum heating block. The solutions were mixed and heated for 24 h until large blue block crystals had formed. The block crystals were collected using a Buchner funnel and filter paper and the crystals were washed with water (2 x 5 mL) and ether (3 x 5 mL) (0.0069 g, 73% yield). IR (neat): 3369, 3109, 1635, 1553, 1449, 1400, 1083, 1023, 964 cm^{-1}. Anal. Calcd for $C_{24}H_{44}Cu_6N_{18}O_{28}S_5\cdot 13H_2O$: C, 15.94; H, 3.90; N, 13.94. Found: C, 15.97; H, 3.55; N, 13.68.

Synthesis of 4 utilizing the same reaction conditions as 3. Copper(II) sulphate pentahydrate (0.0367 g, 0.147 mmol) and **2** (0.0140 g, 0.0735 mmol) were added to separate 4 mL scintillation vials and dissolved with 1 mL and 2 mL of water, respectively. The vials were heated to 85 °C for 30 min in an aluminum heating block. The solutions were mixed and heated for an additional 48 h until large blue block crystals had formed. The block crystals were collected using a Buchner funnel and filter paper and the crystals were washed with water (2 x 5 mL) and ether (3 x 5 mL) (0.0065 g, 15% yield).

Synthesis of 4 from 3. **3** (10.0 mg, 0.00405 mmol) was added to a 4 mL scintillation vial containing 0.5 mL of water and heated to 85 °C in an aluminum

heating block. After heating the mixture for 48 h, single crystals of **4** were separated under a microscope utilizing their distinct shape and color. These collected crystals yielded 2.8 mg of **4**. (33% yield). Single crystal and powder X-ray diffraction measurements were collected on the separated crystals. The structure of the separated **4** was confirmed by single crystal X-ray diffraction and PXRD.

Time dependent reactions of 4 from 3. **3** (10.0 mg, 0.00405 mmol) was added to a 4 mL scintillation vial containing 0.5 mL of water. The mixture was then heated to 85 ℃ in an aluminum heating block and powder X-ray diffraction pattern were taken at specific time intervals to monitor the reaction as shown in Figure 3.

X-ray Structure Determinations. Data was collected on a Bruker SMART APEXII three circle diffractometer equipped with a CCD area detector and operated at 1,800 W power (45 kV, 40 mA) to generate Mo Kα radiation (λ = 0.71073 Å). The incident X-ray beam was focused and monochromated using Bruker Excalibur focusing optics. A single crystal of **3** was mounted on nylon CryoLoops (Hampton Research) with Paratone-N (Hampton Research) frozen at -173 ºC, while a single crystal of **4** was mounted in a glass capillary (Hampton Research) and flame sealed and cooled to 5 ºC. Initial scans of each specimen were taken to obtain preliminary unit cell parameters and to assess the mosaicity (i.e. breadth of spots between frames) of the crystal to select the required frame width for data collection. For all cases frame widths of 0.5º were judged to be

appropriate and full hemispheres of data were collected using the *Bruker APEX2* software suite to carry out overlapping ϕ and ω scans at detector setting of $2\theta = 28^{o}$. Following data collection, reflections were sampled from all regions of the Ewald sphere to re-determine unit cell parameters for data integration. Following exhaustive review of collected frames the resolution of the dataset was judged, and, if necessary, regions of the frames where no coherent scattering was observed were removed from consideration for data integration using the *Bruker SAINTplus* program.[26] Data was integrated using a narrow frame algorithm and were subsequently corrected for absorption. Absorption corrections were performed for both samples using the SADABS program.[26] Space group determination and tests for merohedral twinning were carried out using *XPREP*.[26] In all cases, the highest possible space group was chosen.

Final models were refined anisotropically (with the exception of H atoms). In the case of **3**, hydrogen atoms on the linker were placed in calculated positions and included as riding atoms with isotropic displacement parameters 1.5 times U_{eq} of the attached C atoms; water hydrogens were located by Fourier electron density map and with isotropic displacement parameters 1.5 times U_{eq} of the attached O atoms. In the case of **4**, the crystal loses solvent very quickly, even at -173.15℃. Therefore, the crystal was mounted in a capillary and flame sealed to prevent the loss of solvent during the collection. The data was collected at 5℃. Position disorder of the third sulphate anion (SO_4) was present in the structure. In the final least-squares refinement this disorder was taken into

account by two parts of SO_4 anions: Part 1 contains S2', O33', O30', O31', and O32' with 0.652 occupancy and Part 2 contains S2", O33", O30", O31", and O32" with 0.348 occupancy. Disordered water molecules were present in the structure. SQUEEZE routine was used to simplify and improve the refinement. The presence of large solvent accessible volume and relative poor data quality prevents the anisotropic refinement for all non-hydrogen atoms. Atoms O31, O32 and O33 as well as O30', O31', O32' and O33' were refined iostropically. All structures were examined using the *Addsym* subroutine of PLATON[27] to assure that no additional symmetry could be applied to the models.

Powder X-ray experiments. Powder X-ray diffraction (PXRD) data were collected using a Panalytical Empyrean θ-2θ diffractometer in reflectance Bragg-Brentano geometry. Cu-Kα radiation (λ = 1.5406 Å; 1,800 W, 45kV, 40 mA) was focused using a planar Gobel Mirror riding the Kα line. A 0.25 mm divergence slit was used for all measurements. Diffracted radiation was detected using a PIXcel[3d] detector [(6° 2θ sampling width) equipped with a Ni monochrometer]. All samples were mounted onto a zero background quartz plate fixed on a sample holder by dropping powders and then leveling the sample surface. The best counting statistics were achieved by using a 0.0131º 2θ step scan from 4 – 50° with an exposure time of 81.6 s per step and a revolution spin rate of 4 s.

Chapter 3

Three-dimensional breathing MOFs

A version of this chapter was originally published by Christopher R. Murdock, Zheng Lu, and David M. Jenkins:

Murdock, Christopher R.; Lu, Zheng; Jenkins, David M. "Effects of Solvation on the Framework of a Breathing Copper MOF Employing a Semirigid Linker." *Inorg. Chem.* **2013**, *52*, 2182-2187.

All work presented herein is the work of Chris Murdock with assistance in crystallography by Zheng Lu.

Abstract

A semi-rigid di-1,2,4-triazole ligand leads to the formation of the MOF $[Cu_2(\mathbf{L})_2(SO_4)(Br)_2]\bullet xH_2O$ (**1**). The framework structure of **1** flexes reversibly upon removal or addition of water to form semi-hydrated ($[Cu_2(\mathbf{L})_2(SO_4)(Br)_2]\bullet 4H_2O$) and dehydrated ($[Cu_2(\mathbf{L})_2(SO_4)(Br)_2]\bullet 0H_2O$) MOFs, **1′** and **1″**, respectively. Single crystal X-ray analysis demonstrated that the 2-butene subunit of the ligand rotates between two positions for **1** and **1′** causing a change in solvent accessible volume in the framework. This double hinge within the semi-rigid ligand is a built-in breathing mechanism and suggests a novel approach for a general synthesis of breathing MOFs.

Introduction

Due to their potential importance in applications such as gas separations,[24a, 28] liquid separations,[29] chemical sensing,[9b, 9d] and even drug

delivery,[30] breathing MOFs (metal-organic frameworks) have become an important class of multi-functional porous materials. Breathing MOFs undergo a reversible expansion and contraction of the void space in the framework due to the presence or absence of guest molecules.[6a, 6b, 8] A simple flexing of the framework to accommodate its guest frequently leads to highly selective guest adsorption.[6b, 9d, 30a] For example, selective gas adsorption has been demonstrated for separations of CO_2 versus CH_4,[9b, 28a-d] N_2,[9b, 24a, 28a, 28d, 28f] and H_2,[28d-f] respectively. Given their ability to exhibit high guest selectivity and the challenge for their preparation, synthetic methodologies for the rational synthesis of breathing MOFs are sorely desired.[6a, 6b, 8]

Myriad strategies have been pursued to synthesize 3D breathing materials that change their void space as a function of guest.[6a, 6b, 8] Kitagawa describes three classes of 3D breathing materials: 2D coordination polymer layers that are connected by a flexible ligand in the third dimension (Class a), 1D coordination polymer chains that form a rhombus (or certain other geometric shapes) in the other two dimensions (Class b), and 3D interpenetrated grids (Class c) (Figure 3.1).[8] The breathing MOFs from Class a have demonstrated large breathing behavior with a range of flexible linkers between their 2D polymeric layers.[6c, 31] However, the synthesis of additional MOFs of this type is challenging because it remains a struggle to control the number of linkers between each 2D layer.[31] In a similar manner, while interpenetrated grids have shown phase transitions upon solvation/desolvation, which can selectively trap CO_2 in the nanopores at low

pressures,[28d] it is quite challenging to rationally synthesize new variants on this class of MOF because the degree of interpenetration is not predictable.[32] Since the SBUs (secondary building units) of Class b materials are similar to many MOFs that have previously been prepared,[33] this class of breathing MOFs has attracted the most attention.[6d, 9a, 9c, 34]

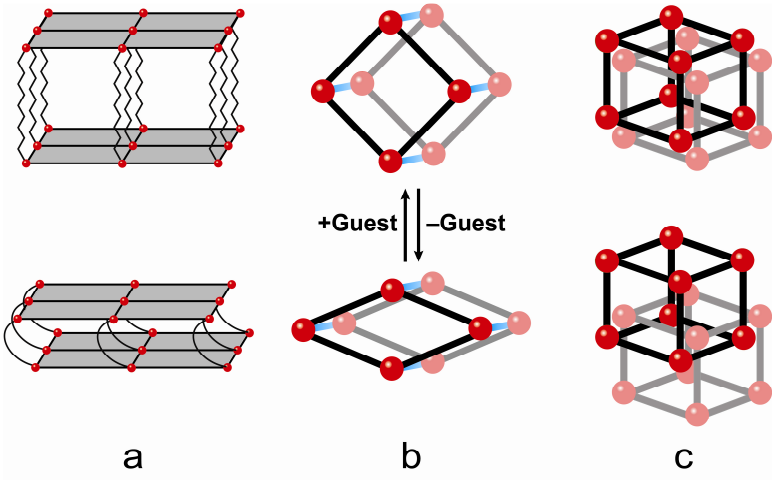


Figure 3.1. Illustration of three classes of 3D breathing materials. All materials are shown expanded on top and contracted on bottom. (a) 2D coordination polymer layers that are connected by a flexible ligand in the third dimension; (b) 1D coordination polymer chains (blue lines) that form a rhombus in the other two dimensions; (c) 3D interpenetrated grids.

Férey and Serre have prepared a series of Class b breathing MOFs.[6d, 9c, 34a-d] The critical feature is a ditopic carboxylate attached to an inorganic brick (SBU) that has a mirror plane. The breathing mechanism is activated by rotation around the O-O axis of the carboxylate (known as the “kneecap”), which requires

an opposite rotation on the opposing side of the SBU.[6b, 34c] While Férey and Serre have effectively described this mechanism and identified examples of this class of breathing MOFs, preparing additional MOFs of this type has been challenging, in part because the inorganic bricks that fit their requirements are quite rare.[6b, 35]

More recently, Long and coworkers reported two other Class b breathing MOFs that utilized 1,4-benzene-di(1*H*-1,2,3-triazole)[28g] or 1,4-benzenedipyrazolate[36] as the bridging ligand instead of a ditopic carboxylate. In the triazole system, the flexing was caused by two separate bending points: a small one within the ligand and the larger one at the metal-ligand interface. For the pyrazolate-based cobalt MOF, the structure undergoes a complex five-step transition that involves a rearrangement at the cobalt center wherein the geometry about the metal ion shifts from square planar to tetrahedral. Notably, the "kneecap," the primary flexing point, in both of their systems is still located at the junction of the ligand and metal.[28g, 36]

A problem with expanding Class b breathing MOFs is that they all depend on the exact interaction of the binding angle between the ligand and the metal. Our objective is to move the "kneecap" from the metal-ligand junction to within the ligand itself. We are developing MOFs utilizing semi-rigid ligands that have two points of rotation between the ditopic binding to the rigid metal-ligand fragment. These double hinges effectively make the ligand act like a "screw," which twists so that the angles of the rhombus shift without any significant effects

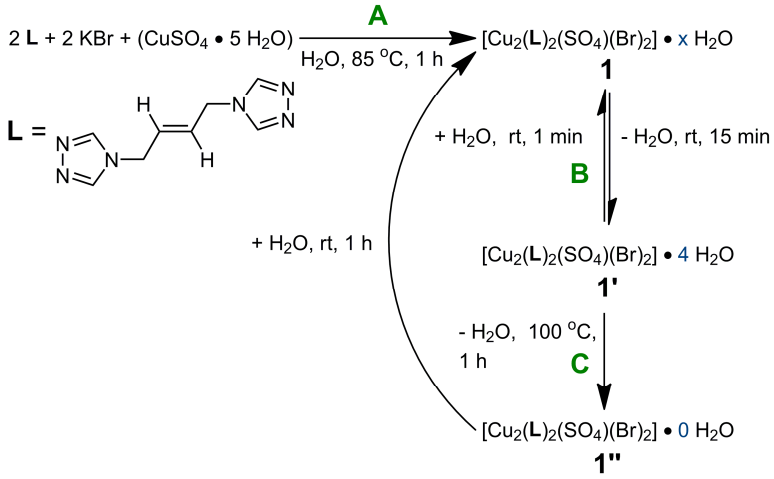
at the metal-ligand binding points. The elegance of this method is that the degree of breathing can be incorporated by judicious choice of semi-rigid ligands that conform to this double hinged design motif.

In this manuscript, we describe the synthesis and characterization of a copper MOF with a semi-rigid linker that displays reversible structural changes due to solvation/desolvation in the framework. Crucially, single crystal characterization shows these structural changes are the result of the rotation of a subunit of the ligand and not a change in the metal-ligand bond, which ultimately affects the void volume of the framework but not the topology. This change in void volume is demonstrated via gas adsorption experiments with an increase in adsorption for both CO_2 and CH_4 as a function of increased water in the pores.

Results and Discussion

We have previously reported the synthesis of the semi-rigid di-1,2,4-triazole, 4,4′-(1,4-(*trans*-2-butene)diyl)bis-(1,2,4-triazole), denoted as **L**.[12] Adding two equivalents of both **L** and potassium bromide to copper sulphate yields $[Cu_2(\mathbf{L})_2(SO_4)(Br)_2]\bullet xH_2O$ (**1**) as blue needle shaped crystals after 1 h at 85 °C (Scheme 3.1, Reaction **A**). Single crystal X-ray studies of the blue needles revealed that compound **1** crystallizes in the $P\bar{1}$ space group. Each octahedral copper center is coordinated by four triazole ligands that form an equatorial plane and two bromides in the axial positions. Adjacent copper atoms along the x-axis are bridged by two triazole fragments using the two terminal nitrogen atoms on

Scheme 3.1. Synthesis of copper MOFs.



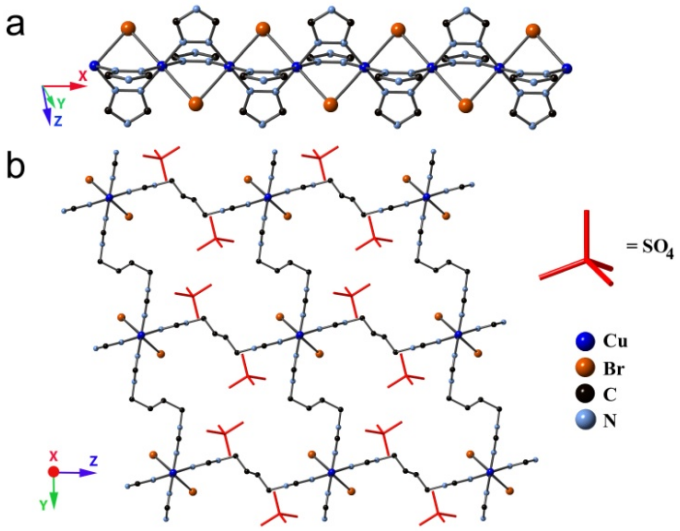


Figure 3.2. X-ray structure of $[Cu_2(\mathbf{L})_2(SO_4)(Br)_2] \cdot xH_2O$, **1**. (a) Crystal structure of **1** showing copper chains formed along x-axis; (b) Crystal structure of **1** showing links between copper chains viewed orthogonal to x-axis.

each triazole and a bridging bromide to form a linear chain (Figure 3.2a). These chains are linked in the other two dimensions by the second triazole moiety of the ligand, forming the three dimensional network, while the sulphates remain in the pores (Figure 3.2b).

While the PXRD of a fresh sample of **1** matches its simulated powder pattern, a considerable shift in the PXRD pattern can be seen in aged samples. Our suspicion for the cause of the shift in the PXRD was a loss of the guest molecules from within the pores. To confirm our suspicion, a time dependent PXRD of **1** was performed and revealed that the pattern of **1** was changed to the semi-hydrated form (**1′**) within 15 min., and the pattern of **1′** is stable for days (Figure 3.3). Additionally, **1′** will fully revert to **1** upon resolvation when a few drops of water are added onto the sample. This reversible process could be repeated multiple times without apparent crystallinity change.

To determine the extent of hydration in **1** and **1′** we conducted TGA measurements. The amount of lattice water that resides in **1** cannot be determined from TGA measurements since MOF **1** loses the excess water very quickly at room temperature to give **1′**. Immediate removal of **1** from a water bath results in a TGA trace shown in Figure 3.4. The initial weight loss can be attributed primarily to surface water.[37] MOF **1′**, on the other hand, loses 8.9% of its mass at 86 ^{o}C which is consistent with four water molecules in the pores (Figure 3.4). From the weight loss, we can deduce the formula for **1′** is

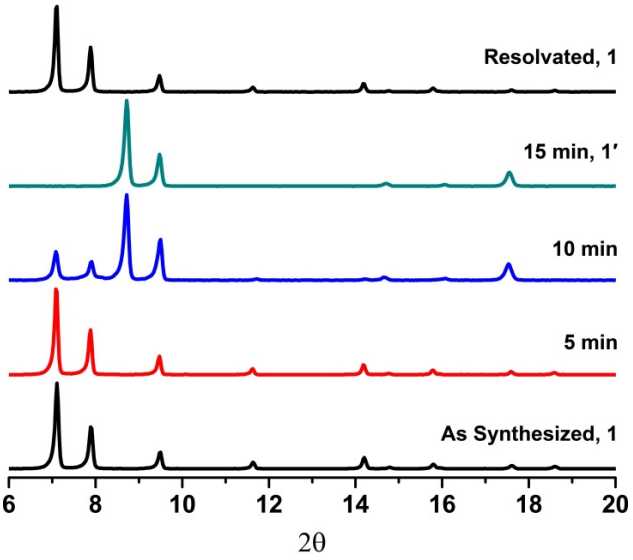


Figure 3.3. Powder pattern X-ray diffraction measurements taken of samples showing effects of solvation. **1′** is fully formed from **1** within 15 min. **1** can be reformed by resolvating the sample of **1′**. The intensity was normalized for each pattern.

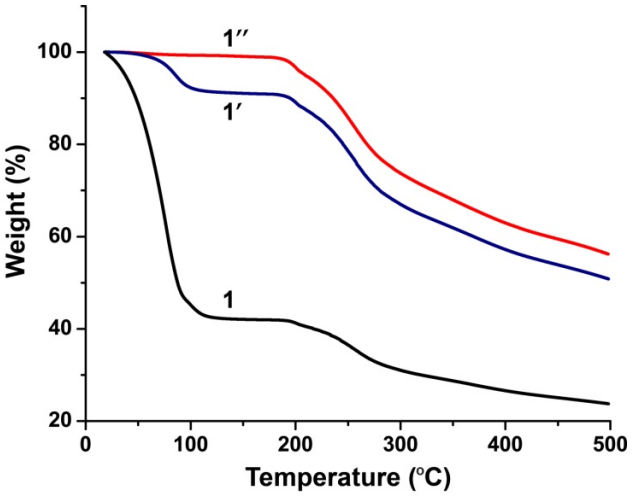


Figure 3.4. TGA measurements for all Copper MOFs**.**

$[Cu_2(\mathbf{L})_2(SO_4)(Br)_2]\bullet 4H_2O$ (Scheme 3.1). Notably, the TGA trace for **1** shows additional weight loss at the same temperature leading us to conclude that by 86 ^oC we have already formed **1′**.

To further understand this reversible process, single crystal X-ray diffraction was performed on a carefully air dried single crystal of **1**. Air dried **1** (compound **1′**) maintains the macroscopic morphology of blue needles, but the space group changes to *C*2/*c*. The X-ray crystal structure demonstrated that the topologies of **1** and **1′** are the same and that there was no appreciable change along the vector containing the Cu-Br bonds (Figure 3.2 and Figure 3.5).

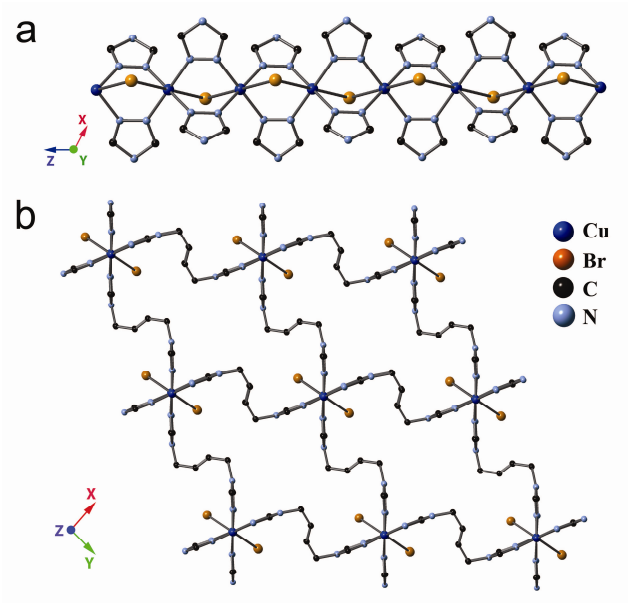


Figure 3.5. X-ray structure of $[Cu_2(\mathbf{L})_2(SO_4)(Br)_2] \bullet 4H_2O$, **1′**. (a) Crystal structure of **1′** showing copper chains formed along z-axis; (b) Structure of **1′** showing links between copper chains viewed orthogonal to the z-axis. Sulphates have been omitted for clarity.

Despite having the same topologies, several structural differences between **1** and **1′** are observed. A significant change in the axis lengths on the rhombus perpendicular to the 1D coordination polymer chains is detected with the vertical height decreasing by over 2.3 Å (Figure 3.6a and b). Furthermore, in contrast to Long's system, a small decrease in axial length of 0.4 Å was also noted.[28g] These changes to the size of the pore channels lead to a 29% increase in density between **1** (1.224 g/cm^3) and **1′** (1.584 g/cm^3). Although the solvent molecules within the framework were not located due to poor crystallinity, the solvent accessible volume in each framework was calculated using PLATON.[27] The solvent accessible volume of **1** is 21% larger than **1′** (35.6% for **1** versus 14.8% for **1′**).

To understand what causes these structural differences between **1** and **1′** we evaluated the positions of the bridging ligand, **L**, in relation to the 1D chain composed of Cu and Br atoms. MOF **1** has two crystallographically distinct bridging 1,2,4-di-triazoles (Figure 3.6a, shown in red and green highlights). The 2-butene portion of **L** highlighted in green in Figure 3.6a is pointed almost orthogonal to the yz-plane. The dihedral angle between the two planes composed of the 1D coordination polymer chain (the Cu and Br atoms), and the 2-butene portion of **L** is 33°. The second distinct bridging **L** highlighted in red in Figure 3.6a has a dihedral angle of 82° between the 1D coordination polymer chain and the 2-butene.

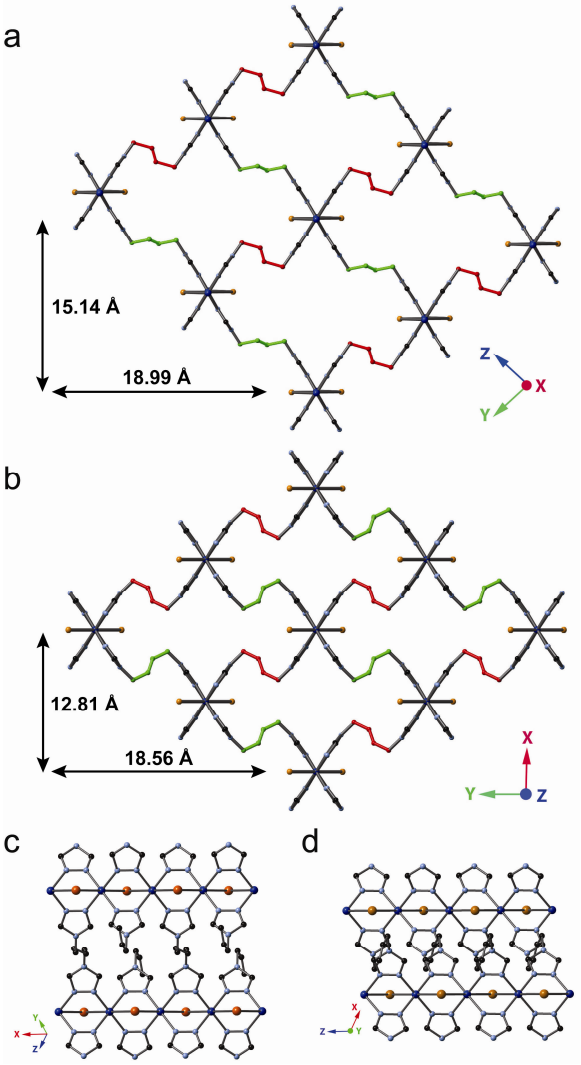


Figure 3.6. Comparison of X-ray structures. In (a) and (b): Distances shown are rhombus axes. Red and green highlights are 2-butene subunits of ligand that correspond to same position in **1** and **1′**; (a) Crystal structure of **1** viewed orthogonal to x-axis. (b) Crystal structure of **1′** viewed orthogonal to z-axis; (c) Crystal structure of **1** viewed along the x-axis; (d) Crystal structure of **1′** viewed along the z-axis. In all structures, sulphates have been omitted for clarity.

In MOF **1′**, one of the 2-butene subunits of the bridging ligand **L** has rotated to become the mirror image of the other one and they are no longer crystallographically distinct (Figure 3.6b). The 2-butene portion highlighted in red has barely shifted and has a dihedral angle of 83° with respect to the Cu and Br atoms, but the other 2-butene fragment, highlighted in green, has rotated substantially, now showing a dihedral angle of 97° (Figure 3.6b). This twisting about one pair of 2-butene subunits on the opposite edges of the rhombus causes the Cu-Br layers to pack more tightly (Figure 3.6c and 3.6d) demonstrating that in this system the orientation of the 2-butene subunit acts as the "kneecap." To the best of our knowledge, this result is the first case where the "kneecap" is entirely based in the ligand and not primarily at the metal-ligand junction.

TGA measurements show that **1′** is only partially dehydrated (Figure 3.4), suggesting that it may be possible to give a fully desolvated MOF. If the remaining guest molecules could be removed, the 2-butene subunits may rotate to a different position, which may further decrease the void volume. To investigate the effect of further dehydration on the flexibility of the framework, a fully dehydrated MOF was prepared. A sample of **1′** was heated to 100 °C for 1 hr. A green powder corresponding to $[Cu_2(\mathbf{L})_2(SO_4)(Br)_2]\bullet 0H_2O$ (**1″**) was obtained. A TGA was taken of **1″** and there was no weight loss until the framework itself decomposed, providing evidence the framework had been completely desolvated (Figure 3.4). Due to the poor crystallinity of **1″**, we were

not able to obtain a single crystal. However, a PXRD pattern of **1″** shows that although the material is almost amorphous, one peak persists after heating, which is at $2\theta = 9.4°$. This peak is also present in the PXRD patterns of both **1** and **1′** (Figure 3.3). Indexing of the PXRD patterns of **1** and **1′** indicates this peak represents their (011) and (020) planes, respectively (Figures 3.7 and 3.8). The similarity of these two planes is most clearly seen along the copper-bromide vectors in **1** and **1′** (Figure 3.6c and Figure 3.6d). Conceivably, this same ordered plane exists in the fully dehydrated **1″** while randomly oriented ethylene chains cause disorder, leading to a mostly amorphous state. Finally, if a sample of **1″** is left in water for 1 hour, the adsorption of water allows for the reformation of blue **1** based on PXRD measurements. Attempts at forming **1** from **1″** through the use of water vapor were unsuccessful, and it was determined that only liquid water allowed for the successful reformation of **1**. The newly reformed **1** can then be cycled through **1′** and subsequently **1″**.

The presence of guest molecules within a framework, specifically polar guests such as water, has recently been shown to improve CO_2 adsorption or selectivity.[38] This increase in adsorption by polar guests can be attributed to the significant quadrupole moment of CO_2 which favors interactions such as hydrogen bonding with the guest molecules.[28b, 38a, 38c-e] On the other hand, adsorption of gases, such as CH_4, that exhibit no quadrupole moment is not favored in the presence of polar guests.[28b, 38a, 38c] The flexibility exhibited by this

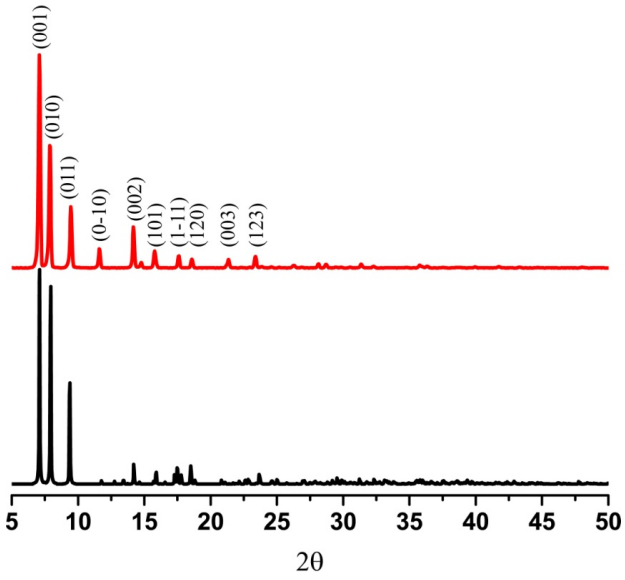


Figure 3.7. PXRD pattern for $[Cu_2(\mathbf{L})_2(SO_4)(Br)_2]\bullet xH_2O$ (**1**): experimental (red) and simulated (black).

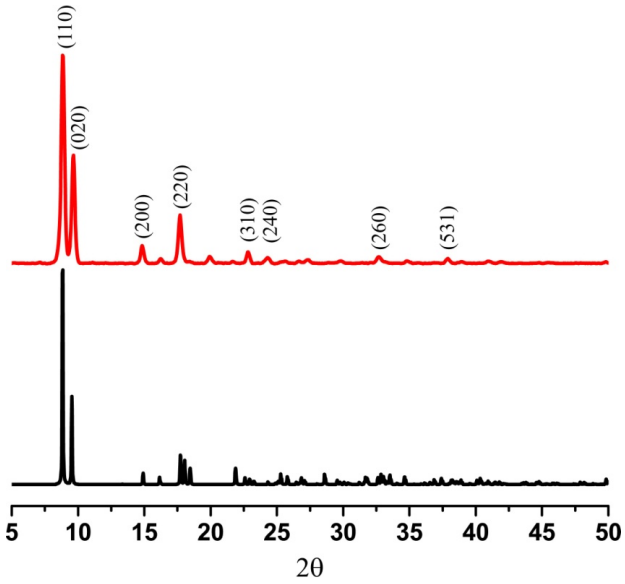


Figure 3.8. PXRD pattern for $[Cu_2(\mathbf{L})_2(SO_4)(Br)_2] \bullet 4H_2O$ (**1′**): experimental (red) and simulated (black).

MOF system as well as the presence of water as a guest molecule piqued our interest in studying their CO_2 adsorption properties, and in particular their selectivity for CO_2 versus non-polar guests, such as CH_4, as a function of guest water molecules. Since no crystal structure could be obtained for **1″**, adsorption isotherms may also provide evidence for the expansion in the solvent accessible volume of **1′** versus **1″**.

Due to the rapid dehydration of **1** to **1′**, adsorption properties of the fully hydrated **1** were not able to be analyzed; however, adsorption isotherms could be performed and compared between the fully dehydrated **1″** and the partially dehydrated **1′**. Figure 3.9 shows both the CO_2 and CH_4 adsorption isotherms for **1′** and **1″** at 298 K. At 1.22 bar, the CO_2 and CH_4 uptakes for **1″** are 0.490 and 0.0285 mmol g^{-1}, respectively. When the framework is expanded to **1′** after careful hydration treatment, the adsorption isotherms drastically change. An increase in adsorption is witnessed, resulting in the uptake of 1.39 mmol g^{-1} of CO_2 and 0.160 mmol g^{-1} of CH_4 at 1.22 bar. Since both CO_2 and CH_4 adsorption increased, the selectivity did not appear to change significantly even though polar guests are present within the framework.

As mentioned above, polar guests, such as water, have been demonstrated to improve the CO_2/CH_4 selectivity due to the different interactions between the guest molecules and adsorbent. By analyzing the isotherms and the transition from **1″** to **1′**, the adsorption behavior experienced does not follow the normal trend and, instead, the adsorption of water and expansion of the

framework allows for an increase in both CO_2 and CH_4 adsorption for **1′** when compared to **1″**. In other systems, the presence of water has been shown to decrease CH_4 adsorption, therefore increasing selectivity for CO_2.[28b, 38a, 38c] A plausible explanation for the increase in adsorption for both CO_2 and CH_4 in **1′** is the expansion of the framework in addition to any interactions with the guest water molecules present.

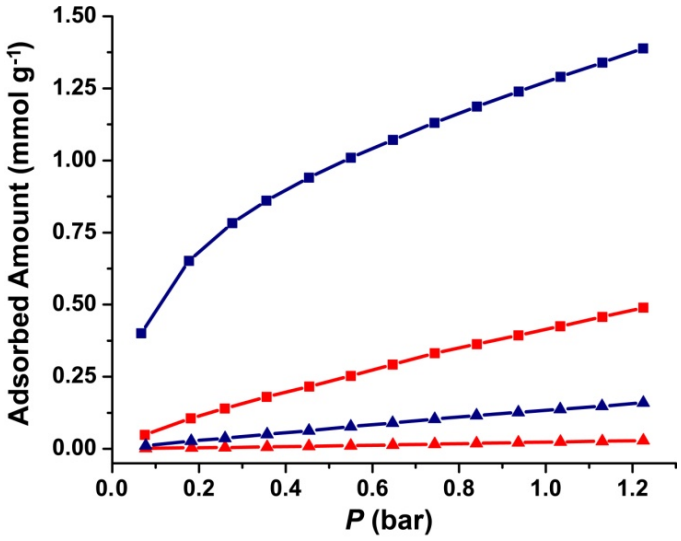


Figure 3.9. CO_2 (squares) and CH_4 (triangles) depict adsorption isotherms for $[Cu_2(\mathbf{L})_2(SO_4)(Br)_2]\bullet xH_2O$ (**1′**) (blue) and $[Cu_2(\mathbf{L})_2(SO_4)(Br)_2]\bullet 0H_2O$ (**1″**) (red) at 298 K.

Conclusion

In conclusion, a three-dimensional copper MOF was synthesized that changes its framework structure as a function of the quantity of interstitial water

molecules. The orientation of the semi-rigid di-1,2,4-triazole ligand adjusts as a function of hydration, and this process is reversible at room temperature. Furthermore, the MOF loses much of its crystallinity when the remaining water molecules are removed (as seen in **1″**), but **1** can be recovered in its powder form by addition of water. Single crystal X-ray diffraction demonstrates that this breathing MOF constructed with semi-rigid linkers has the ability to self-adjust the solvent accessible volume according to the amount of solvent present while maintaining the same topology. Notably, the "kneecap" in this breathing system lies within the ligand itself and not at the metal-ligand juncture. The quantity of gases adsorbed increased for both CO_2 and CH_4 with a structural change that was facilitated by addition of guest water molecules. Finally, the selectivity of CO_2 versus CH_4 adsorption is not increased with water in the pores which is contrary to what is typically observed for MOFs that have been partially hydrated. Since similar semi-rigid linkers are easy to synthesize and their flexibility can be modulated, this strategy could lead to a large family of porous materials that change their void space as a function of guest adsorption.

Experimental

The compound 4,4′-(1,4-(*trans*-2-butene)diyl)bis-(1,2,4-triazole) (notated below as "**L**") was prepared as described previously.[12] All other reagents were purchased from commercial vendors and used without purification. Infrared spectra were collected on a Thermo Scientific Nicolet iS10 with a Smart iTR accessory for attenuated total reflectance. Thermogravimetric analysis (TGA)

data were collected on a TA Instruments TGA Q50 under N_2. Carbon, hydrogen, and nitrogen analyses were obtained from Atlantic Microlab, Norcross, GA. Single crystal diffraction data was collected on a Bruker SMART APEX II three circle diffractometer equipped with a CCD area detector and operated at 1,800 W power (45 kV, 40 mA) to generate Mo Kα radiation (λ = 0.71073 Å). The incident X-ray beam was focused and monochromated using Bruker Excalibur focusing optics. Single crystals of **1** and **1′** were mounted on nylon CryoLoops (Hampton Research) with Paratone-N (Hampton Research) and frozen at -100 ℃ and -173 ℃, respectively. The sulphate anions in both cases are heavily disordered. Due to the large void volume, water molecules were not located. In both cases, SQUEEZE routine was used to simplify and improve the refinements. Additionally, all structures were examined using the *Addsym* subroutine of PLATON[27] to assure that no additional symmetry could be applied to the models. Powder X-ray diffraction (PXRD) data was collected using a Panalytical Empyrean θ-2θ diffractometer in reflectance Bragg-Brentano geometry. Cu-Kα radiation (λ = 1.5406 Å; 1,800 W, 45 kV, 40 mA) was focused using a planar Gobel Mirror riding the Kα line. Gas adsorption measurements were collected at 298 K on a Micromeritics ASAP 2020.

Synthesis of $[Cu_2(L)_2(SO_4)(Br)_2]\cdot xH_2O$, 1. Copper(II) sulphate pentahydrate (9.18 mg, 0.0367 mmol) and a mixture of potassium bromide (8.75 mg, 0.0735 mmol) and **L** (14.0 mg, 0.0735 mmol) were added to separate 4 mL scintillation vials and dissolved with 1 mL and 2 mL of water, respectively. The vials were

heated to 85 °C for 30 min in an aluminum heating block. The solutions were mixed and heated for an additional 1 hr until large blue crystalline needles had formed. The crystalline material was collected from the mother liquor and washed with H_2O to remove excess ligand. IR (neat): 3349, 3135, 1640, 1561, 1497, 1444, 1401, 1377, 1360, 1280, 1216, 1088, 1066, 1046, 972, 944, 880, 742, 680 cm^{-1}. Crystal data for **1** $C_{16}H_{20}Br_2Cu_2N_{12}O_4S$, M = 763.40, triclinic, space group $P\bar{1}$, a = 7.260(16), b = 11.77(3), c = 13.15(3) Å, α = 74.55(3), β = 76.47(3), γ = 76.55(3)°. V = 1036(4) $Å^3$, Z = 1, ρ_{calc} = 1.224 Mg m^{-3}, μ(Mo Kα) = 3.036 mm^{-1}. 7844 collected reflections, 2839 crystallographically independent reflections [R_{int} = 0.1421], θ_{max} = 23.34°, Goodness-of-fit = 1.028. R_1 = 0.1711, wR_2 = 0.3766 [I>2∑(I)]; R_1 = 0.2125, wR_2 = 0.4152 (all data).

Synthesis of $[Cu_2(L)_2(SO_4)(Br)_2]\cdot 4H_2O$, 1′. Air drying **1** for 15 min resulted in the formation of the partially dehydrated framework, **1′**, and remained as blue crystalline needles (5.6 mg, 37% yield; yield was based on starting copper sulphate). IR (neat): 3362, 3138, 2964, 1636, 1560, 1496, 1444, 1401, 1377, 1361, 1279, 1261, 1214, 1089, 1064, 1046, 974, 948, 879, 797, 742, 680 cm^{-1}. Anal. Calcd. for $C_{16}H_{20}Br_2Cu_2N_{12}O_4S\cdot 4H_2O$: C, 23.00; H, 3.38; N, 20.12. Found: C, 22.54; H, 3.75; N, 18.63. Crystal data for **1′**: $C_{16}H_{20}Br_2Cu_2N_{12}O_4S$, M = 763.40, monoclinic, space group $C2/c$, a = 12.813(6), b = 18.557(8), c = 7.259(3) Å, β = 111.973(5)°. V = 1600.7(12) $Å^3$, Z = 2, ρ_{calc} = 1.584 Mg m^{-3}, μ(Mo Kα) = 3.930 mm^{-1}. 2919 collected reflections, 622 crystallographically independent reflections

[R_{int} = 0.0912], θ_{max} = 18.75°, Goodness-of-fit = 1.465. R_1 = 0.1148, wR_2 = 0.3305 [I>2∑(I)]; R_1 = 0.1366, wR_2 = 0.3534 (all data).

Synthesis of $[Cu_2(L)_2(SO_4)(Br)_2]\cdot 0H_2O$, 1″. A sample of **1′** was heated to 100 ℃ in a 20 mL scintillation vial in an aluminum heating block. A green powder, **1″**, was formed after 1 hr of heating. Anal. Calcd for $C_{16}H_{20}Br_2Cu_2N_{12}O_4S$: C, 25.17; H, 2.64; N, 22.02. Found: C, 24.43; H, 2.90; N, 20.97.

Time dependent reactions for the desolvation/resolvation of 1. **1** was synthesized according to the above method and an immediate PXRD was taken of the as synthesized crystals. PXRD patterns were then taken at 5, 10, and 15 minutes to monitor the dehydration process. Upon desolvation, the powder was resolvated by adding 5 drops of H_2O and gently soaking up any excess solvent. A PXRD pattern was then taken at 15 minutes to show the desolvated phase and this process was repeated again as can be seen in Figure 3.

TGA Measurements. Thermogravimetric analysis (TGA) data were collected on a TA Instruments TGA Q50 under N_2. All TGAs were collected at a ramp rate of 5° C per minute under N_2 atmosphere. A TGA of **1** was obtained by soaking a sample of **1′** in water for 1 hr. A PXRD was taken of a small sample of the material to ensure the sample was in the correct phase as **1**. Upon removal from solution, excess water was collected using filter paper and a TGA was immediately collected. A TGA of **1′** was obtained after placing a sample in a desiccator for 24 h using the same initial sample as **1**.

Gas Adsorption Measurements. Gas adsorption measurements were collected at 298 K on a Micromeritics ASAP 2020. Gas adsorption measurements were performed on a fresh sample of **1′** which was verified by PXRD. The sample was first degassed at 100°C for one hour to form the completely dehydrated framework **1″** and CO_2 and CH_4 measurements were collected at 298 K. After data collection, 2 mL of H_2O was added to the sample and allowed to soak for 1 hr. After soaking, the sample was collected and washed with acetone and placed in a desiccator for 24 h. A PXRD was taken to verify the sample was in the **1′** phase prior to CO_2 and CH_4 measurements.

Chapter 4

Two-dimensional MOFs

A version of this chapter was originally published by Christopher R. Murdock, Nicholas William McNutt, David J. Keffer, and David M. Jenkins:

Murdock, Christopher R.; Mcnutt, Nicholas W.; Keffer, David J.; Jenkins, David M. "Rotating phenyl rings as a guest-dependent switch in 2D MOFs." *J. Am. Chem. Soc.* **2014**, *136*, 671-678.

All work presented herein is the work of Chris Murdock and has been modified from the above publication.

Abstract

A semi-rigid di-1,2,4-triazole ligand binds in a *syn* conformation between copper(I) chains to form a series of two-dimensional metal-organic frameworks that display a topology of fused 1D metal-organic nanotubes. These anisotropic frameworks undergo two different transformations in the solid state as a function of solvation. The 2D sheet layers can expand or contract, or, more remarkably, the phenyl ring can rotate between two distinct positions. Rotation of the phenyl ring allows for the adjustment of the tube size, depending on the guest molecules present. This "gate" effect along the 1D tubes has been characterized through single crystal X-ray diffraction. The transformations can also be followed by powder X-ray diffraction and solid state ^{13}C CP MAS NMR. Whereas PXRD cannot differentiate between transformations, solid state ^{13}C CP MAS NMR can be employed to directly monitor phenyl rotation as a function of solvation, suggesting that this spectroscopic method is a powerful approach for monitoring

breathing in this novel class of frameworks. Finally, isoreticular frameworks which contain extended naphthyl and biphenyl linkers have been synthesized and characterized. Isoreticular synthesis is an important concept in MOF chemistry, but isoreticular synthesis utilizing more flexible linkers has never before been demonstrated. The ability of extended di-triazole ligands to bind in a similar *syn* conformation allows for the future testing of additional "gate" effects.

Introduction for Gate Switching Breathing: Rotating Phenyl Rings

Since breathing MOFs (metal-organic frameworks) can switch between opened and closed configurations, these advanced materials have been proposed for applications such as gas separations,[1b, 6a, 7a, 7c-e, 39] liquid separations,[7c-e, 39d] chemical sensing,[1b, 6a, 7a, 7c, 7e, 39a, 39b, 39d, 40] and even hazardous waste adsorption.[7a, 39d, 41] The existence of multiple stable states combined with a fine tuning of the pore properties allows breathing MOFs to exhibit highly selective guest adsorption.[9b, 28b, 28f, 42] Guest selective pore-opening and step-wise adsorption as a function of pressure or concentration result in pore properties that can be modified, leading to an increased interest in the synthesis of additional breathing MOF systems.[6a, 7a, 43] Since breathing MOFs are multipurpose porous materials with numerous potential applications, the development of rational synthetic methodologies for their preparation is indispensable.

One constructive approach for designing breathing MOFs begins by determining where the hinges or "kneecap" should be on the porous material.[7c, 39b] Kitagawa proposed a system for 3D materials wherein the dimension of porosity could be either 1D (tubes), 2D (sheets), or 3D (interpenetrated).[7b] Of the breathing MOFs that fall within this classification, most flex at the metal ligand interface, which means that the exact interaction between the ligand and the metal determines whether the MOF can flex.[7c, 7e, 39b] To avoid this limitation in the synthesis of breathing MOFs, researchers have investigated routes that move the "kneecap" away from the metal-ligand interface to the ligand itself. Wang, Oliver, and Vittal have independently demonstrated that double-hinged ligands can act like a screw to pull the layers in 2D MOFs together as a function of guest (Figure 4.1, top), while our research has shown the same screw-like effect with 1D rhombic pores allowing the rhombus to be pinched shut as a function of guest (Figure 4.1, middle).[11a, 11b, 44] Placing the "kneecap" solely on the ligand allows for fixed metal-ligand binding points, but it is clear from the dearth of examples that a more robust synthetic strategy is required.

An alternative approach to building breathing MOFs whose "kneecap" is located solely on the ligand involves preparing an anisotropic framework where a moiety of the linker can swivel to block the pore as a function of guest. The concept of applying linker rotation to block the pore has been implied with the development of frameworks in which a subunit of the linker can undergo free

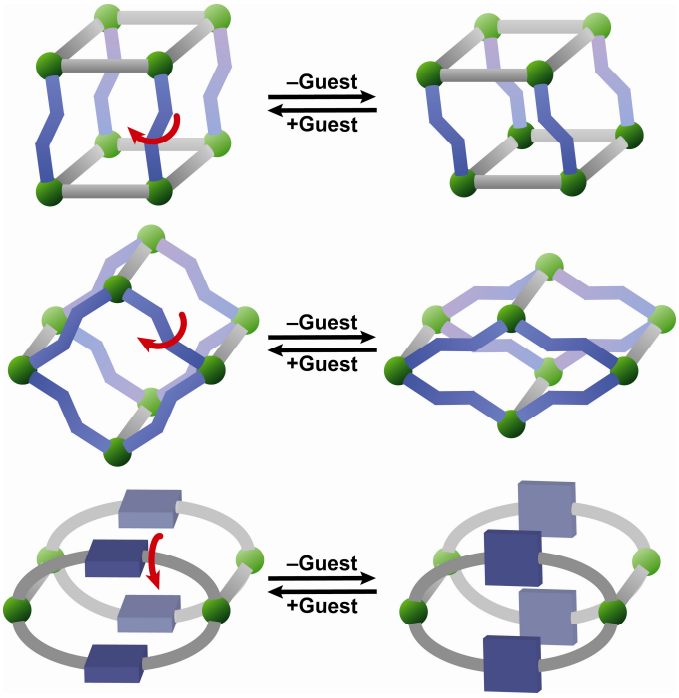


Figure 4.1. Graphical depiction of methods in which the "kneecap" is placed solely on the ligand. Double-hinged ligands can be used to pull together rigid 2D sheets (top) or 1D chains (middle), or a subunit of the ligand can rotate to open and close the pore (bottom). Green spheres represent metal centers or secondary building units (SBUs) and gray and blue components represent rigid and flexible portions of the ligand, respectively.

rotation.[1b, 7d, 45] However, to form a breathing MOF, the linker must rotate between fixed positions that would allow for a more effective "gate" effect to occur as the pore is opened and closed. A depiction of an anisotropic metal-organic framework that demonstrates this "gate" effect is shown in Figure 4.1 (bottom). This "gate" opening effect would not be dependent on the metal centers and would potentially allow for a wide range of pore sizes to be synthesized in a highly isoreticular manner with only modest changes to the swiveling subunit. Another advantage of employing a "gate" mechanism is that the rotating subunit may be able to be monitored directly through solid state spectroscopic methods, such as ^{13}C CP MAS NMR, which is a boon when crystallographic data is not available.

While aryl rings are an obvious component of the rotating "gate," only limited examples have been reported to date. Kitagawa and coworkers prepared a pillared-layer cadmium coordination polymer wherein the aryl ring rotated as a function of hydration, as determined by single crystal diffraction. The total motion between the open and closed states of their framework, however, is quite complex since, upon dehydration, the "gate" will close concurrently with a contraction of the distance between the layers.[46] More recently, Yang, Schröder, and coworkers prepared a cobalt MOF that exhibited adsorption isotherms consistent with breathing. Based on grand canonical Monte Carlo simulations, PXRD, and IR experiments, they concluded that the pyridyl rings in their linkers rotate in the presence of CO_2 to open the channels.[47] To date, a rotating "gate"

framework has not been fully characterized both by single crystal diffraction and additional spectroscopic methods where rotation is solely at the aryl unit.

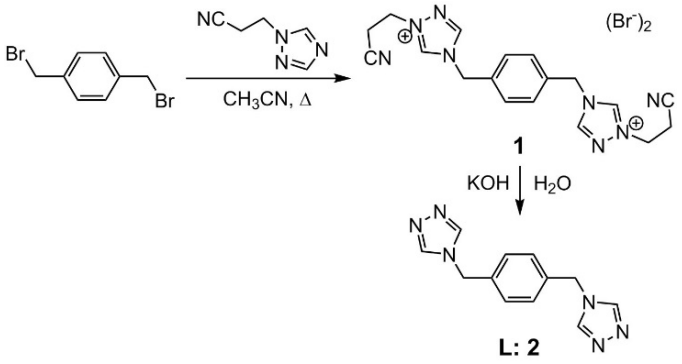
We have synthesized a 2D copper sheet MOF that has a topology of 1D nanotubes fused along the copper chains. The backbone of the framework is formed by a bidentate semi-rigid linker in a *syn* conformation whose phenyl subunit rotates between parallel and perpendicular positions as a function of guest solvent. These phenyl rotations open and close the 1D tubes. Crucially, each orientation of the phenyl ring has been confirmed by single crystal and powder X-ray diffraction, and, more notably, the rotating "gate" effect has been observed, for the first time, by ^{13}C CP MAS NMR. This direct spectroscopic technique could be highly valuable for testing additional MOFs that breathe by the same "gate" rotating mechanism, reducing the need for single crystal diffraction to prove the existence of each state.

Results and Discussion for Gate Switching Breathing: Rotating Phenyl Rings

We have previously reported the synthesis of a semi-rigid di-1,2,4-triazole containing a 2-butene subunit[48] and have expanded this methodology to incorporate a central xylene moiety. Following the method of Horváth,[23] the addition of 1,2,4-triazole-1-propanenitrile to 1,4-bis(bromomethyl)benzene leads to the formation of the intermediate **1** in 94% yield (Scheme 4.1). Subsequent cleavage of the propanenitrile group with potassium hydroxide yields the product

4,4′-(1,4-(xylene)diyl)bis(1,2,4-triazole) (**L: 2**) in 84% yield. The ligand **L** (**2**) can be further purified via recrystallization from water.

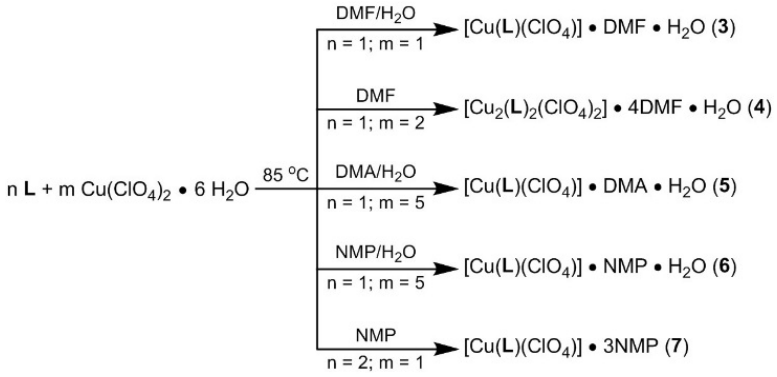
Scheme 4.1. Di-triazole ligand synthesis.



Our previous published results with the semi-rigid linker, 4,4′-(1,4-(trans-2-butene)diyl)bis(1,2,4-triazole), have demonstrated that it is possible to prepare multiple copper MOFs as a function of varying reaction conditions including solvent, metal to ligand ratio, and starting metal salt.[11b, 48] To canvas the reaction space of this new double-hinged ligand **2**, several different reaction conditions were attempted (Scheme 4.2).

The addition of one equivalent of both **L** and copper perchlorate to a mixture of N,N-dimethylformamide (DMF) and water leads to the formation of [Cu(**L**)(ClO_4)] • DMF • H_2O (**3**) (Scheme 4.2, top). Colorless crystalline needles that are suitable for X-ray diffraction are obtained after heating the reaction mixture for 24 h at 85 °C. Single crystal X-ray diffraction shows that each

Scheme 4.2. Synthesis of copper frameworks utilizing various solvents and metal to ligand ratios.



tetrahedral Cu(I) center is coordinated to four triazole ligands (Figure 4.2A). Adjacent copper atoms are bridged by two triazole ligands to form an equatorial plane, resulting in the formation of a linear chain (Figure 4.2B). The semi-rigid ligand exhibits a *syn* conformation to form a 2D layered structure with neighboring copper chains (Figure 4.2C).[39c, 49] Since the triazole ligands bridge the copper centers in an alternating manner, the overall topology is a 2D sheet (Figure 4.2C). Guest DMF molecules fill the pores of the framework, while the perchlorate anions are packed between the sheet layers.

While framework **3** resembles a 2D network, the actual connectivity does not resemble a two-dimensional square grid.[50] The topology is more comparable to a set of fused 1D metal-organic nanotubes (MONTs)[51] due to the existence of channels along the y-axis (Figure 4.2C). The result of this topology is an anisotropic framework in which porosity is controlled through the size of the 1D

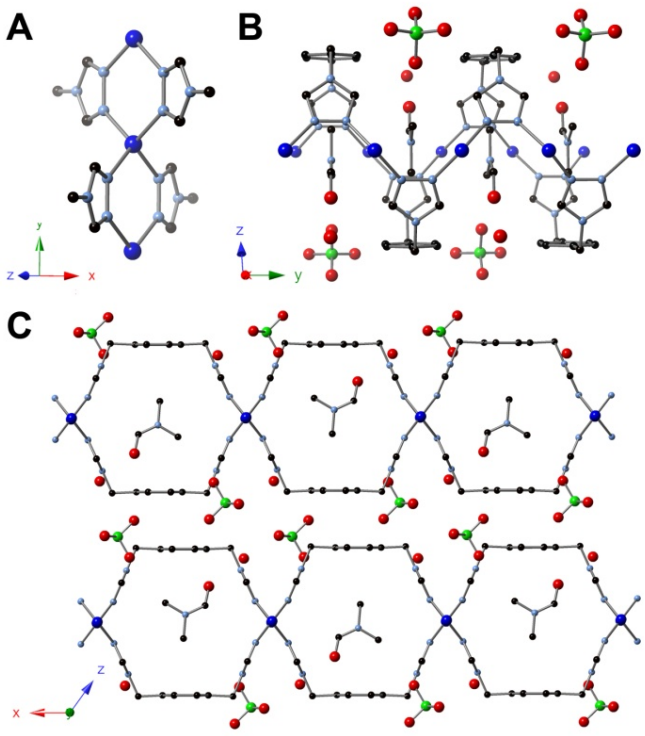


Figure 4.2. X-ray structure of [Cu(**L**)(ClO_4)] • DMF • H_2O, **3**. (A) Crystal structure of **3** showing the copper connectivity. (B) Crystal structure of **3** showing copper chains along the y-axis. (C) Crystal structure of **3** viewed orthogonal to the y-axis showing the fused-tube topology. Blue, light blue, black, green, and red spheres represent Cu, N, C, Cl, and O, respectively. All hydrogen atoms have been omitted for clarity.

pores. The size of these pores are in turn set by the size and shape of the *syn* conformed ligand.

By using DMF as a solvent and a two-to-one metal to ligand ratio, a variant of **3** was obtained. The framework, $[Cu_2(\mathbf{L})_2(ClO_4)_2] \cdot 4DMF \cdot H_2O$ (**4**), was collected as colorless needles after heating in DMF at 85 ℃ for 36 h (Scheme 4.2). The crystalline needles are in the same $C_{2/m}$ space group as **3**, but an increase in the unit cell volume was observed. Crystallographic studies revealed the same connectivity with Cu(I) centers bridged by triazole ligands, resulting in a fused 1D MONT structure similar to **3** (Figure 4.3). While DMF molecules remain within the voids as in **3**, additional DMF molecules are now

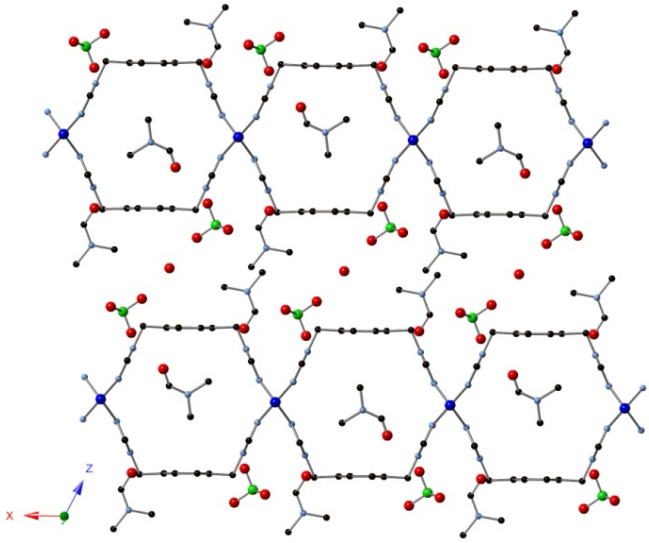


Figure 4.3. Crystal structure of $[Cu_2(\mathbf{L})_2(ClO_4)_2] \cdot 4DMF \cdot H_2O$, **4**, viewed orthogonal to the y-axis showing the fused-tube topology.

located between the layers. The π–π interactions are disrupted in order to accommodate the additional guest molecules, which increases the distance between the layers from 3.8 Å to 7.3 Å (Figure 4.3).

As part of our screening of reaction conditions as a function of solvent, we employed structurally similar N,N'-dimethylacetamide (DMA) as a cosolvent with water in the framework reaction. Upon addition of one equivalent of **L** with five equivalents of copper perchlorate, [Cu(**L**)(ClO_4)] • DMA • H_2O (**5**) was obtained as colorless needles after heating two weeks at 85 °C (Scheme 4.2). The structure of **5** was topologically identical to that of **3** — consisting of Cu(I) centers bridged by two triazole ligands to form a fused-tube structure — but there was one major structural change (Figure 4.4): the orientation of the phenyl ring had rotated 90° compared to **3**! Whereas the phenyl rings are parallel to one another in **3**, resulting in layers which are stacked through π–π interactions, the phenyl moiety in **5** is perpendicular to the orientation of the tubes. This rotation of the phenyl rings breaks the π–π interactions and allows for a migration of the solvent from within the pore to between the rotated phenyl rings (Figure 4.2 and 4.4). Despite repeated efforts, we were unsuccessful in preparing a bulk quantity of framework **5**.

Even though framework **5** was not isolable, the existence of the phenyl ring in a perpendicular rather than parallel fashion piqued our interest in synthesizing additional 2D fused MONTs. Although dynamic transformations

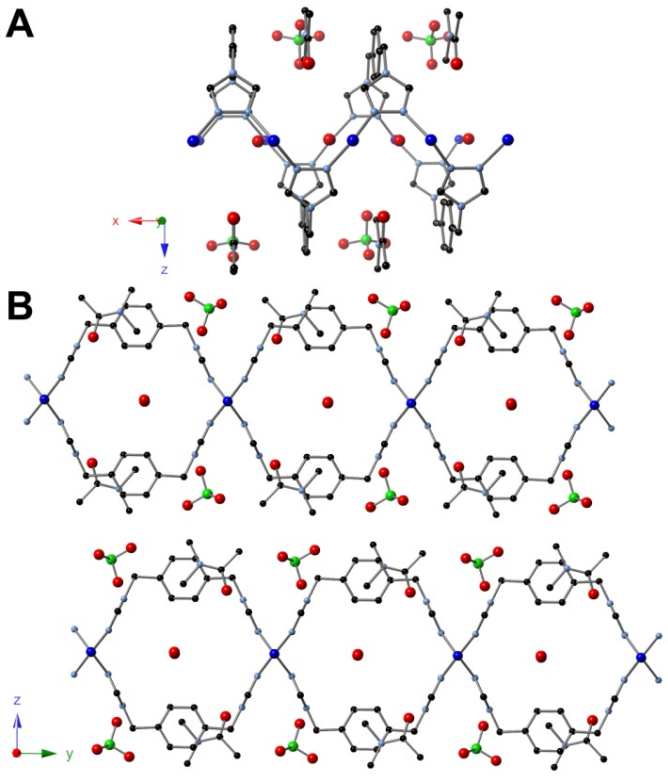


Figure 4.4. X-ray structure of [Cu(**L**)(ClO_4)] • DMA • H_2O, **5**. (A) Crystal structure of **5** showing copper chains along the x-axis. (B) Crystal structure of **5** viewed orthogonal to the x-axis showing the fused-tube topology.

within MOFs have been studied, including the continuous rotation of phenyl rings,[45] the ability to control the rotation between two fixed states would provide a valuable gating technique for porous materials. The ability to switch between different states is only beneficial if the framework is anisotropic, and the existence of 1D pores in frameworks **3**-**5** provides an ideal platform to study switchable phenyl rotation that can change the pore size.

Given the differences in frameworks **3** and **5**, we desired to attempt to synthesize two frameworks that contain the *same* solvent and show both aryl ring positions. N-methyl-2-pyrrolidone (NMP) was used as a reaction medium to synthesize additional frameworks due to its structural similarity to DMF and DMA. Using a combination of NMP and water, [Cu(**L**)(ClO_4)] • NMP • H_2O (**6**) was obtained after two weeks of heating at 85 °C with a metal to ligand ratio of five-to-one (Scheme 4.2). The topologically similar framework again crystallized in the $C_{2/m}$ space group and is analogous to that of **3**, except that the DMFs within the pores are now replaced with guest NMP molecules (Figure 4.5). The phenyl moiety remained in a parallel fashion showing π–π stacking between the layers with a layer distance of 3.8 Å.

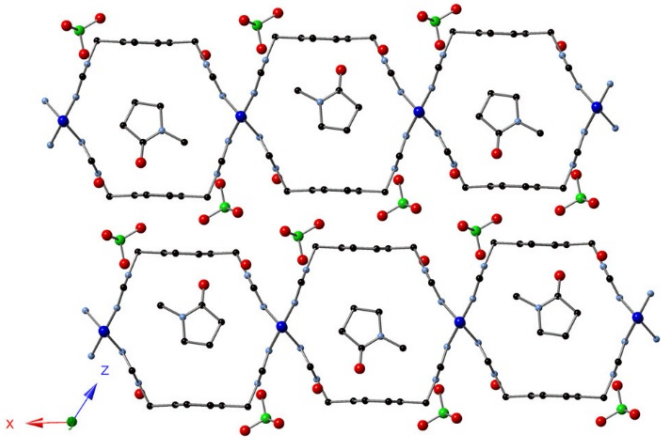


Figure 4.5. Crystal structure of [Cu(**L**)(ClO_4)] • NMP • H_2O, **6**, viewed orthogonal to the y-axis showing the fused-tube topology.

When only NMP is used as a reaction solvent with a two-to-one ligand to metal ratio, [Cu(**L**)(ClO_4)] • 3NMP (**7**) is formed as colorless needles after three days of heating at 85 °C (Scheme 4.2). Crystallographic studies revealed that the framework crystallizes in the $P\bar{1}$ space group and that the connectivity resembles the previously-described frameworks **3**-**6**. Notably, the phenyl moiety is rotated 76° as compared to **6** (Figure 4.6). In a similar manner to **5**, guest NMP molecules are now located between the rotated phenyl rings as well as within the tubular pores. Examination of the estimated pore sizes in frameworks **6** and **7** yields dimensions of 9.0 Å x 10.5 Å for **6** and 4.9 Å x 10.7 Å for **7**.

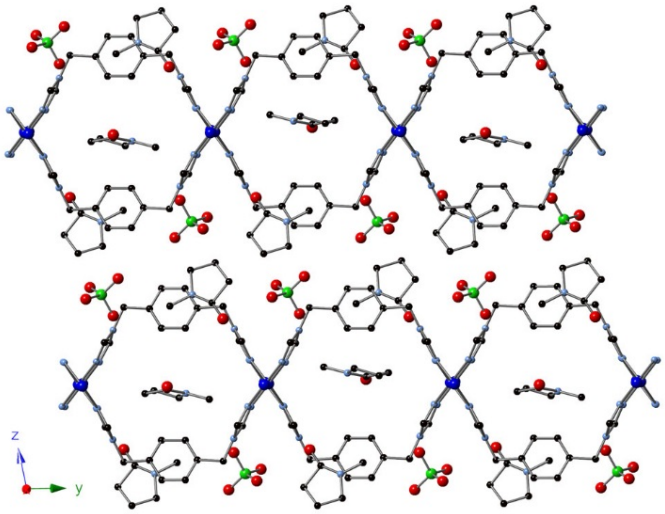


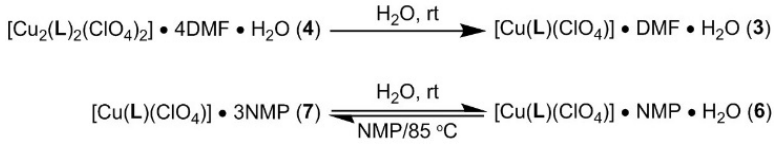
Figure 4.6. Crystal structure of [Cu(**L**)(ClO_4)] • 3NMP, **7**, viewed orthogonal to the x-axis showing the fused-tube topology.

The synthesis of **7** demonstrates that we have prepared a pair of anisotropic frameworks in which the phenyl moiety exists in two distinct

orientations while containing the *same* solvent, NMP, within the lattice. The only variation between frameworks **6** and **7** with regards to elemental composition is that **6** has one guest water molecule while **7** has two additional NMPs. Since the phenyl moiety can crystallographically exist in two distinct positions, the ability to switch the phenyl orientation as a function of solvation is clearly plausible. Nevertheless, for this pore gating effect to be practical, an in situ monitoring technique that does not rely on single crystal X-ray diffraction must be developed.

Once an assortment of isoreticular systems had been synthesized, the next step was to determine whether transitions could occur in the solid state as a function of solvation. Two pairs of frameworks and their transitions could be monitored: **4** to **3** and **7** to **6** (Scheme 4.3). The first pair features a separation of the 2D sheet layers while the second pair involves the rotation of the phenyl ring that makes up the backbone of the 1D tubular topology. Although single crystal X-ray analysis can confirm which state a breathing MOF is in for one crystal, PXRD measurements are commonly employed to investigate transformations to the bulk material.[6d, 28g, 46, 52]

Scheme 4.3. Conversion between framework states as a function of solvent.



The first pair of frameworks investigated was **3** and **4**, each of which contains different amounts of DMF in their formulas that causes expansion or contraction of the sheet layers (Scheme 4.2, Figures 4.2 and 4.3). Since **3** and **4** have distinct PXRD patterns, an experiment that monitored the dynamic transformation as a function of solvent was possible. Two PXRDs were collected on the same powder sample: an as-synthesized sample of **4** and a sample of **4** that was subsequently soaked in water for 1 h and the PXRD recollected (Figure 4.7). PXRD patterns were matched with simulated spectra to confirm phase purity before and after addition of solvent. As expected, the spacing between the 2D sheets can be monitored with PXRD.

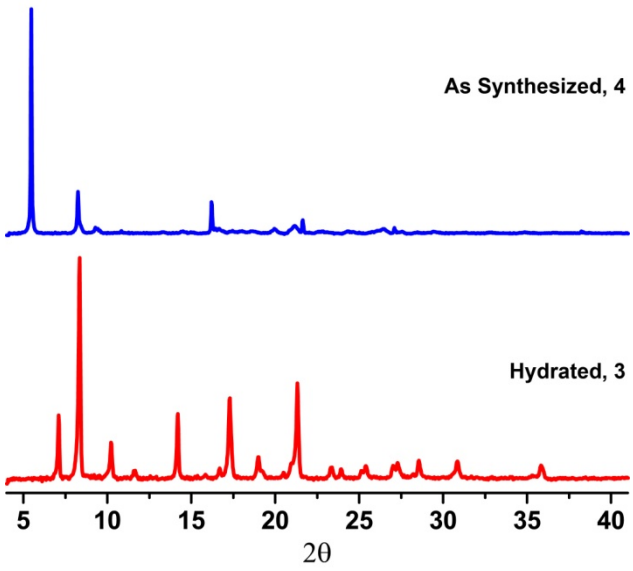


Figure 4.7. Powder pattern X-ray diffraction measurements taken for a sample of $[Cu_2(\mathbf{L})_2(ClO_4)_2] \cdot 4DMF \cdot H_2O$ (**4**) and after exposure to water for 1 h. The PXRD pattern matches **3**. Intensity was normalized for each pattern.

The ability to monitor phenyl rotation as a function of solvent with PXRD is of greater interest. Monitoring the rotation of the phenyl rings by PXRD was tested by taking three X-ray measurements: an initial sample of **7**, a hydrated sample of **7** that was first soaked in water and subsequently soaked in a water and NMP mixture, and a sample that was resoaked in pure NMP and heated to 85 °C for 8 h (Figure 4.8). PXRD measurements confirmed that the bulk material transforms from **7** to **6** and back to **7**.

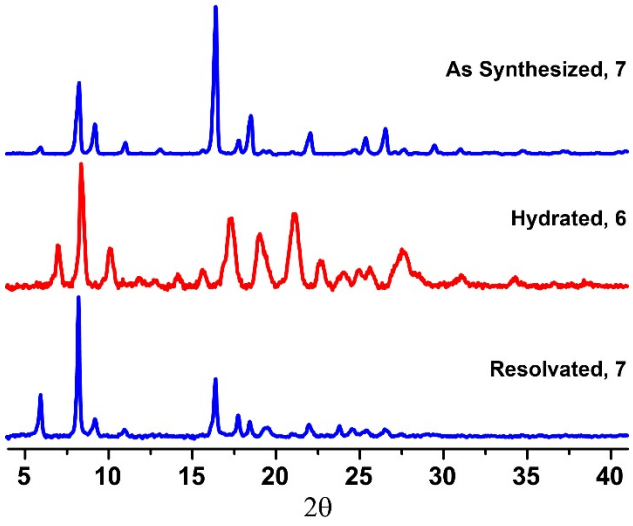


Figure 4.8. Powder pattern X-ray diffraction measurements taken for a sample of [Cu(**L**)(ClO_4)] • 3NMP (**7**), after exposure to water and NMP for 1 h, and resolvation with NMP for 8 h at 85 °C. Intensity was normalized for each pattern.

Although PXRD measurements confirm that transformations occur between the different states for these sheet MOFs, an alternative spectroscopic

technique, solid state NMR, can provide more useful information for monitoring dynamic transitions in the solid state. Solid state NMR has been used extensively to characterize MOFs,[53] and, in particular, it is a powerful tool for thev determination of rotation rates of aryl rings.[45] The rotation of aryl rings to locked positions, therefore, offers an ideal case for demonstrating the efficacy of this technique.

Nevertheless, solid state ^{13}C CP MAS NMR has rarely been employed to effectively monitor the transition between fixed positions in breathing MOFs.[54] In two instances, the twisting motions at metal-ligand "kneecaps" (and the accompanying aryl rings) on zinc MOFs have been observed as a function of guests.[54b, 54c] The resonances either shift as a function of breathing state or, more constructively, split into multiple resonances as the carbon atoms are rendered inequivalent in their new conformation. However, no ^{13}C CP MAS NMR measurements have been performed where the breathing motion occurs solely on the ligand.

Prior to collecting solid state ^{13}C CP MAS NMR of the frameworks, it is critical to assign appropriate peak positions for **2** in the solution state NMR. HSQC and HMBC spectra were collected for **2** in DMSO-d_6, along with 1D ^{1}H and ^{13}C NMR, which allowed for absolute assignments of all of the distinct carbons on the ligand (See experimental section and Figures 4.9 and 4.10). The central aryl carbons have a resonance at 128.16 ppm and the ipso carbons have

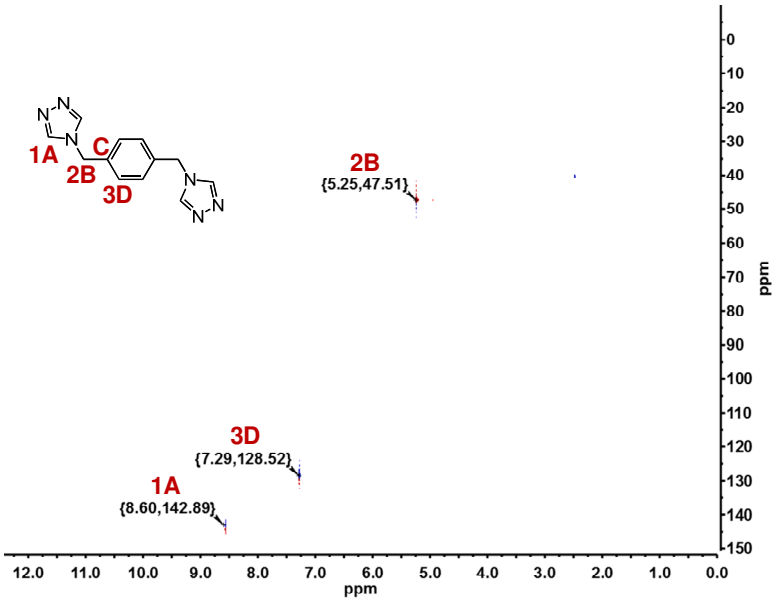


Figure 4.9. HSQC in DMSO-d_6.

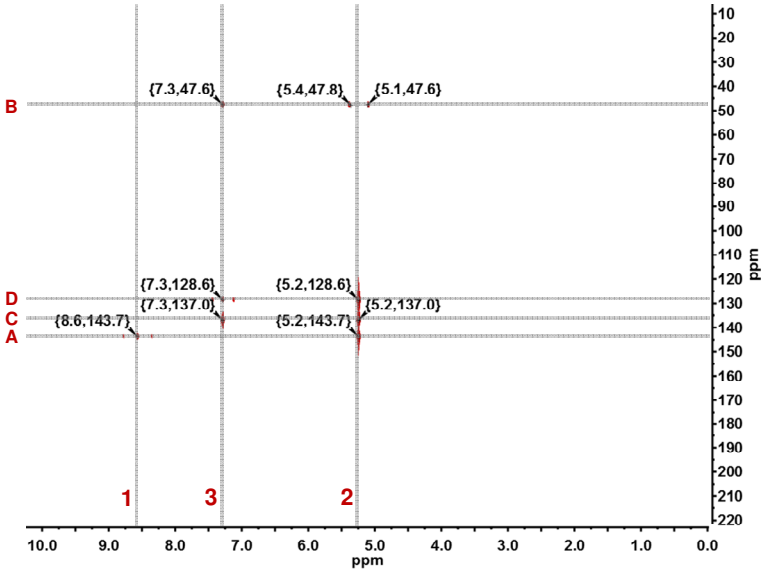


Figure 4.10. HMBC in DMSO-d_6.

a resonance at 136.54 ppm in the solution NMR. These resonances were also confirmed with a ^{13}C CP MAS NMR of **2** (Figure 4.11).

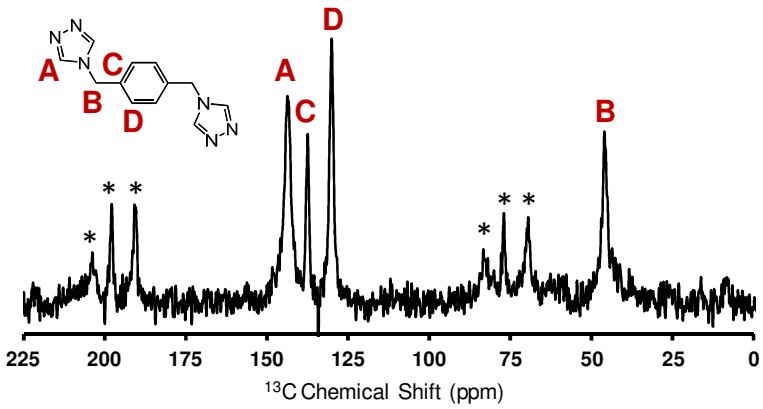


Figure 4.11. ^{13}C CP MAS NMR of ligand (* denote spinning sidebands).

Once the ^{13}C NMR spectrum of **2** was assigned, we could compare those values to the solid state ^{13}C CP MAS NMR spectra of the frameworks. A spectrum of **3**, including a portion of the structure and a blow-up of the aryl region, can be seen in Figure 4.12. The resonance at 49.3 ppm is attributed to the methylene carbon of the triazole ring, while resonances at 131.0, 132.5, 136.0, 136.6, and 144.8 ppm are assigned to the aryl carbons. Although the ligand **2** is highly symmetric in solution, the symmetry of the aryl carbons is lost in the solid state due to the different local environments of the aryl atoms. This break in symmetry is due to the solvent and anion molecules within the framework.

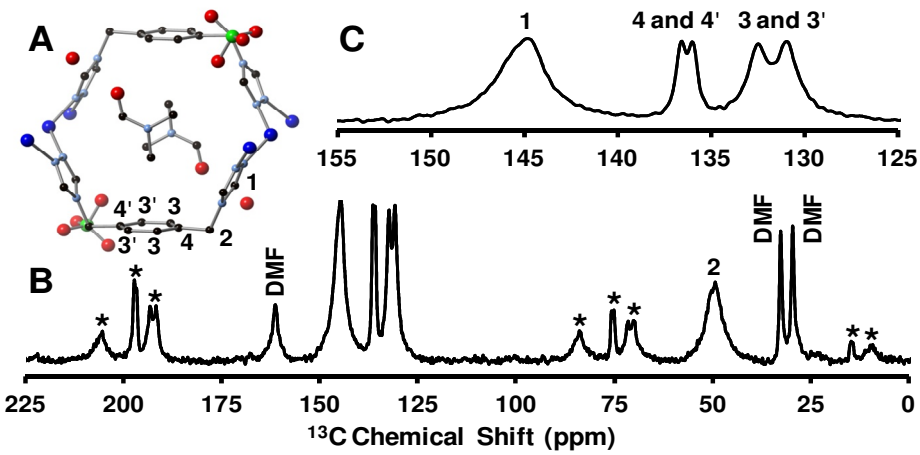


Figure 4.12. ^{13}C CP MAS NMR of [Cu(**L**)(ClO_4)] • DMF • H_2O, **3**. (A) Highlighted portion of the crystal structure of **3** with labeled carbon atoms. (B) Full solid state ^{13}C CP MAS NMR spectrum of **3**. * denote spinning sidebands. (C) Highlight of the aryl region of the spectrum of **3** with labeled peaks.

Framework solvent can also be located via NMR analysis and is a powerful tool for monitoring phase transitions as a function of solvation.[54b, 54c] The solid state ^{13}C CP MAS NMR for **3** shows three peaks for DMF (Figure 4.12). These correspond to the DMF molecules that are present in the 1D channel. A comparison of the spectrum of **3** to **4** shows that there is no significant difference on the aryl region of the spectrum, but an additional set of DMF peaks are observed at 35.5, 39.6, and 166.9 ppm (Figure 4.13). These additional resonances are due to the presence of two DMF molecules that exhibit different local environments, one contained within the pore and one between the layers.

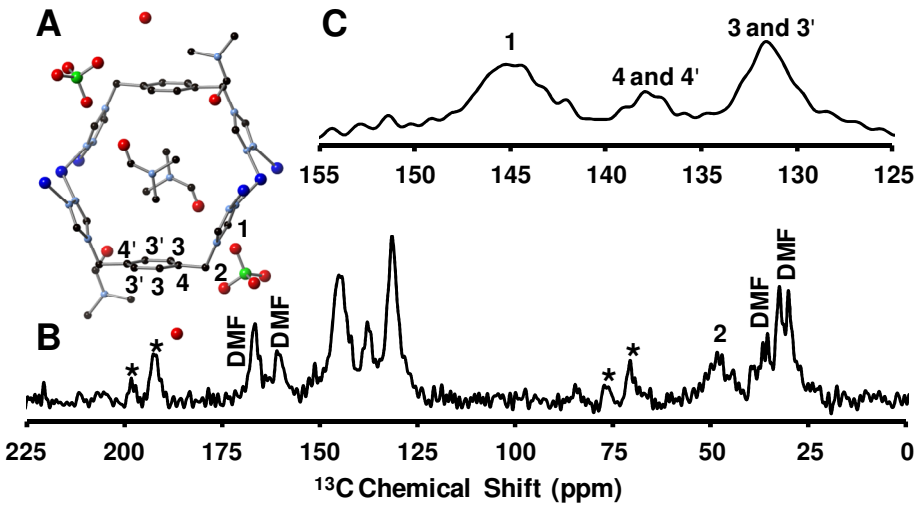


Figure 4.13. ^{13}C CP MAS NMR of $[Cu_2(\mathbf{L})_2(ClO_4)_2]$ • 4DMF • H_2O, **4**. (A) Highlighted portion of the crystal structure of **4** with labeled carbon atoms. (B) Full solid state ^{13}C CP MAS NMR spectrum of **4** collected at -75 ℃. * denote spinning sidebands. (C) Highlight of the aryl region of the spectrum of **4** with labeled peaks.

Analysis of solid state NMR for frameworks **6** and **7** allowed us to correlate peak positions with rotation of the aryl ring in the solid state. The ^{13}C CP MAS NMR of **6** is similar to **3**, with the aryl carbons yielding four peaks at 131.7, 133.4, 135.3, and 136.7 ppm due to a break in symmetry (Figure 4.14). Despite a change in solvent in the tubular pore, there is little change in peak position of the aryl ring resonances. The triazole and methylene carbons both exhibit two peaks each at 46.6 and 49.8 ppm and 145.3 and 146.9 ppm (Figure 4.14), whereas in **3**

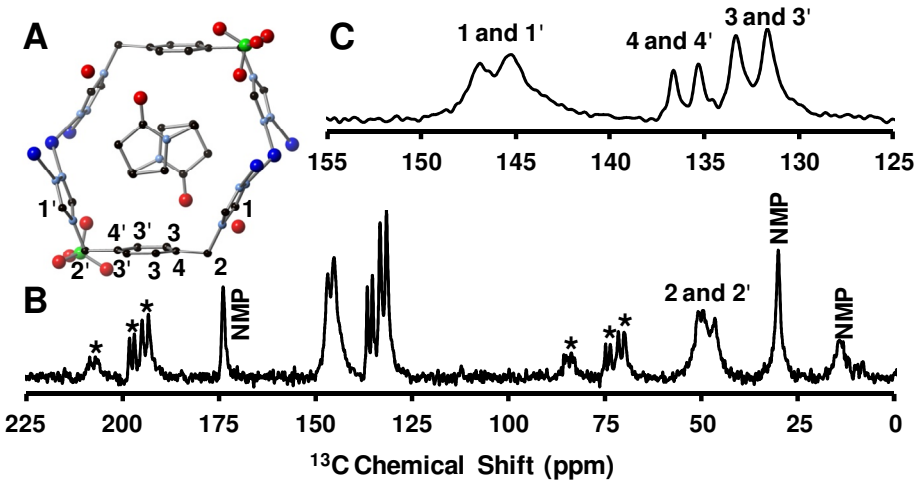


Figure 4.14. ^{13}C CP MAS NMR of [Cu(**L**)(ClO_4)] • NMP • H_2O, **6**. (A) Highlighted portion of the crystal structure of **6** with labeled carbon atoms. (B) Full solid state ^{13}C CP MAS NMR spectrum of **6**. * denote spinning sidebands. (C) Highlight of the aryl region of the spectrum of **6** with labeled peaks.

only one peak is present for each carbon. The triazole and methylene carbons exhibit two separate resonances because there is a slight tilt of the ligand from right to left (Figure 4.5), leading to each individual pore being asymmetric and, ultimately, the ligand being asymmetric.

When analyzed by ^{13}C CP MAS NMR, framework **7** exhibits a single broad peak for the methylene and triazole carbons with resonances at 49.7 and 146.6 ppm, respectively, which is in contrast to **6** (Figure 4.15). The resonances for the aryl carbons are now at 125.9 (broad), 135.9, and 137.0 ppm. The broad resonance at 125.9 ppm corresponds to the now four inequivalent “3” carbons in

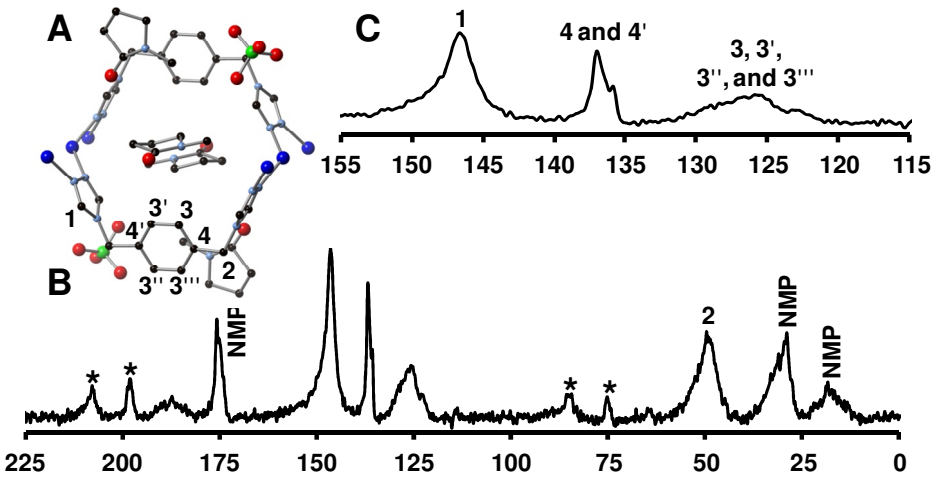


Figure 4.15. ^{13}C CP MAS NMR of [Cu(**L**)(ClO_4)] • 3NMP, **7**. (A) Highlighted portion of the crystal structure of **7** with labeled carbon atoms. (B) Full solid state ^{13}C CP MAS NMR spectrum of **7**. * denote spinning sidebands. (C) Highlight of the aryl region of the spectrum of **7** with labeled peaks.

the phenyl ring. This increased ring heterogeneity, combined with a possible increase in the chemical shift distribution, leads to this broader peak. Notably, the peaks for the 4 and 4' carbons have barely shifted between **6** and **7**. The only significant change to the solid state NMR spectrum is the resonances that correlate to the aryl carbons that moved with the framework, which demonstrates that solid state NMR can differentiate between different breathing modes for the bulk material.

In addition to evaluating the pure phase frameworks by solid state NMR, we monitored the change in frameworks as a function of solvation. A solid state ^{13}C CP MAS NMR spectrum of a sample of **4** was collected, and the sample was

then soaked in water for 1 h. The ^{13}C CP MAS NMR of hydrated **4** was collected and compared with isolated **3**. A match was obtained between the isolated **3** and hydrated **4** (Figure 4.16), which demonstrated that NMR was successful for monitoring breathing of the framework.

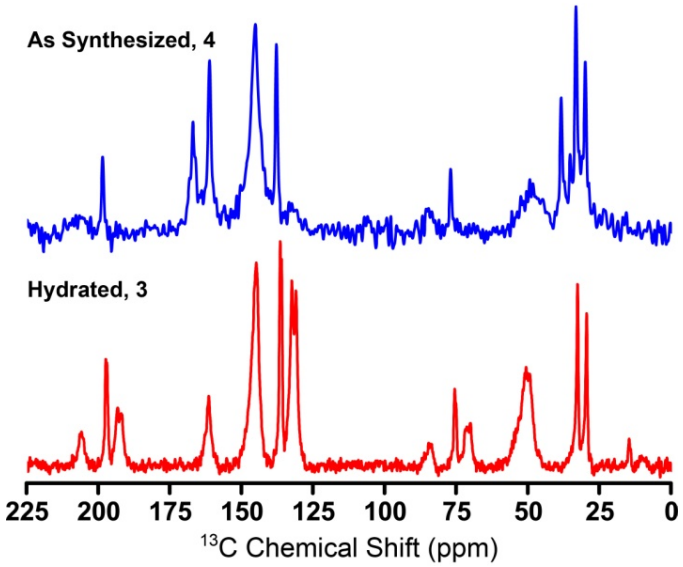


Figure 4.16. ^{13}C CP MAS NMR following the dynamic transition of $[Cu_2(\mathbf{L})_2(ClO_4)_2] \cdot 4DMF \cdot H_2O$ (**4**) to $[Cu(\mathbf{L})(ClO_4)] \cdot DMF \cdot H_2O$ (**3**) upon hydration.

To monitor aryl rotation between **7** and **6**, a solid state ^{13}C CP MAS NMR of a freshly prepared sample of **7**, which had been verified by PXRD, was collected. The sample was subsequently soaked in water for 1 h, and the NMR was again collected (Figure 4.17). When hydrated **7** is compared to a ^{13}C CP MAS NMR of pure **6**, the spectrum was found to be identical. The same sample

of hydrated **7** (i.e. **6**) was therefore soaked in NMP in an attempt to reproduce framework **7**. Although soaking in NMP under ambient conditions did not reproduce **7**, heating the sample at 85 °C for 8 h resulted in an NMR that was a direct match with the as-synthesized framework **7** (Figure 4.17). These experiments demonstrate that ^{13}C CP MAS NMR is an effective technique to monitor framework breathing in the solid state.

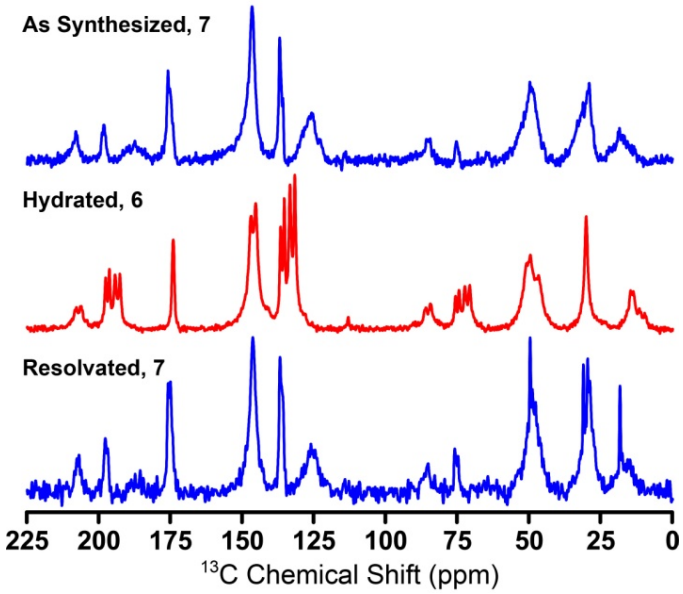


Figure 4.17. ^{13}C CP MAS NMR spectrum of [Cu(**L**)(ClO_4)] • 3NMP (**7**), after exposure to water for 1 h, and resolvation with NMP for 8 h at 85 °C.

Conclusion for Gate Switching Breathing: Rotating Phenyl Rings

A series of two-dimensional MOFs that display a topology of fused 1D metal-organic nanotubes was synthesized, and the frameworks undergo two

different transformations in the solid state as a function of solvation. A semi-rigid di-1,2,4-triazole ligand connects one-dimensional copper chains through a *syn* conformation to form a tubular architecture. The phenyl rings between the 1,2,4-triazoles are either parallel or perpendicular to the tube. The first transformation involves the 2D sheet layers expanding or contracting as a function of DMF concentration. More notably, DMA and NMP cause the phenyl ring to rotate perpendicular to the tube orientation. All of these framework transformations were initially determined by single crystal X-ray diffraction and powder X-ray diffraction. Since the breathing mode of phenyl rotation is solely ligand based, we believed that solid state ^{13}C CP MAS NMR would be a powerful tool to elucidate this switching mechanism between the parallel and perpendicular modes of the phenyl ring. Unlike PXRD, solid state ^{13}C CP MAS NMR could directly monitor phenyl rotation as a function of solvation, demonstrating that this is an effective approach for monitoring changes to a breathing framework that occur solely through "gate" switching of the ligand.

Experimental for Gate Switching Breathing: Rotating Phenyl Rings

The compound 1,2,4-triazole-1-propanenitrile[23] was prepared as described previously. All other reagents were purchased from commercial vendors and used without purification. ^{1}H and $^{13}C\{^{1}H\}$ NMR spectra were recorded at ambient temperature on a Varian Mercury 300 MHz or a Varian VNMRS 500 MHz narrow-bore broadband system. ^{1}H and ^{13}C NMR chemical

shifts were referenced to the residual solvent. Solid ^{13}C CP MAS NMR samples were recorded on a Varian Inova 400 MHz spectrometer and referenced to an external adamantane sample. All mass spectrometry analyses were conducted at the Mass Spectrometry Center located in the Department of Chemistry at the University of Tennessee. The DART analyses were performed using a JEOL AccuTOF-D time-of-flight (TOF) mass spectrometer with a DART (direct analysis in real time) ionization source from JEOL USA, Inc. (Peabody, MA). The ESI/MS analyses were performed using a QSTAR Elite quadrupole time-of-flight (QTOF) mass spectrometer with an electrospray ionization source from AB Sciex (Concord, Ontario, Canada). Infrared spectra were collected on a Thermo Scientific Nicolet iS10 with a Smart iTR accessory for attenuated total reflectance. Thermogravametric analysis data were collected on a TA Instruments TGA Q50 under N_2. Carbon, hydrogen, and nitrogen analyses were obtained from Atlantic Microlab, Norcross, GA.

Synthesis of 4,4'-[1,4-(xylene)diyl]bis-(1-(2-cyanoethyl)-1,2,4-triazolium) dibromide, 1. 1,4-bis(bromomethyl)-benzene (10.0 g, 0.0378 mol) and 1,2,4-triazole-1-propanenitrile (20.0 g, 0.164 mol) were added to a 100 mL round bottom flask and diluted with acetonitrile (35 mL). The reaction was heated to reflux until a white precipitate had formed after 1 h. The reaction was cooled to rt and diethyl ether (35 mL) was added to the reaction mixture, followed by drying under reduced pressure. The crude solid product was washed with acetonitrile (3 x 30 mL) and dried under reduced pressure to yield the pure product (18.0 g,

93.8% yield). ^{1}H NMR (DMSO-d_6, 499.72 MHz): δ 10.46 (s, 2H), 9.49 (s, 2H), 7.60 (s, 4H), 5.65 (s, 4H), 4.74 (t, J = 6.5 Hz, 4H), 3.25 (t, J = 6.5 Hz, 4H). ^{13}C{^{1}H} NMR (DMSO-d_6, 125.66 MHz): δ 144.90, 143.37, 134.31, 129.47, 117.66, 50.04, 47.25, 17.30. IR (neat): 3102, 3019, 2980, 2254, 1820, 1584, 1517, 1442, 1419, 1395, 1381, 1366, 1339, 1315, 1285, 1226, 1195, 1145, 1069, 1043, 1024, 980, 916, 879, 833, 782, 739, 672 cm^{-1}. ESI/MS (m/z): [M-Br]$^{+}$ 427.05, [M-2Br]$^{2+}$ 174.07. Anal. Calcd for $C_{18}H_{20}Br_2N_8$: C, 42.54; H, 3.97; N, 22.05. Found: C, 42.75; H, 3.88; N, 21.88.

Synthesis of 4,4′-(1,4-(xylene)diyl)bis(1,2,4-triazole), L, 2. Potassium hydroxide (7.96 g, 0.142 mol) and **1** (18.0 g, 0.0355 mol) were added to a 500 mL Erlenmeyer flask containing 200 mL of water. After 2 h, the product precipitated from solution as a white powder and was filtered and washed with water (3 x 50 mL) and acetonitrile (3 x 50 mL). The pure product was dried under reduced pressure to yield 7.52 g (83.7 % yield). ^{1}H NMR (DMSO-d_6, 499.72 MHz): δ 8.59 (s, 4H), 7.30 (s, 4H), 5.26 (s, 4H). ^{13}C{^{1}H} NMR (DMSO-d_6, 125.66 MHz): δ 143.21, 136.54, 128.16, 47.14. IR (neat): 3130, 3117, 2994, 1672, 1532, 1513, 1458, 1434, 1420, 1381, 1362, 1344, 1278, 1218, 1207, 1179, 1122, 1075, 1015, 985, 963, 859, 817, 760, 739, 708, 681 cm^{-1}. Anal. Calcd for $C_{12}H_{12}N_6$: C, 59.99; H, 5.03; N, 34.98. Found: C, 60.13; H, 5.10; N, 34.86.

Synthesis of [Cu(L)(ClO_4)] • DMF • H_2O, 3. Copper(II) perchlorate hexahydrate (0.0272 g, 0.0735 mmol) and **L** (0.0177 g, 0.0735 mmol) were added to separate 4 mL scintillation vials and dissolved in 1 mL of water and 2 mL of DMF,

respectively. The vials were heated to 85 °C for 30 min in an aluminum heating block, followed by mixing of the solutions and additional heating. After heating for 24 h, colorless needles formed and were isolated and washed with water and acetone to yield the pure product (12.5 mg, 34.4 % yield). IR (neat): 3617, 3123, 1980, 1672, 1601, 1543, 1499, 1476, 1455, 1432, 1382, 1336, 1254, 1213, 1192, 1170, 1088, 1004, 961, 931, 885, 860, 835, 811, 752, 718, 680, 656 cm^{-1}. Anal. Calcd for $C_{12}H_{12}ClCuN_6O_4$•DMF•H_2O: C, 36.44; H, 4.28; N, 19.83. Found: C, 37.42; H, 4.12; N, 20.37.

Synthesis of $[Cu_2(L)_2(ClO_4)_2]$ • 4DMF • H_2O, 4. Copper(II) perchlorate hexahydrate (0.0545 g, 0.147 mmol) and **L** (0.0177 g, 0.0735 mmol) were added to separate 4 mL scintillation vials and dissolved in 1 and 2 mL of DMF, respectively. The vials were heated to 85 °C for 1 h in an aluminum heating block, followed by mixing of the solutions and additional heating. After heating for 36 h, colorless needles formed and were isolated and washed with DMF and acetone to yield the pure product (34.0 mg, 41.4 % yield). IR (neat): 3124, 2920, 1673, 1544, 1458, 1382, 1336, 1255, 1211, 1191, 1171, 1087, 1005, 963, 931, 884, 836, 811, 753, 719, 681, 657. Anal. Calcd for $C_{24}H_{24}Cl_2Cu_2N_{12}O_8$•4DMF•$H_2O$: C, 38.71; H, 4.87; N, 20.06. Found: C, 37.98; H, 4.41; N, 20.02.

Synthesis of $[Cu(L)(ClO_4)]$ • DMA • H_2O, 5. Copper(II) perchlorate hexahydrate (0.136 g, 0.368 mmol) and **L** (0.0177 g, 0.0735 mmol) were added to separate 4 mL scintillation vials and dissolved in 1 mL of water and 2 mL of DMA,

respectively. The vials were heated to 85 °C for 1 h in an aluminum heating block, followed by mixing of the solutions and additional heating. After heating for 2 weeks, colorless needles formed that could not be isolated in bulk.

Synthesis of $[Cu(L)(ClO_4)] \cdot NMP \cdot H_2O$, 6. Copper(II) perchlorate hexahydrate (0.136 g, 0.368 mmol) and **L** (0.0177 g, 0.0735 mmol) were added to separate 4 mL scintillation vials and dissolved in 1 mL of water and 2 mL of NMP, respectively. The vials were heated to 85 °C for 30 min in an aluminum heating block, followed by mixing of the solutions and additional heating. After heating for 2 weeks, colorless needles formed and were isolated and washed with water and acetone to yield the pure product (26.4 mg, 68.9 % yield). IR (neat): 3597, 3117, 1681, 1624, 1541, 1500, 1452, 1423, 1404, 1332, 1295, 1262, 1210, 1191, 1170, 1089, 1069, 1000, 960, 931, 895, 834, 811, 748, 717, 680, 651 cm^{-1}. Anal. Calcd for $C_{12}H_{12}ClCuN_6O_4 \cdot NMP \cdot H_2O$: C, 39.24; H, 4.45; N, 18.84. Found: C, 38.85; H, 3.94; N, 19.33.

Synthesis of $[Cu_2(L)_2(ClO_4)_2] \cdot 3NMP$, 7. Copper(II) perchlorate hexahydrate (0.0136 g, 0.0367 mmol) and **L** (0.0177 g, 0.0735 mmol) were added to separate 4 mL scintillation vials and dissolved in 1 and 2 mL of NMP, respectively. The vials were heated to 85 °C for 30 min in an aluminum heating block, followed by mixing of the solutions and additional heating. After heating for 3 d, colorless needles formed and were isolated and washed with NMP and acetone to yield the pure product (8.80 mg, 19.9 % yield). IR (neat): 3596, 3117, 1680, 1624, 1540, 1501, 1452, 1423, 1405, 1391, 1367, 1331, 1295, 1261, 1209, 1193, 1170,

1119, 1091, 1069, 1000, 960, 931, 895, 833, 811, 749, 717, 679 cm^{-1}. Anal. Calcd for $C_{39}H_{51}Cl_2Cu_2N_{15}O_{11}$•3NMP: C, 42.43; H, 4.66; N, 19.03. Found: C, 42.34; H, 4.86; N, 18.65.

X-ray Structure Determinations. Data was collected on a Bruker SMART APEXII three circle diffractometer equipped with a CCD area detector and operated at 1,800 W power (45 kV, 40 mA) to generate Mo Kα radiation (λ = 0.71073 Å). The incident X-ray beam was focused and monochromated using Bruker Excalibur focusing optics. Single crystals were mounted on nylon CryoLoops (Hampton Research) with Paratone-N (Hampton Research) and frozen at -100 ºC and -173 ºC, respectively. Initial scans of each specimen were taken to obtain preliminary unit cell parameters and to assess the mosaicity (i.e. breadth of spots between frames) of the crystal to select the required frame width for data collection. For all cases frame widths of 0.5º were judged to be appropriate and full hemispheres of data were collected using the *Bruker APEX2* software suite to carry out overlapping ϕ and ω scans at detector setting of 2θ = 28°. Following data collection, reflections were sampled from all regions of the Ewald sphere to re-determine unit cell parameters for data integration. Following exhaustive review of collected frames the resolution of the dataset was judged, and, if necessary, regions of the frames where no coherent scattering was observed were removed from consideration for data integration using the *Bruker SAINTplus* program.[26] Data was integrated using a narrow frame algorithm and was subsequently corrected for absorption. Absorption corrections were

performed for both samples using the SADABS program.[26] Space group determination and tests for merohedral twinning were carried out using *XPREP*.[26] In all cases, the highest possible space group was chosen.

Final models were refined anisotropically (with the exception of H atoms). In the case of **3** and **4**, hydrogen atoms were not located on water molecules due to the poor crystallinity. In the case of **7**, poorer diffraction data prevented the anisotropic refinement of all solvent atoms. Additionally, one NMP molecule (within the voids) was refined using half occupancy due to disorder which led to the satisfactory refinement using anisotropic treatment. All structures were examined using the *Addsym* subroutine of PLATON[27] to assure that no additional symmetry could be applied to the models.

Powder X-ray experiments. Powder X-ray diffraction (PXRD) data was collected using a Panalytical Empyrean θ-2θ diffractometer in reflectance Bragg-Brentano geometry. Cu-Kα radiation (λ = 1.5406 Å; 1,800 W, 45 kV, 40 mA) was focused using a planar Gobel Mirror riding the Kα line. A 0.25 mm divergence slit was used for all measurements. Diffracted radiation was detected using a PIXcel^{3d} detector [(6° 2θ sampling width) equipped with a Ni monochrometer]. All samples were mounted onto a zero background quartz plate fixed on a sample holder by dropping powders and then leveling the sample surface. The best counting statistics were achieved by using a 0.0394º 2θ step scan from 3 – 50° with an exposure time of 119.85 s per step and a revolution spin rate of 4 s.

Solid-State NMR. All spectra were recorded on a Varian INOVA 400 MHz NMR operating at Lamor frequencies of 100.54 MHz for ^{13}C. A Chemagnetic and DOTY CP MAS NMR probe were used with a 5 mm rotor and a spin rate of 6 kHz. In all ^{13}C experiments, spectra were referenced to adamantane peaks at 38.68 and 29.6 ppm. A collection at -75 °C using the Chemagnetics CP MAS NMR probe was required for **4**, potentially due to molecular motion which occurred at the frequency corresponding to the decoupling field strength. All other measurements were carried out under ambient conditions.

Monitoring the transition from 4 to 3 using PXRD. **4** was synthesized according to the above method and a PXRD was collected to ensure purity. The sample was then soaked in 2 mL of water for 1 h. After soaking in water for 1 h, a PXRD was again collected and matched the PXRD for **3** which can be seen in Figure 7.

Monitoring the transition from 7 to 6 using PXRD. **7** was synthesized according to the above method and a PXRD was collected to ensure purity. The sample was soaked in 2 mL of water for 30 min, followed by soaking in 2 ml of a 2:1 mixture of NMP and water for 2 h. After soaking for 2 h, a PXRD was again collected and matched the PXRD for isolated **6**. Finally, the sample was collected and soaked in 2 mL NMP for 8 h at 85 °C. The PXRD collected confirmed the formation of **7** as seen in Figure 8. Attempts at reforming **7** under ambient conditions were unsuccessful, and heat was required for the process to occur.

Monitoring the transition from 4 to 3 using ^{13}C CP MAS NMR. **4** was synthesized according to the above method and a PXRD was collected to ensure purity. A ^{13}C CP MAS NMR was collected on the sample, followed by soaking the recollected sample in 2 mL of H_2O for 1 h. After soaking in H_2O for water, a PXRD was again collected and matched the PXRD for **3**. The collection of another ^{13}C CP MAS NMR on the hydrated **4** confirmed the transition from **4** to **3** upon soaking in water, which can be seen in Figure S16.

Monitoring the transition from 7 to 6 using ^{13}C CP MAS NMR. **7** was synthesized according to the above method and a PXRD was collected to ensure purity. A ^{13}C CP MAS NMR was collected on the sample, followed by soaking the recollected sample in 2 mL of H_2O for 1 h. After soaking, a ^{13}C CP MAS NMR was collected on the hydrated **7** and confirmed the transition from **7** to **6** upon soaking in water, which can be seen in Figure 12. The sample of hydrated **7**(**6**) was collected and soaked in 2 mL of NMP. The sample was subsequently heated to 85 °C for 8 h and a final ^{13}C CP MAS NMR was collected on the sample, confirming the formation of **7**.

Introduction for Isoreticular Synthesis

Metal-Organic Frameworks (MOFs) are a class of porous materials currently under rigorous investigation due to their large surface areas and ability to adsorb a multitude of guests within their crystalline lattice.[1a, 1c-e] The high degree of tunability within MOFs has led to a plethora of highly stable, porous frameworks with applications ranging from gas and liquid separations to catalysis

to luminescence.[3a, 3c-h, 14a, 55] As the apertures in MOFs dictate the transport and storage properties of the material, methods aimed at logical design are therefore a must for advancement in the selective sorption of guests.[2a, 2d, 5] One concept of logical design, the use of reticular synthesis in MOFs, has allowed the prediction of final structures as a function of varying organic linker.[2b-d] However, with emerging classes of MOFs such as breathing MOFs which stray from the traditional secondary building units (SBUs), additional reticular synthesis techniques are in dire need.[6a, 6b, 7e, 8]

The use of reticular synthesis in MOFs has focused primarily on the use of rigid organic ligands comprised of multiple carboxylate functionalities. The employment of carboxylates locks metal ions into directional clusters through a chelate effect, allowing for points of extension to define predictable geometric shapes, or secondary building units (SBUs). The establishment of reaction conditions which favor the *in situ* formation of specific SBUs requires advanced organic methods as the geometry of the linker will play an important role in the dimensionality obtained.[2a, 2d] Once favorable reaction conditions are determined, linkers containing the same shape but varying lengths can be employed to create a series of isoreticular frameworks.[2b, 2c]

While architectural design in MOFs has made great advances in recent years, examples in which the resulting framework is a variant of the designed topology are continuously emerging. The limit of the isoreticular principle was recently investigated by Férey who introduced small flexible endings to the

periphery of a previously employed tritopic ligand for MOF synthesis.[56] The introduction of flexibility to the shell of the ligand in MIL-112 resulted in vast structural changes as compared to MIL-103 which possessed the original rigid ligand. Although both MOFs have close formulation, the free rotation due to methylene groups in MIL-112 no longer forces a strict C_3 symmetry and allows other lower energy configurations to exist.[56]

As Férey's work provides an example for the limits of reticular synthesis, our group has been focusing on the use of similar semi-rigid ligands for MOF preparation in hopes of overcoming these limitations. Recent results have demonstrated that incorporation of a semi-rigid di-1,2,4-triazole containing a central phenyl moiety leads to the formation of a multitude of copper MOFs (Figure 4.18).[11c] Under a variety of reaction conditions, a series of 2D MOFs comprised of rigid 1D metal fragments bridged by *syn* conformed di-triazoles were obtained.[11c] In order to test the reticular synthesis of MOFs containing semi-rigid di-triazoles, ligands with extended naphthyl and biphenyl central moieties were synthesized. Utilizing similar reaction conditions, frameworks with the same *syn* conformed topology were obtained, revealing that judicious choice of semi-rigid ligands can in fact lead to the synthesis of isoreticular frameworks.

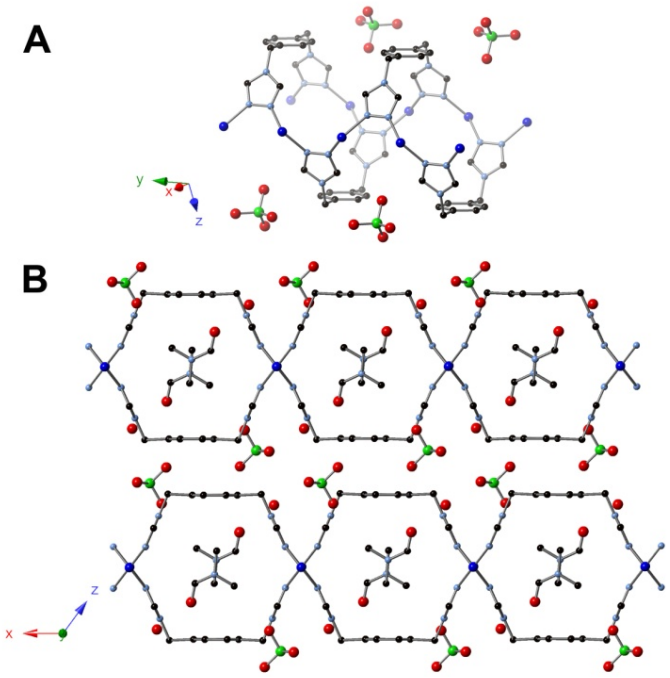


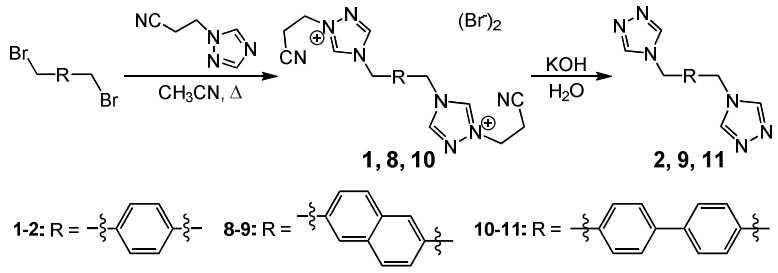
Figure 4.18. X-ray structure of [Cu(**L**)(ClO_4)] • DMF • H_2O, **3**. (A) Crystal structure of **3** showing copper chains along the y-axis. (B) Crystal structure of **3** viewed orthogonal to the y-axis showing the fused-tube topology.

Results and Discussion for Isoreticular Synthesis

We have previously reported the synthesis of 4,4′-(1,4-(xylene)diyl)bis(1,2,4-triazole), a di-1,2,4-triazole ligand containing a central xylene moiety.[11c] By following the method of Horváth,[23] the final di-triazole can be obtained in two steps: addition of 1,2,4-triazole-1-propanenitrile to 1,4-bis(bromomethyl)benzene leads to the formation of intermediate **1**, followed by cleavage of the propanenitrile group with potassium hydroxide to yield the final product **2**. A generalized reaction for di-triazole synthesis can be seen in

Scheme 4.4. This generalized scheme can be utilized to form extended linkers, of which a central naphthyl and biphenyl moiety were selected. By selecting linkers which contain larger core moieties, a systematic illustration of the effect of ligand size on framework synthesis can be studied. By following the method of Horváth, naphthyl and biphenyl intermediates **8** and **10** were synthesized with yields of 70 and 84%, respectively. Cleavage of the dinitrile groups with potassium hydroxide results in formation of **9** and **11** with respective yields of 94% and 86% (Scheme 4.4).

Scheme 4.4. General synthesis of di-triazole ligands.



Previously published results with the semi-rigid linker 4,4′-(1,4-(xylene)diyl)bis(1,2,4-triazole) demonstrated that it is possible to prepare copper MOFs as a function of varying reaction conditions including solvent and metal to ligand ratio.[11c] A key feature of the MOFs synthesized through the use of the semi-rigid ligand **2** is the ability to obtain an identical topology under various reaction conditions. Single crystal X-ray diffraction revealed that for all solvents studied, the 2D frameworks maintain an overall topology resembling a set of

fused 1D metal-organic nanotubes (MONTs). Tetrahedral Cu(I) centers are formed by coordination to four triazole ligands, and a linear chain results as adjacent copper atoms are bridged by two triazoles to form an equatorial plane. Importantly, the neighboring copper chains are linked to form 1D tubes as a result of the ligand adopting a *syn* geometry with anions packing between the 2D layers. Therefore, the frameworks are anisotropic with the size of the 1D tubes being controlled by the semi-rigid ligand employed.[11c] With the aim of increasing tube size as a function of ligand, replacing ligand **2** with extended linkers **L2** (**9**) and **L3** (**11**) would allow for the synthesis of a series of frameworks if the di-triazoles maintain a *syn* conformation.

To test the reaction space of the newly synthesized extended ligands, ligand **L2** (**9**) with a central naphthyl moiety was first subjected to a variety of reaction conditions. The addition of two equivalents of **L2** and one equivalent of copper perchlorate to a mixture of N,N-dimethylacetamide (DMA) and water led to the formation of [Cu(**L2**)(ClO_4)] • DMA • H_2O (**12**). Heating the reaction mixture at 85 ℃ for 24 h leads to colorless crystals suitable for X-ray diffraction. Single crystal X-ray diffraction shows, in fact, that a similar topology is obtained using the di-triazole containing a central naphthyl moiety (Figure 4.19). Tetrahedral Cu(I) centers are linked in an alternating manner by di-triazole ligands which adopt a *syn* conformation (Figure 4.19A), leading to formation of a 2D framework composed of 1D anisotropic pores (Figure 4.19B). Guest DMA

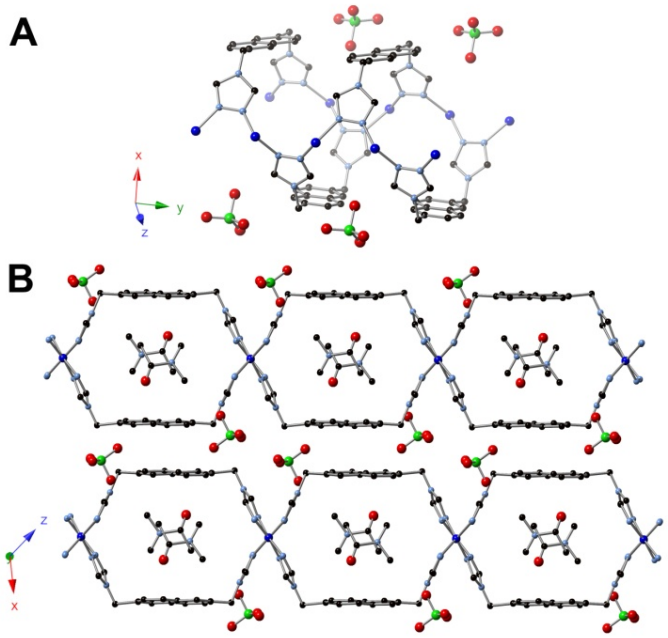


Figure 4.19. X-ray structure of [Cu(**L2**)(ClO_4)] • DMA • H_2O, **12**. (A) Crystal structure of **12** showing copper chains along the y-axis. (B) Crystal structure of **12** viewed orthogonal to the y-axis showing the fused-tube topology.

molecules are located within the pores, and perchlorate anions are within the sheet layers. As the size of the *syn*-conformed ligand controls the size of the pores, an increase in the pore volume was expected upon increasing ligand size. A comparison of channel dimensions reveals an increase in width with pore sizes increasing from 8.9 x 11.0 Å when using a central phenyl moiety to 8.9 x 12.9 Å in **12**. Therefore, as expected, only the width of the pore increased as the length of the central moiety of the ligand increased from phenyl to naphthyl.

With a similar fused-MONT topology being obtained through the use of a naphthyl moiety, the next step in obtaining a series of isoreticular frameworks is

to examine the reaction space of **L3** (**11**) containing a biphenyl moiety. In a similar manner to synthesis of **12**, addition of two equivalents of **L3** and one equivalent of copper perchlorate to a mixture of N,N-diethylformamide (DEF) and water leads to the formation of [Cu(**L3**)(ClO_4)] • DEF (**13**). Single crystals of **13** suitable for X-ray analysis are obtained after heating at 85 ℃ for 24 h. X-ray diffraction studies revealed an identical topology using the extended ligand **L3**, allowing for a series of isoreticular frameworks to be synthesized. Tetrahedral Cu(I) centers (Figure 4.20A) linked by *syn*-conformed **L3** results in a 2D

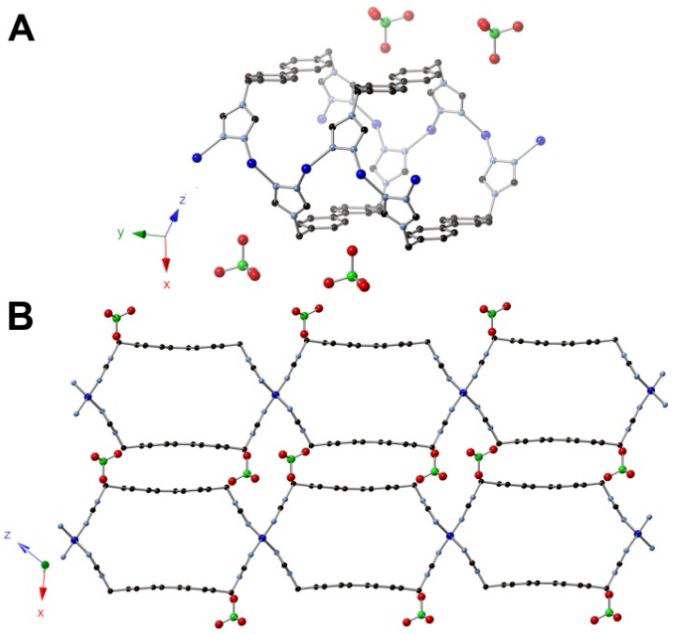


Figure 4.20. X-ray structure of [Cu(**L3**)(ClO_4)] • DEF, **13**. (A) Crystal structure of **13** showing copper chains along the y-axis. (B) Crystal structure of **13** viewed orthogonal to the y-axis showing the fused-tube topology.

framework with 1D anisotropic pores (Figure 4.20B). Channel dimensions reveal a pore size of 8.9 x 15.5 Å for **13**, an increase from 8.9 x 12.9 Å in **12**. Guest DEF molecules fill the tubular pores while anions are located between the sheets.

By increasing the central core of the di-triazole ligand from phenyl to naphthyl to biphenyl, a systematic increase in the pore size was observed for each resulting MOF. More specifically, adjusting the central moiety within the di-triazole allows for adjustment of the width of the pore. The pore width was increased from 11.0 Å when using **L1** to 12.9 Å in **12** using **L2**, and finally 15.5 Å in **12** using **L3**. Therefore, through judicious ligand choice, the pore size can be controlled in a precise manner and can increase in width by more than 4 Å!

In addition to single crystal X-ray diffraction, all MOFs synthesized were characterized by PXRD analysis. PXRD provides a characterization method for bulk analysis[2c, 6d, 9d] and all MOF PXRDs were compared to simulated data obtained from the crystal structure. PXRD, combined with elemental analysis and TGA, provided full compositional characterization of the isoreticular frameworks.

Conclusion for Isoreticular Synthesis

Through the use of semi-rigid di-triazoles, a series of isoreticular frameworks was synthesized. Di-triazoles containing central phenyl, naphthyl, and biphenyl moieties were synthesized and employed in framework synthesis to study the effect of central moiety on MOF pore size. In all cases, the semi-rigid

ligand adopts a *syn* conformation to bridge rigid metal fragments, leading to the formation of a 2D sheet which resembles a set of fused MONTs. Solvent molecules lie within the voids of the frameworks while anions are located between the sheet layers. As all frameworks synthesized reveal identical topologies, increasing the central moiety from phenyl to biphenyl resulted in an increase in the width of the pore by 4.5 Å. The height of the pores remains constant as only the central portion of the bridging ligand is varied. The preferred binding by the di-triazoles has allowed, to our knowledge, for the first study of reticular synthesis in a non-rigid system. The ability to engineer MOFs with flexible linkers opens up a new door of possibilities for the rational synthesis and applications of flexible frameworks. Future studies will focus on the study of gas adsorption as a function of semi-rigid linker employed. The ability to tailor the pore size will allow for the fine-tuning of sorption properties for both storage and selectivity.

Experimental for Isoreticular Synthesis

The compound 1,2,4-triazole-1-propanenitrile[23], ligands **1** and **2**[11c], as well as framework **3**[11c], were prepared as described previously. All other reagents were purchased from commercial vendors and used without purification. ^{1}H and $^{13}C\{^{1}H\}$ NMR spectra were recorded at ambient temperature on a Varian Mercury 300 MHz or a Varian VNMRS 500 MHz narrow-bore broadband system. ^{1}H and 13C NMR chemical shifts were referenced to the residual solvent. Solid 13C CP MAS NMR samples were recorded on a Varian Inova 400 MHz spectrometer and

referenced to an external adamantane sample. All mass spectrometry analyses were conducted at the Mass Spectrometry Center located in the Department of Chemistry at the University of Tennessee. The ESI/MS analyses were performed using a QSTAR Elite quadrupole time-of-flight (QTOF) mass spectrometer with an electrospray ionization source from AB Sciex (Concord, Ontario, Canada). Infrared spectra were collected on a Thermo Scientific Nicolet iS10 with a Smart iTR accessory for attenuated total reflectance. Thermogravametric analysis data were collected on a TA Instruments TGA Q50 under N_2. Carbon, hydrogen, and nitrogen analyses were obtained from Atlantic Microlab, Norcross, GA.

Synthesis of 4,4'-[naphthalene-2,6-diylbis(methylene)]bis-(1-(2-cyanoethyl)-1,2,4-triazolium) dibromide, 8. 2,6-bis(bromomethyl)naphthalene (2.00 g, 0.00635 mol) and 1,2,4-triazole-1-propanenitrile (1.56 g, 0.0128 mol) were added to a 100 mL round bottom flask and diluted with acetonitrile (40 mL). The reaction was subsequently heated to reflux for 24 h. The reaction was cooled to rt and the crude solid product was washed with acetonitrile (3 x 30 mL) and dried under reduced pressure. The crude product was again added to a 100 mL round bottom flask along with an additional quantity of 1,2,4-triazole-1-propanenitrile (1.56 g, 0.0128 mol) and diluted with 40 mL of acetonitrile. The reaction was again heated to reflux for 24 h, and this process of reflux followed by washing was repeated an additional third time to ensure completion of the reaction. After the third reflux, the reaction was cooled to rt and diethyl ether (35 mL) was added

to the reaction mixture, followed by drying under reduced pressure. The crude solid product was washed with acetonitrile (3 x 30 mL) and dried under reduced pressure to yield the pure product (2.51 g, 70.2% yield). ^{1}H NMR (DMSO-d_6, 499.72 MHz): δ 10.44 (s, 2H), 9.52 (s, 2H), 8.08 (s, 2H), 8.02 (d, J = 8.4 Hz, 2H), 7.68 (d, J = 8.4 Hz, 2H), 5.80 (s, 4H), 4.75 (t, J = 6.3 Hz, 4H), 3.25 (t, J = 6.3 Hz, 4H). ^{13}C{^{1}H} NMR (DMSO-d_6, 125.66 MHz): δ 145.08, 143.50, 132.55, 131.98, 129.00, 127.93, 126.73, 117.70, 50.63, 47.26, 17.34. IR (neat): 3097, 3018, 2977, 2256, 1822, 1580, 1518, 1441, 1419, 1381, 1339, 1317, 1290, 1258, 1230, 1182, 1166, 1139, 1067, 1043, 1023, 979, 918, 840, 766, 718, 676 cm^{-1}. ESI/MS (m/z): [M-Br]$^{+}$ 477.11, [M-2Br]$^{2+}$ 199.10. Anal. Calcd for $C_{22}H_{22}Br_2N_8$: C, 47.33; H, 3.97; N, 20.07. Found: C, 47.36; H, 3.92; N, 19.97.

Synthesis of 4,4'-[4,4'-bitolyl]bis-(1-(2-cyanoethyl)-1,2,4-triazolium) dibromide, 10. 4,4'-bis(bromomethyl)-1,1'-biphenyl (2.00 g, 0.00588 mol) was added to a 100 mL round bottom flask which had 1,2,4-triazole-1-propanenitrile (1.437 g, 0.0118 mol) and the mixture was diluted with acetonitrile (40 mL). The reaction was heated to reflux for 24 h, followed by cooling the reaction to rt and washing the precipitate with diethyl ether (30 mL), and then dried under reduced pressure. The crude white solid was then washed with acetonitrile (3 x 30 mL) and dried under reduced pressure to yield the pure product (2.75 g, 84.1 % yield). ^{1}H NMR (DMSO-d_6, 499.72 MHz) δ 10.40 (s, 2H), 9.51 (s, 2H), 7.78 (d, J = 8.3 Hz, 4H), 7.63 (d, J = 8.2 Hz, 4H), 5.65 (s, 4H), 4.74 (t, J = 6.3 Hz, 4H), 3.25 (t, J = 6.3 Hz, 4H). ^{13}C{^{1}H} NMR (DMSO-d_6, 125.66 MHz): δ 144.97, 143.38,

139.92, 133.01, 129.56, 127.32, 117.71, 50.21, 47.25, 17.31. IR (neat): 3101, 3032, 3018, 2982, 2254, 1820, 1584, 1519, 1500, 1439, 1419, 1393, 1381, 1367, 1341, 1297, 1215, 1182, 1143, 1068, 1043, 1024, 1005, 980, 965, 916, 849, 833, 816, 787, 756, 708 cm^{-1}. ESI/MS (*m*/*z*): $[M-Br]^+$ 503.11, $[M-2Br]^{2+}$ 212.14. Anal. Calcd for $C_{24}H_{24}Br_2N_8$: C, 49.33; H, 4.14; N, 19.18. Found: C, 49.31; H, 4.08; N, 18.90.

Synthesis of 4,4′-[naphthalene-2,6-diylbis(methylene)]bis(1,2,4-triazole), L2, 9. Potassium hydroxide (1.01 g, 0.0179 mol) and **8** (2.50 g, 0.00448 mol) were added to a 50 mL Erlenmeyer flask containing 25 mL of water. The product precipitated from solution as a white powder, and the crude product was filtered after stirring for 24 h and washed with water (3 x 50 mL), acetonitrile (3 x 50 mL), and tetrahydrofuran (3 x 50 mL). The pure product was dried under reduced pressure to yield 1.22 g (94.1 % yield). ^{1}H NMR (DMSO-d_6, 499.72 MHz): δ 8.66 (s, 4H), 7.91 (d, *J* = 8.5 Hz, 2H), 7.79 (s, 2H), 7.46 (d, *J* = 8.5 Hz, 2H), 5.45 (s, 4H). ^{13}C{^{1}H} NMR (DMSO-d_6, 125.66 MHz): δ 143.33, 134.67, 132.24, 128.62, 126.28, 126.14, 47.63. IR (neat): 3102, 3037, 2941, 1648, 1608, 1529, 1465, 1448, 1387, 1351, 1338, 1276, 1255, 1192, 1178, 1129, 1076, 974, 951, 918, 903, 881, 828, 762, 694 cm^{-1}. Anal. Calcd for $C_{16}H_{14}N_6$: C, 66.19; H, 4.86; N, 28.95. Found: C, 65.69; H, 5.00; N, 28.24.

Synthesis of 4,4′-(4,4'-bitolyl)bis(1,2,4-triazole), L3, 11. Potassium hydroxide (1.17 g, 0.0208 mol) and **10** (2.90 g, 0.00521 mol) were added to a 50 mL Erlenmeyer flask containing 25 mL of water. After 24 h, the product precipitated

from solution as a white powder and was filtered and washed with water (3 x 50 mL), acetonitrile (3 x 50 mL), and tetrahydrofuran (3 x 50 mL). The pure product was dried under reduced pressure to yield 1.40 g (85.2 % yield). ^{1}H NMR (DMSO-d_6, 499.72 MHz) δ 8.65 (s, 4H), 7.66 (d, J = 7.7 Hz, 4H), 7.38 (d, J = 7.8 Hz, 4H), 5.32 (s, 4H). ^{13}C{^{1}H} NMR (DMSO-d_6, 125.66 MHz): δ 143.27, 139.25, 136.05, 128.29, 127.12, 47.21. IR (neat): 3089, 3029, 2962, 1664, 1613, 1522, 1500, 1458, 1439, 1403, 1378, 1361, 1336, 1316, 1207, 1179, 1169, 1074, 1006, 976, 967, 950, 889, 854, 833, 796, 755, 746, 712, 693 cm^{-1}. Anal. Calcd for $C_{16}H_{14}N_6$: C, 68.34; H, 5.10; N, 26.56. Found: C, 67.80; H, 5.18; N, 25.77.

Synthesis of [Cu(L2)(ClO_4)] • DMA • H_2O, 12. Copper(II) perchlorate hexahydrate (0.0136 g, 0.0367 mmol) and **L2** (0.0213 g, 0.0735 mmol) were added to separate 4 mL scintillation vials and dissolved in 1 mL of water and 2 mL of DMA, respectively. The vials were heated to 85 °C for 30 min in an aluminum heating block, followed by mixing of the solutions and additional heating. After heating for 24 h, colorless needles formed and were isolated and washed with water and acetone to yield the pure product (7.10 mg, 42.8 % yield). IR (neat): 3371, 3114, 1633, 1586, 1551, 1446, 1395, 1377, 1340, 1214, 1194, 1091, 1071, 1001, 968, 942, 907, 874, 818, 802, 767, 750, 732, 697 cm^{-1}. Anal. Calcd for $C_{16}H_{14}ClCuN_6O_4$•DMA•H_2O: C, 43.01; H, 4.51; N, 17.56. Found: C, 42.99; H, 3.76; N, 17.35.

Synthesis of [Cu(L3)(ClO_4)] • DEF, 13. Copper(II) perchlorate hexahydrate (0.0136 g, 0.0367 mmol) and **L3** (0.0232 g, 0.0735 mmol) were added to

separate 4 mL scintillation vials and dissolved in 1 mL of water and 2 mL of DEF, respectively. The vials were heated to 85 ℃ for 30 min in an aluminum heating block, followed by mixing of the solutions and additional heating. After heating for 24 h, colorless needles formed and were isolated and washed with water and acetone to yield the pure product (2.40 mg, 13.1 % yield). IR (neat): 3618, 3133, 2968, 2917, 2870, 2838, 1661, 1605, 1545, 1503, 1455, 1432, 1396, 1380, 1355, 1336, 1307, 1262, 1210, 1189, 1085, 1008, 973, 942, 859, 819, 754, 703, 684 cm^{-1}. Anal. Calcd for $C_{18}H_{16}ClCuN_6O_4$•DEF: C, 47.59; H, 4.69; N, 16.89. Found: C, 47.59; H, 4.63; N, 16.84.

X-ray Structure Determinations. Data was collected on a Bruker SMART APEXII three circle diffractometer equipped with a CCD area detector and operated at 1,800 W power (45 kV, 40 mA) to generate Mo Kα radiation (λ = 0.71073 Å). The incident X-ray beam was focused and monochromated using Bruker Excalibur focusing optics. Single crystals were mounted on nylon CryoLoops (Hampton Research) with Paratone-N (Hampton Research) and frozen at -100 ºC and -173 ºC, respectively. Initial scans of each specimen were taken to obtain preliminary unit cell parameters and to assess the mosaicity (i.e. breadth of spots between frames) of the crystal to select the required frame width for data collection. For all cases frame widths of 0.5º were judged to be appropriate and full hemispheres of data were collected using the *Bruker APEX2* software suite to carry out overlapping ϕ and ω scans at detector setting of 2θ = 28°. Following data collection, reflections were sampled from all regions of the

Ewald sphere to re-determine unit cell parameters for data integration. Following exhaustive review of collected frames the resolution of the dataset was judged, and, if necessary, regions of the frames where no coherent scattering was observed were removed from consideration for data integration using the *Bruker SAINTplus* program.[26] Data was integrated using a narrow frame algorithm and was subsequently corrected for absorption. Absorption corrections were performed for both samples using the SADABS program.[26] Space group determination and tests for merohedral twinning were carried out using *XPREP*.[26] In all cases, the highest possible space group was chosen. Final models were refined anisotropically (with the exception of H atoms).

Chapter 5

One-dimensional MOFs

Abstract

Employment of semi-rigid di-1,2,4-triazoles has led to the reticular synthesis of a series of metal-organic nanotubes (MONTs). The di-triazole ligands adopt a *syn* conformation between rigid metal chains while appropriate anion choice provides a "capping" of the metal fragments, leading to nanotube formation. MONT structures depend on the metal center employed with Cu(I) centers adopting a tetrahedral geometry and capping bromide anions while Ag(I) centers adopt a seesaw geometry in which nitrate anions provide a cap for the metal centers. Utilizing Cu(II) centers allows for an additional example with formation of square pyramidal metal centers upon MONT synthesis. The pore size of the MONTs is adjusted by changing the central portion of the double-hinged ligand, allowing for a general synthesis of MONTs. Adsorption properties of MONTs as a function of pore size revealed selective uptake of CO_2 and CH_4 with copper MONTs exhibiting the highest uptake.

Introduction

Metal-Organic Frameworks (MOFs) are a new class of materials which possess highly tunable pores through the use of reticular synthesis.[2b-d] Due to their precise architectural control during synthesis, MOFs have been tailored and investigated for applications ranging from gas separation and storage to catalysis.[3b-e, 3g, 3h, 14a] Despite the vast number of 2D and 3D MOFs which have been developed, the design of their 1D counterpart remains in its infancy.[51d]

Since the discovery of carbon nanotubes and their electronic properties,[57] an interest in tubular nanomaterials has emerged with a push towards the use of coordination chemistry to design materials which incorporate metals and elements other than carbon.[51d] Metal-organic nanotubes (MONTs) have only recently emerged as a 1D variant of MOFs and, despite the fact that only a limited number of MONTs have been synthesized, they have already shown promise in highly selective adsorptions.[58] With the potential of MONTs largely unexplored and a majority of reports focusing solely on structural details,[51c, 59] the development of rational methodologies which allow for their preparation and study is essential.

Despite the interest in a general synthesis for MONTs, only a few approaches have been successful for preparing frameworks with infinite chains. The limited MONT literature reveals three strategies for their preparation, including the use of a curling-up mechanism to form helical chains, a four-column pillared approach, or a two-column pillared approach (Figure 5.1).[51d] Examples include Qiu and coworkers who have recently demonstrated the first use of a "rolling up" mechanism to undergo a sheet-to-tube conversion,[60] while Kitagawa and coworkers have investigated the oxidative polymerization of square-shaped building blocks to form infinite four-column pillared MONTs.[58a] While four-column pillared MONTs can be prepared in a more rational manner than helical chains, the resulting pore size is difficult to control as it is particularly challenging to form any shape other than a square. The two-column pillar approach, however,

allows for the height and width to be controlled separately and ultimately allows for the adjustment of the void space through appropriate ligand choice. Two-column pillared MONTs generally employ the use of flexible organic molecules which can adopt a *cis* conformation to bridge metal centers, as demonstrated by Du and Sun.[51c, 59b]

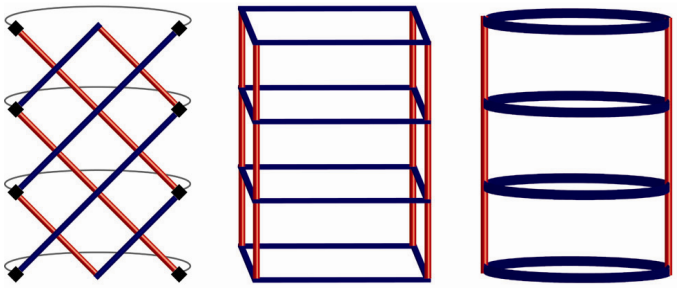


Figure 5.1. Pictorial representation of the three classes of MONTs: helical chains formed by a curling up mechanism (left), 4-column pillars (center), and 2-column pillars (right).

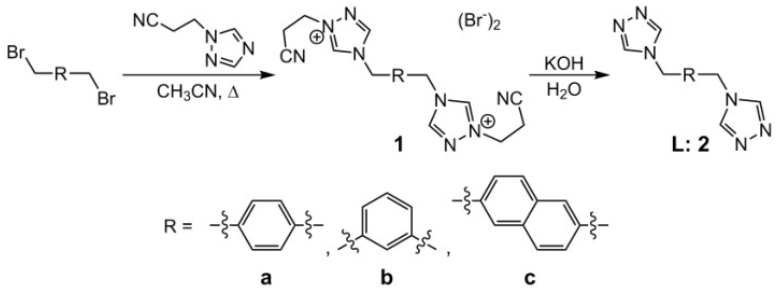
Our previous research with semi-rigid di-1,2,4-triazoles has demonstrated that 2D copper MOFs can be synthesized that display a topology similar to fused 1D nanotubes.[11c] In a similar manner to Du and Sun's MONTs,[51c, 59b] the bidentate semi-rigid linker adopts a *syn* conformation to link rigid metal fragments and form a 2D network. By employing reaction conditions which favor the formation of MONTs rather than 2D MOFs, we have developed a general synthetic strategy for nanotube formation using di-1,2,4-triazoles. As the size of the tube can be adjusted by ligand choice, adjusting the central portion of the

double-hinged ligand allows for a method to control the pore size. We believe that a general method for the reticular synthesis of MONTs has not been previously achieved and these materials are porous, allowing for the first test of gas adsorption as a function of pore size in MONTs.

Results and Discussion

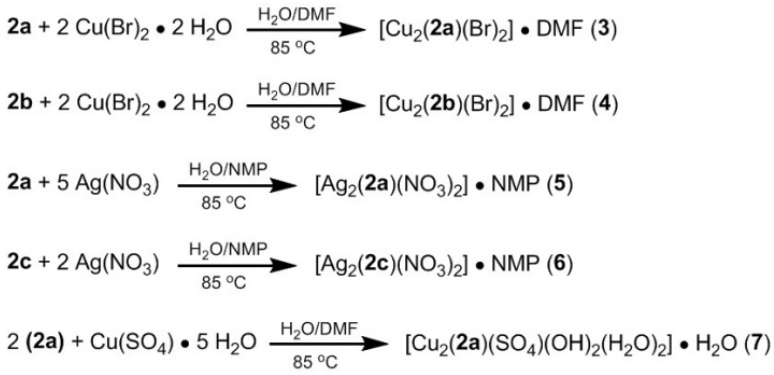
We have previously reported the synthesis of semi-rigid di-1,2,4-triazoles[11b, 12] and have most recently expanded this methodology to incorporate a central xylene moiety.[11c] Following the method of Horváth,[23] 4,4′-(1,4-(xylene)diyl)bis(1,2,4-triazole) is formed via a two-step process: the addition of 1,2,4-triazole-1-propanenitrile to 1,4-bis(bromomethyl)benzene leads to the formation of intermediate **1a**, followed by cleavage of the propanenitrile groups with potassium hydroxide to yield final product **2a** (Scheme 5.1). Following a similar reaction scheme, we have expanded our ligand library to encompass additional central moieties. Specifically, di-triazole derivatives containing *m*-xylene and naphthalene central moieties were synthesized. Intermediates **1b** and **1c** were synthesized using the appropriate bis(bromomethyl) starting material, resulting in yields of 90% and 70%, respectively. Cleavage of the propanenitrile group leads to formation of 4,4′-(1,3-(xylene)diyl)bis(1,2,4-triazole), **2b** and 4,4′-[naphthalene-2,6-diylbis(methylene)]bis(1,2,4-triazole), **2c** (Scheme 5.1).

Scheme 5.1. Synthesis of di-triazole ligands for MONT formation.



Previous results with the semi-rigid linker 4,4′-(1,4-(xylene)diyl)bis(1,2,4-triazole), **2a**, have demonstrated that through the use of copper perchlorate, multiple MOFs can be synthesized by varying reaction conditions such as solvent and metal to ligand ratio.[11c] To further assess the reactivity of ligand **2a** and newly synthesized ligands **2b** and **2c**, a variety of reaction conditions including changes to metal salt, solvent, and metal to ligand ratios were investigated (Scheme 5.2).

Scheme 5.2. Synthesis of frameworks utilizing various metals, solvents, and metal to ligand ratios.



The reaction space of previously synthesized **2a** was first examined through the use of additional metal salts. Addition of one equivalent of **2a** and two equivalents of copper bromide to a mixture of N,N-dimethylformamide (DMF) and water leads to the formation of $[Cu_2(\mathbf{2a})(Br)_2]$ • DMF (**3**) (Scheme 5.2, top). Heating the reaction mixture for 2 weeks at 85 °C resulted in colorless crystalline needles suitable for X-ray diffraction. Single crystal X-ray diffraction shows that each Cu(I) center is coordinated to two triazoles and two bromides, leading to a tetrahedral geometry about the metal center with an N1-Cu-N1′ bond angle of 140° (Figure 5.2A). Linear chains are formed as adjacent copper atoms are bridged by one triazole moiety and one bromide, and the linear chains are linked by the di-triazole ligand. This linking of two linear chains by the di-triazole induces formation of a two-pillared MONT, one of the aforementioned general classes of MONTs. As previously reported for **2a**, the semi-rigid ligand adopts a *syn* conformation. However, whereas in previous studies the triazole ligands bridged the copper centers in an alternating manner to form a 2D sheet, the presence of bromides along the rigid copper chains allows for a "capping" of the framework, leading to a 1D MONT instead of a 2D sheet (Figure 5.2B). Guest DMF molecules fill the pores of the framework which have dimensions of 9.3 x 9.9 Å.

As the study of MONTs remains in its infancy,[51d] the formation of **3** piqued our interest in further studying the use of semi-rigid di-triazoles for nanotube

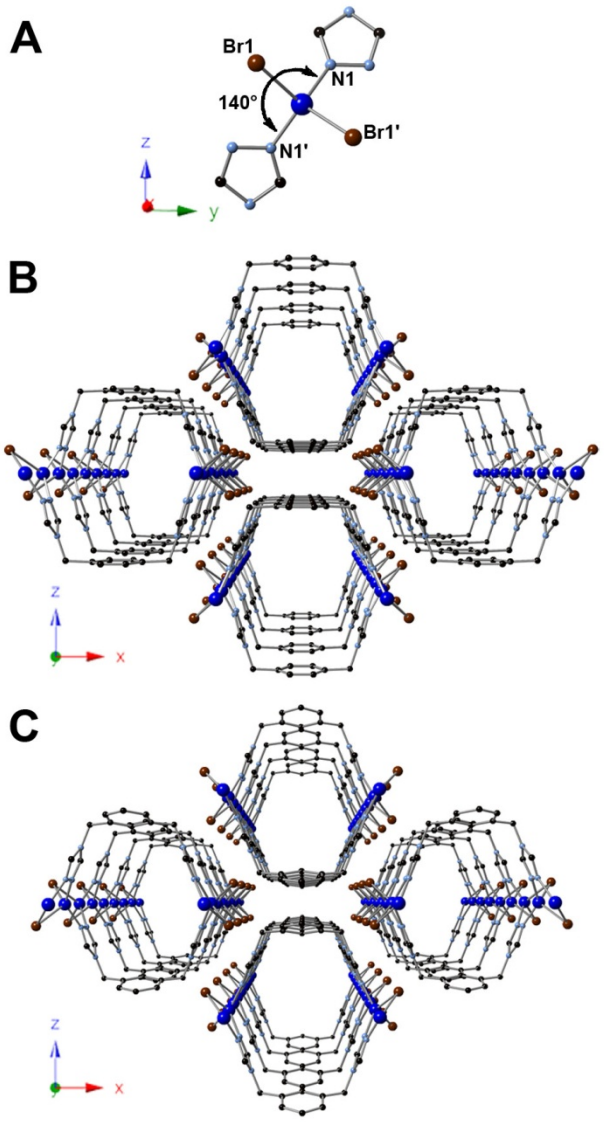


Figure 5.2. X-ray structures of $[Cu_2(\mathbf{2a})(Br)_2]$ • DMF, **3**, and $[Cu_2(\mathbf{2b})(Br)_2]$ • DMF, **4**. (A) Highlighted portion of the tetrahedral copper coordination geometry in MONTs **3** and **4**. (B) Crystal structure of **3** viewed orthogonal to y-axis showing packing of the MONT. (C) Crystal structure of **4** viewed orthogonal to the y-axis showing packing of the MONT. Solvent DMF molecules omitted for clarity.

formation. As the aforementioned di-triazoles only vary in their central moiety, other MONT structures should be attainable under similar reaction conditions. The synthesis of additional frameworks through a two-pillared approach would allow for the first reticular synthesis of MONTs.

To test the ability of additional di-triazoles to form MONTs, di-triazole **2b** was first tested under similar reaction conditions. By replacing di-triazole **2a** with **2b**, the analogous framework $[Cu_2(\mathbf{2b})(Br)_2]$ • DMF (**4**) (Scheme 5.2) was synthesized under identical reaction conditions, demonstrating that in fact the formation of MONTs can occur in a reticular fashion. One equivalent of **2b** combined with two equivalents of copper bromide in a DMF and water mixture led to formation of colorless crystals of **4** after heating at 85 °C for 5 days. X-ray diffraction studies of **4** revealed identical connectivity to that of **3** (Figure 5.2C). Tetrahedral Cu(I) centers coordinated to two triazoles and two bromides with a N1-Cu-N1′ bond angle of 137° form linear chains which are linked by the di-triazole ligand. The *syn* conformation of **2b** and the presence of "capping" bromides allows for the formation of MONT **4** with guest DMF molecules again residing within the tubular pores. As the use of different di-triazoles allows for MONTs with varying pore sizes to be synthesized, the pore size of **3** versus **4** was examined. A decrease in pore dimensions from 9.3 x 9.9 Å in **3** to 9.1 x 9.5 Å in **4** was observed and, although only a slight decrease, shows how ligand choice can fine-tune the properties of the synthesized MONT.

To further examine the reticular synthesis of MONTs using di-triazoles, additional metal salts were tested. As MONTs **3** and **4** involve the use of a d^{10} metal center, employing additional group 11 metal centers with the same oxidation state will allow for a broader approach for MONT synthesis. Therefore, as an initial survey of metal centers, the use of silver(I) metal salts was carried out.

Addition of one equivalent of **2a** and five equivalents of silver nitrate to a mixture of N-methyl-2-pyrrolidone (NMP) and water led to the formation of $[Ag_2(\mathbf{2a})(NO_3)_2] \bullet$ NMP (**5**) (Scheme 5.2). Heating for 24 h at 85 °C resulted in colorless crystals suitable for X-ray diffraction. Single crystal X-ray diffraction shows that each Ag(I) center is coordinated to two triazoles and two nitrates. In contrast to **4**, the silver exhibits a distorted seesaw geometry with an N1-Ag-N2′ bond angle of 162° (Figure 5.3A). The silver centers are coordinated to two triazoles and two nitrate anions with linear chains forming as adjacent metal centers are bridged through one triazole moiety and a bidentate nitrate anion. Nitrate anions behave as bromides in MONTs **3** and **4**, providing a “cap” for the metal centers and leading to formation of a 1D network with guest NMP molecules filling the tubular pores (Figure 5.3B).

With the synthesis of MONT **5** showing nanotube formation is a more generalizable approach and does not solely rely on copper metal centers, the possibility of synthesizing additional silver MONTs was addressed. Upon

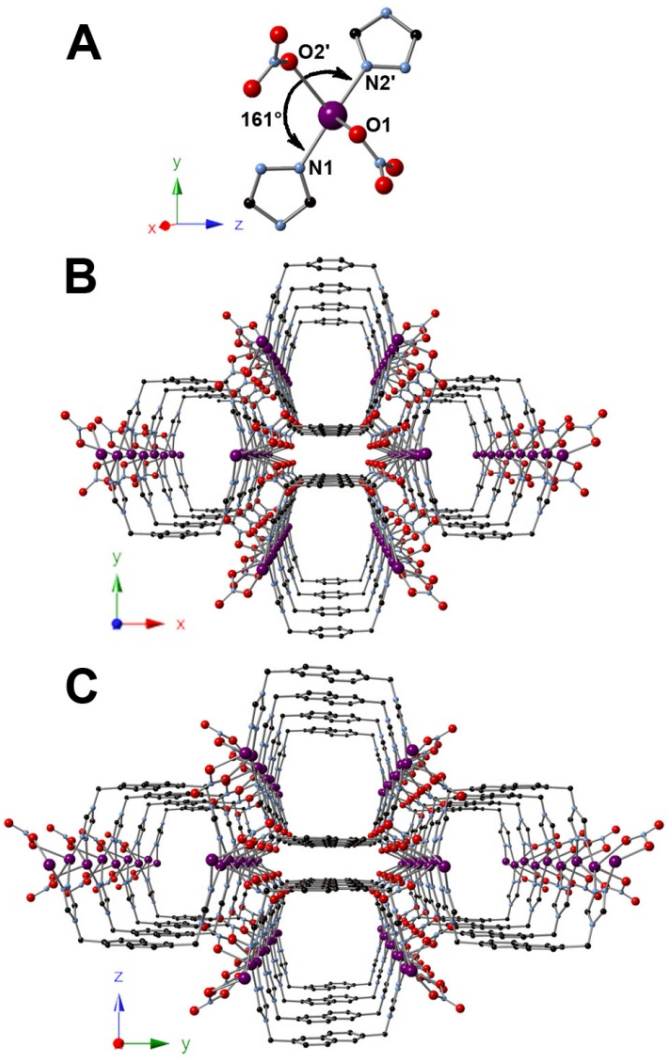


Figure 5.3. X-ray structures of $[Ag_2(\mathbf{2a})(NO_3)_2]$ • NMP, **5**, and $[Ag_2(\mathbf{2c})(NO_3)_2]$ • NMP, **6**. (A) Highlighted portion of the seesaw silver coordination geometry in MONTs **5** and **6**. (B) Crystal structure of **5** viewed orthogonal to z-axis showing packing of the MONT. (C) Crystal structure of **6** viewed orthogonal to the x-axis showing packing of the MONT. Guest NMP molecules omitted for clarity.

addition of one equivalent of di-triazole **2c** and two equivalents of silver nitrate in an NMP and water mixture, formation of MONT [Ag_2(**2a**)$(NO3)_2$] • NMP (**6**) (Scheme 5.2) occurred. Colorless needles suitable for X-ray diffraction were obtained after heating at 85 °C for 24 h. X-ray diffraction revealed identical connectivity to that of **5** (Figure 5.3C). Ag(I) centers exhibiting a seesaw geometry are bridged by triazoles and nitrates with an N1-Ag-N2′ bond angle of 160° to form linear chains which, combined with the *syn* geometry adopted by **2c**, results in MONT formation. Guest NMP molecules are again located within the pores. As di-triazole **2c** contains a central naphthalene moiety whereas **2a** contains a central phenyl moiety, an increase in pore dimensions is observed. A measurement of pore size in **6** reveals 1D channels of 10.3 x 10.5 Å while MONT **5** contains channels with dimensions of 8.7 x 10.6 Å. Therefore, through reticular synthesis, the pore size of the resulting MOFs can be tuned as a function of di-triazole used.

Through additional testing of reaction conditions, the employment of copper sulfate resulted in the formation of [Cu_2(**2a**)$(SO_4)(OH)_2(H_2O)_2$] • H_2O (**7**) (Scheme 5.2). Heating at 85 °C for 2 wks resulted in the formation of blue crystalline needles. X-ray diffraction revealed a different copper coordination environment than previous copper MONTs **3** and **4**. Each copper(II) center is coordinated to two triazole moieties, two bridging hydroxides, and a water molecule to give a square pyramidal geometry (Figure 5.4A). Adjacent copper

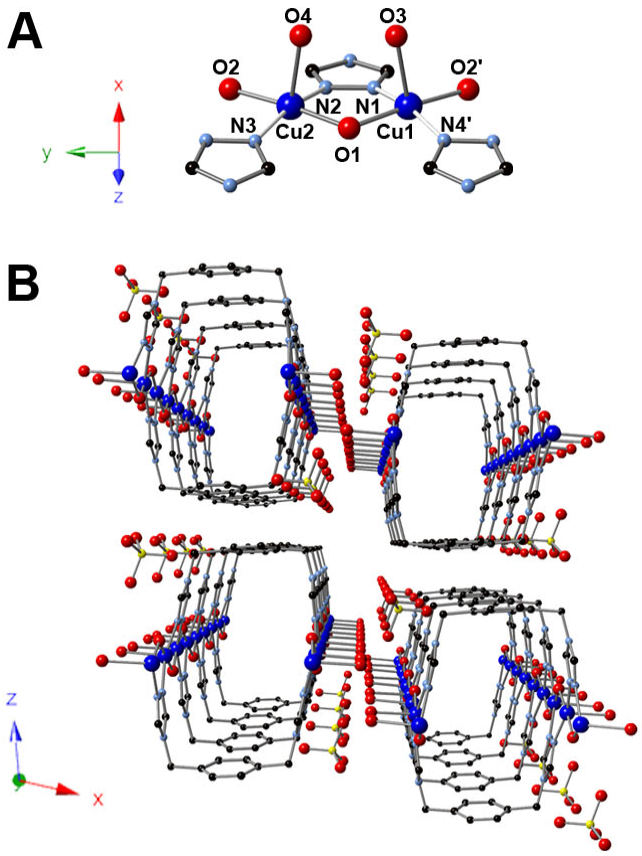


Figure 5.4. X-ray crystal structure of $[Cu_2(\mathbf{2a})(SO_4)(OH)_2(H_2O)_2] \cdot H_2O$, **7**. (A) Highlighted portion of the square pyramidal copper coordination geometry in MONT **7**. (B) Crystal structure of **7** viewed orthogonal to y-axis showing packing of the MONT. Guest water molecules omitted for clarity.

atoms are bridged by triazole and hydroxide moieties to yield linear chains which are again linked by the *syn* conformed di-triazole (Figure 5.4B). Solvent waters lie within the voids while sulfate anions are located between the 1D MONTs. The 1D pores within **7** yield dimensions of 7.6 x 10.7 Å.

Employing a variety of reaction conditions has led to the formation of MONTs with multiple di-triazoles. As PXRD is employed as a characterization method for bulk analysis, all MONT PXRDs have been analyzed and confirm stable packing of the 1D materials in the solid state (see Experimental section). Additionally, all MONTs are insoluble in common solvents.

The presence of 1D channels, combined with the inherent anisotropy in MONTs **3**-**7**, piqued our interest in studying their adsorption properties and permanent porosity. Each MONT synthesized exhibits a different pore size, depending on metal center and the resulting geometry as well as the di-triazole selected. As copper and silver MONTs have been synthesized with multiple ligands, a system has been developed in which pore size is predictable and controllable, allowing for sorption studies to be performed. To our knowledge, the wide variety of pore sizes in **3**-**7** allows, for the first time, a chance to probe the selectivity of MONTs for gas adsorption. Only a single MONT paper has reported CO_2 adsorption with most previous research focusing on synthesis and structure and not separation properties.

As an initial study of the effect of pore size on gas adsorption, copper MONTs **3**, **4**, and **7** were analyzed. Prior to adsorption studies, MONT

frameworks were activated by solvent exchange to remove initial guest solvent followed by heating overnight (See Experimental for details). MONT **3** was activated by Soxhlet extraction with methanol prior to adsorption studies while MONT **7** was activated by solvent exchange with methanol to remove guest DMF molecules. After multiple attempts with different activation methods, guest DMF molecules within the pores of **4** were not removed and therefore **4** did not exhibit any gas uptake. MONTs **3** and **7**, however, showed selective uptake of CO_2 and CH_4 with all other gases tested (N_2, H_2, and O_2) having no uptake. Figure 5.5 shows both CO_2 and CH_4 adsorption isotherms for **3** and **7** at 298 K. Maximum CO_2 and CH_4 uptakes for **3** at 1.22 bar are 1.58 and 0.658 mmol g^{-1}, respectively. Adsorption values for **7** were only marginally higher at 1.22 bar with an uptake of 1.70 mmol g^{-1} for CO_2 and 0.704 mmol g^{-1} for CH_4. Although MONT **7** exhibits higher adsorption values than **3**, the pore size of **7** is smaller. This increase in adsorption for **7** is likely due to the exposure of open metal sites upon heating as axially coordinated water molecules are removed.

Due to the selective adsorption of CO_2 and CH_4 by MONTs **3** and **7**, we continued our sorption studies by analyzing silver MONTs **5** and **6**. Both silver MONTs were activated by solvent exchange with methanol for 2 weeks to remove guest NMP molecules, followed by heating overnight. Analysis of MONTs **5** and **6** would allow for a direct study of the effect of pore size on adsorption as the only difference is the di-triazole used during synthesis. Both

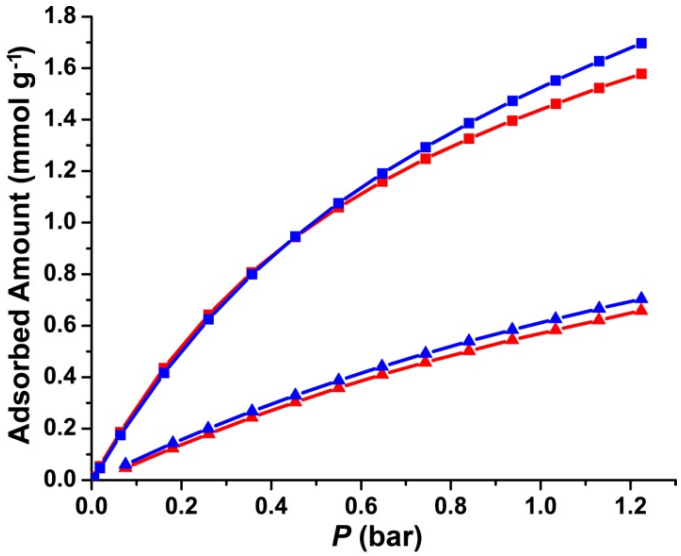


Figure 5.5. CO_2 (squares) and CH_4 (triangles) depict adsorption isotherms for MONTs $[Cu_2(\mathbf{2a})(Br)_2]$ • DMF (**3**) (red) and $[Cu_2(\mathbf{2a})(SO_4)(OH)_2(H_2O)_2]$ • H_2O (**7**) (blue).

CO_2 and CH_4 adsorption isotherms for **5** and **6** are shown in Figure 5.6 with the same axes to allow comparison to previous copper MONTs. MONT **5**, containing a central xylene moiety and therefore a smaller pore size compared to **6**, exhibited a maximum uptake of 0.607 and 0.248 mmol g^{-1} for CO_2 and CH_4, respectively, at 1.22 bar. MONT **6** displayed increased uptakes for both CO_2 and CH_4 with respective maximum values of 0.960 and 0.302 mmol g^{-1} at 1.22 bar. The increased pore size in **6** therefore allowed a higher maximum uptake of CO_2 and improved CO_2 vs. CH_4 selectivity as CH_4 uptake increased only slightly as compared to **5**. Adsorption studies of MONTs **5** and **6** show how ligand choice plays an important role in determining both gas selectivity and uptake, even

though **5** and **6** display a reduction in total uptake by one half as compared to **3** and **7**.

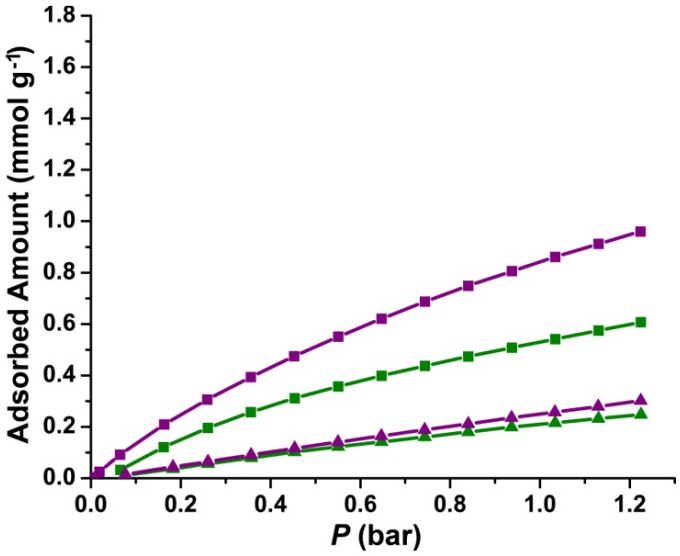


Figure 5.6. CO_2 (squares) and CH_4 (triangles) depict adsorption isotherms for MONTs [Ag_2(**2a**)$(NO3)_2$] • NMP (**5**) (green) and [Ag_2(**2c**)$(NO3)_2$] • NMP (**6**) (purple).

Conclusion

A series of metal-organic nanotubes containing semi-rigid di-1,2,4-triazoles have been synthesized through the use of reticular design. Di-triazoles adopt a *syn* conformation to link rigid metal chains while appropriate anion choice provides a "cap" for the rigid metal fragments, leading solely to nanotube formation. The use of 1,2,4-triazoles has led to a generalized synthetic strategy in which the size of the tube can be adjusted through judicious ligand choice.

Ligands containing central *m*-xylene, *p*-xylene, and naphthalene moieties were utilized and allowed for the first systematic study of gas adsorption in MONTs. Copper MONTs **3** and **7** exhibited the highest CO_2 and CH_4 uptake for MONTs studied. Ag MONTs **5** and **6** allowed for a more direct comparison of pore size on gas adsorption as the only difference is the central moiety of the di-triazole used during synthesis. Adsorption studies on **5** and **6** showed that ligand choice has a large impact on uptake and selectivity as the naphthalene moiety in **6** allowed for increased CO_2 uptake and CO_2/CH_4 selectivity. Future research will focus on the synthesis of MONTs containing additional di-triazoles, allowing for both improved gas uptake and selectivity.

Experimental

The compound 1,2,4-triazole-1-propanenitrile[23], 4,4'-[1,4-(xylene)diyl]bis-(1-(2-cyanoethyl)-1,2,4-triazolium) dibromide (**1a**)[11c], and 4,4′-(1,4-(xylene)diyl)bis(1,2,4-triazole) (**2a**)[11c] were prepared as described previously. Synthesis of ligands **1c** and **2c** were discussed previously (see Chapter 4, Experimental for Isoreticular Synthesis). All other reagents were purchased from commercial vendors and used without purification. ^1H and $^{13}C\{^1H\}$ NMR spectra were recorded at ambient temperature on a Varian Mercury 300 MHz or a Varian VNMRS 500 MHz narrow-bore broadband system. ^1H and ^{13}C NMR chemical shifts were referenced to the residual solvent. All mass spectrometry analyses were conducted at the Mass Spectrometry Center located in the Department of Chemistry at the University of Tennessee. The ESI/MS analyses were

performed using a QSTAR Elite quadrupole time-of-flight (QTOF) mass spectrometer with an electrospray ionization source from AB Sciex (Concord, Ontario, Canada). Infrared spectra were collected on a Thermo Scientific Nicolet iS10 with a Smart iTR accessory for attenuated total reflectance. Thermogravametric analysis data were collected on a TA Instruments TGA Q50 under N_2. Carbon, hydrogen, and nitrogen analyses were obtained from Atlantic Microlab, Norcross, GA. Gas adsorption measurements were collected on a Micromeritics ASAP 2020.

Synthesis of 4,4'-[1,3-(xylene)diyl]bis-(1-(2-cyanoethyl)-1,2,4-triazolium) dibromide, 1b. 1,3-Bis(bromomethyl)benzene (3.00 g, 0.0114 mol) was added to a 100 mL round bottom flask which had 1,2,4-triazole-1-propanenitrile (2.77 g, 0.0228 mol) and the mixture was diluted with acetonitrile (40 mL). The reaction was heated to reflux until a white precipitate had formed after 1 h. The reaction was cooled to rt and the precipitate was washed with diethyl ether (10 mL), and then dried under reduced pressure. The crude white solid was then washed with acetonitrile (3 x 30 mL) and dried under reduced pressure to yield the pure product (4.46 g, 89.8% yield). ^{1}H NMR (DMSO-d_6, 499.72 MHz): δ 10.45 (s, 2H), 9.47 (s, 2H), 7.73 (s, 1H), 7.58 – 7.50 (m, 3H), 5.62 (s, 4H), 4.74 (t, J = 6.3 Hz, 4H), 3.25 (t, J = 6.3 Hz, 4H). ^{13}C{^{1}H} NMR (DMSO-d_6, 125.66 MHz): δ 144.93, 143.43, 134.17, 129.83, 129.53, 129.39, 117.70, 50.24, 47.26, 17.31. IR (neat): 3019, 2906, 2257, 1818, 1569, 1523, 1492, 1446, 1427, 1413, 1367, 1339, 1323, 1281, 1249, 1230, 1184, 1149, 1068, 1043, 980, 943, 926, 911, 839, 758, 726,

667, 666 cm^{-1}. ESI/MS (*m*/*z*): $[M\text{-}Br]^+$ 427.14, $[M\text{-}2Br]^{2+}$ 174.11. Anal. Calcd for $C_{18}H_{20}Br_2N_8$: C, 42.54; H, 3.97; N, 22.05. Found: C, 42.75; H, 3.88; N, 21.88.

Synthesis of 4,4′-(1,3-(xylene)diyl)bis(1,2,4-triazole), 2b. Potassium hydroxide (1.33 g, 0.0236 mol) and **1b** (3.00 g, 0.00598 mol) were added to a 50 mL Erlenmeyer flask containing 30 mL of water. After stirring for 24 h, the solution was extracted with a 1:1 ethanol:chloroform solution (5 X 30 mL) and dried under reduced pressure to yield a crude product. The crude product contained potassium bromide impurities, but did not interfere with subsequent syntheses. ^{1}H NMR (DMSO-d_6, 499.72 MHz): δ 8.59 (s, 4H), 7.39 (t, J = 7.4 Hz, 1H), 7.28 (s, 1H), 7.23 (d, J = 7.6 Hz, 2H), 5.27 (s, 4H). ^{13}C{^{1}H} NMR (DMSO-d_6, 125.66 MHz): δ 143.22 , 137.31 , 129.42 , 127.35 , 126.97 , 47.32. IR (neat): 3388, 3108, 2967, 1639, 1611, 1593, 1524, 1460, 1445, 1387, 1354, 1334, 1246, 1226, 1180, 1156, 1090, 1071, 975, 951, 894, 878, 847, 824, 783, 751, 725, 681 cm^{-1}

Synthesis of $[Cu_2(2a)(Br)_2]$ • DMF, 3. Copper(II) bromide dihydrate (0.0381 g, 0.147 mmol) and **2a** (0.0177 g, 0.0735 mmol) were added to separate 4 mL scintillation vials and dissolved in 1 mL of water and 2 mL of DMF, respectively. The vials were heated to 85 °C for 30 min in an aluminum heating block, followed by mixing of the solutions and additional heating. After heating for 2 wks, colorless needles formed and were isolated and washed with water and acetone to yield the pure product (30.7 mg, 79.3 % yield). IR (neat): 3106, 2995, 1668, 1540, 1499, 1472, 1431, 1380, 1334, 1252, 1211, 1180, 1113, 1080, 1025, 1010,

867, 832, 808, 750, 716, 653, 638, 628 cm^{-1}. Anal. Calcd for $C_{12}H_{12}Br_2Cu_2N_6$•DMF: C, 30.01; H, 3.19; N, 16.33. Found: C, 29.90; H, 3.06; N, 16.26.

Synthesis of $[Cu_2(2b)(Br)_2]$ • DMF, 4. Copper(II) bromide dihydrate (0.0381 g, 0.147 mmol) and **2b** (0.0177 g, 0.0735 mmol) were added to separate 4 mL scintillation vials and dissolved in 1 mL of water and 2 mL of DMF, respectively. The vials were heated to 85 °C for 30 min in an aluminum heating block, followed by mixing of the solutions and additional heating. After heating for 5 days, colorless needles formed and were isolated and washed with water and acetone to yield the pure product (24.1 mg, 62.3 % yield). IR (neat): 3111, 3029, 3003, 2944, 1668, 1539, 1500, 1471, 1441, 1394, 1382, 1348, 1335, 1253, 1229, 1185, 1087, 1077, 1008, 971, 907, 858, 761, 725, 683, 674, 656 cm^{-1}. Anal. Calcd for $C_{12}H_{12}Br_2Cu_2N_6$•DMF: C, 30.01; H, 3.19; N, 16.33. Found: C, 29.88; H, 3.16; N, 16.12.

Synthesis of $[Ag_2(2a)(NO_3)_2]$ • NMP, 5. Silver(I) nitrate hexahydrate (0.0625 g, 0.368 mmol) and **2a** (0.0177 g, 0.0735 mmol) were added to separate 4 mL scintillation vials and dissolved in 1 mL of water and 2 mL of NMP, respectively. The vials were heated to 85 °C for 30 min in an aluminum heating block, followed by mixing of the solutions and additional heating. After heating for 24 h, colorless needles formed and were isolated and washed with water and acetone to yield the pure product (37.6 mg, 88.3 % yield). IR (neat): 3429, 3091, 2996, 1671, 1538, 1499, 1468, 1444, 1423, 1327, 1296, 1220, 1206, 1187, 1166, 1116, 1079,

1022, 1003, 983, 906, 836, 823, 806, 768, 746, 739, 717, 687, 638 cm^{-1}. Anal. Calcd for $C_{12}H_{12}Ag_2N_8O_6$•NMP: C, 30.07; H, 3.12; N, 18.56. Found: C, 30.45; H, 3.01; N, 19.56.

Synthesis of $[Ag_2(2c)(NO_3)_2]$ • NMP, 6. Silver(I) nitrate (0.0250 g, 0.147 mmol) and **2c** (0.0213 g, 0.0735 mmol) were added to separate 4 mL scintillation vials and dissolved in 1 mL of water and 2 mL of NMP, respectively. The vials were heated to 85 °C for 30 min in an aluminum heating block, followed by mixing of the solutions and additional heating. After heating for 24 h, colorless needles formed and were isolated and washed with water and acetone to yield the pure product (26.5 mg, 57.2 % yield). IR (neat): 3389, 3093, 2999, 1705, 1672, 1609, 1541, 1503, 1475, 1444, 1323, 1232, 1216, 1195, 1170, 1135, 1112, 1081, 1045, 1024, 978, 920, 901, 824, 768, 745, 721, 691, 642 cm^{-1}. Anal. Calcd for $C_{16}H_{14}Ag_2N_8O_6$•NMP: C, 34.59; H, 3.18; N, 17.29. Found: C, 33.87; H, 2.64; N, 17.52.

Synthesis of $[Cu_2(2a)(SO_4)(OH)_2(H_2O)_2]$ • H_2O, 7. Copper(II) sulfate pentahydrate (0.00918 g, 0.0367 mmol) and **2a** (0.0177 g, 0.0735 mmol) were added to separate 4 mL scintillation vials and dissolved in 1 mL of water and 2 mL of DMF, respectively. The vials were heated to 85 °C for 30 min in an aluminum heating block, followed by mixing of the solutions and additional heating. After heating for 2 wks, blue needles formed and were isolated and washed with water and acetone to yield the pure product (8.60 mg, 87.9 % yield). IR (neat): 3284, 3144, 1671, 1547, 1458, 1394, 1213, 1200, 1142, 1099, 1024,

961, 907, 832, 808, 746, 718 cm^{-1}. Anal. Calcd for $C_{12}H_{18}Cu_2N_6O_8S•H_2O$: C, 26.14; H, 3.66; N, 15.24. Found: C, 26.45; H, 4.22; N, 14.48.

X-ray Structure Determinations. Data was collected on a Bruker SMART APEXII three circle diffractometer equipped with a CCD area detector and operated at 1,800 W power (45 kV, 40 mA) to generate Mo Kα radiation (λ = 0.71073 Å). The incident X-ray beam was focused and monochromated using Bruker Excalibur focusing optics. Single crystals were mounted on nylon CryoLoops (Hampton Research) with Paratone-N (Hampton Research) and frozen at -100 ºC and -173 ºC, respectively. Initial scans of each specimen were taken to obtain preliminary unit cell parameters and to assess the mosaicity (i.e. breadth of spots between frames) of the crystal to select the required frame width for data collection. For all cases frame widths of 0.5º were judged to be appropriate and full hemispheres of data were collected using the *Bruker APEX2* software suite to carry out overlapping ϕ and ω scans at detector setting of $2\theta = 28^{o}$. Following data collection, reflections were sampled from all regions of the Ewald sphere to re-determine unit cell parameters for data integration. Following exhaustive review of collected frames the resolution of the dataset was judged, and, if necessary, regions of the frames where no coherent scattering was observed were removed from consideration for data integration using the *Bruker SAINTplus* program.[26] Data was integrated using a narrow frame algorithm and was subsequently corrected for absorption. Absorption corrections were performed for both samples using the SADABS program.[26] Space group

determination and tests for merohedral twinning were carried out using *XPREP*.[26] In all cases, the highest possible space group was chosen.

Final models were refined anisotropically (with the exception of H atoms). Hydrogen atoms were not placed on solvent molecules due to disorder. Disorder in **4** led to refinement of phenyl atom occupancies as the phenyl moiety is disordered over two positions. Reducing the occupancies accordingly led to satisfactory refinement. In the case of **6**, after multiple attempts at obtaining crystals, poorer diffraction data prevented the anisotropic refinement of all atoms except silver. All structures were examined using the *Addsym* subroutine of PLATON[4] to assure that no additional symmetry could be applied to the models.

Powder X-ray experiments. Powder X-ray diffraction (PXRD) data was collected using a Panalytical Empyrean θ-2θ diffractometer in reflectance Bragg-Brentano geometry. Cu-Kα radiation (λ = 1.5406 Å; 1,800 W, 45 kV, 40 mA) was focused using a planar Gobel Mirror riding the Kα line. A 0.25 mm divergence slit was used for all measurements. Diffracted radiation was detected using a PIXcel[3d] detector [(6° 2θ sampling width) equipped with a Ni monochrometer]. All samples were mounted onto a zero background quartz plate fixed on a sample holder by dropping powders and then leveling the sample surface. The best counting statistics were achieved by using a 0.0394º 2θ step scan from 3 – 50° with an exposure time of 119.85 s per step and a revolution spin rate of 4 s.

Gas Adsorption Measurements. Gas adsorption measurements were performed on fresh samples which had been verified by PXRD. MONTs **3**-**7**

required activation prior to adsorption studies with the activation method depending on the MONT being analyzed. Samples of **5**-**7** were activated by solvent exchange with methanol, exchanging solvent with fresh methanol every 8 h for 2 weeks. MONT **3** was activated by Soxhlet extraction with methanol for 1 week. All samples were degassed at 75 °C for 24 h prior to measurements and CO_2 and CH_4 isotherms were collected at 298 K. Isosteric heats of adsorption (Q_{st}) values were determined by collecting additional CO_2 isotherms at 0 ºC. Attempts at activating MONT **4** were unsuccessful as the guest solvent could not be removed.

Chapter 6

By-Products of MOF Synthesis

Abstract

The employment of semi-rigid di-triazoles, due to their partial flexibility, has led to the synthesis of MOFs with a variety of topologies. As not all frameworks obtained adhere with the theme of the dissertation, additional frameworks of potential interest are included in this chapter as a source for future reference.

Introduction

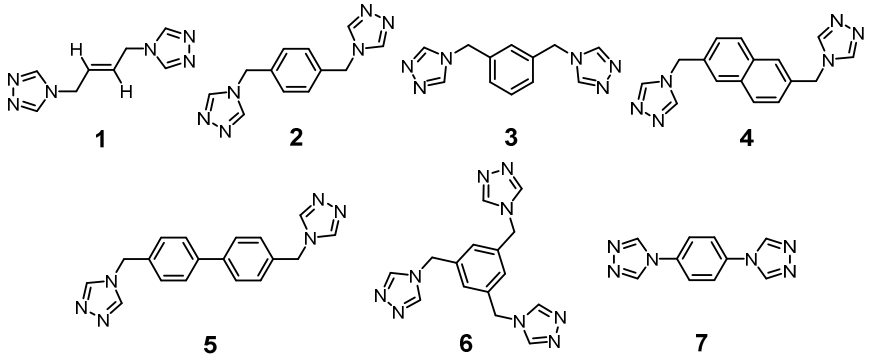
As MOF synthesis is a combinatorial approach, a multitude of MOF structures were obtained through the use of di-triazoles. Many frameworks obtained did not cohere with the theme of the dissertation but they have been included to show the diversity of frameworks that can be synthesized. Additionally, frameworks are reported that contain minor variations to previously published structures such as utilizing different anions in order to show a more broad synthesis. As the additional frameworks have, as of yet, not been fully characterized, only synthesis schemes and single crystal X-ray structures are provided.

Results and Discussion

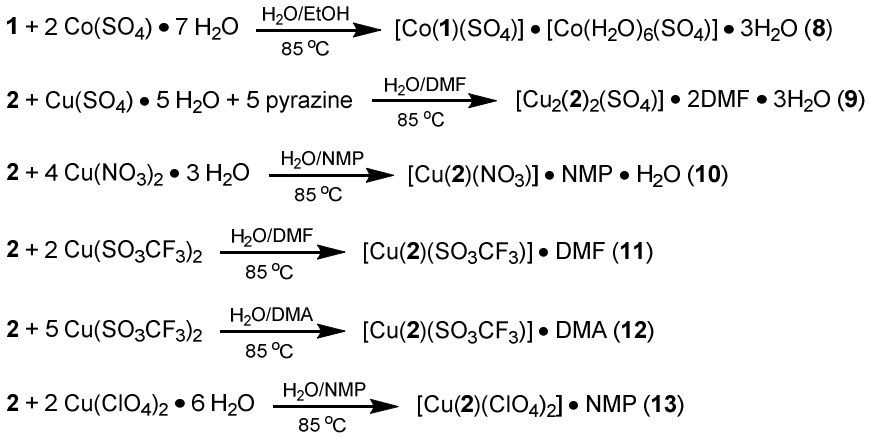
A number of di-triazoles utilized led to the synthesis of additional frameworks as a by-product of MOF synthesis. Di-triazole ligands employed which led to MOF structures included in this chapter are notated in Scheme 6.1. The resulting MOFs yielding structures similar to previously published

frameworks have been notated in Scheme 6.2 and their respective structures shown in Figure 6.1-Figure 6.6. Frameworks have been arranged in accordance with ligand utilized during synthesis and the resulting topologies. In addition, a plethora of MOFs were synthesized which do not match the theme of the dissertation and are reported in Table 6.1 and Table 6.2. MOFs are divided into potentially porous and non-porous structures and the respective ligands and metals used during synthesis and resulting formulas and data file names are listed.

Scheme 6.1. Di-triazoles for MOF synthesis.



Scheme 6.2. Synthesis of frameworks that are structurally analogous to published examples.



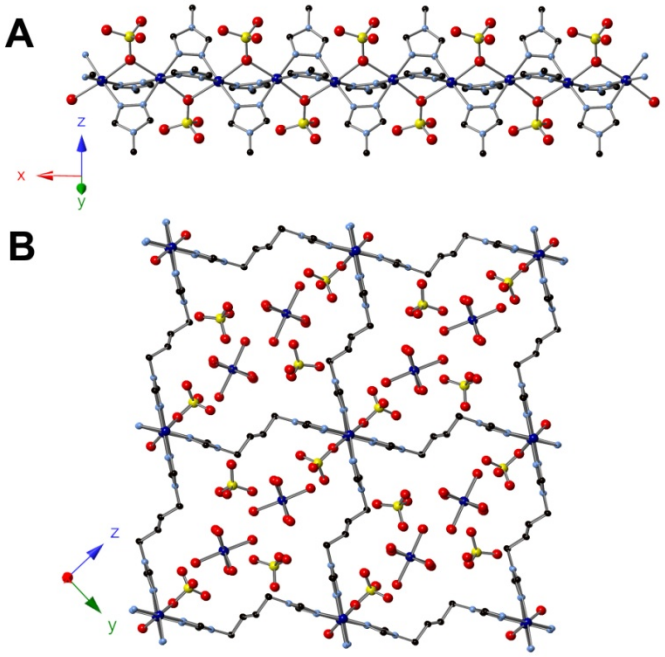


Figure 6.1. X-ray structure of [Co(**1**)(SO_4)] • [Co(H_2O)$_6$(SO_4)] • 3H_2O, **8**. (A) Crystal structure of **8** showing copper chains along the x-axis. (B) Crystal structure of **8** viewed orthogonal to the x-axis showing the fused-tube topology.

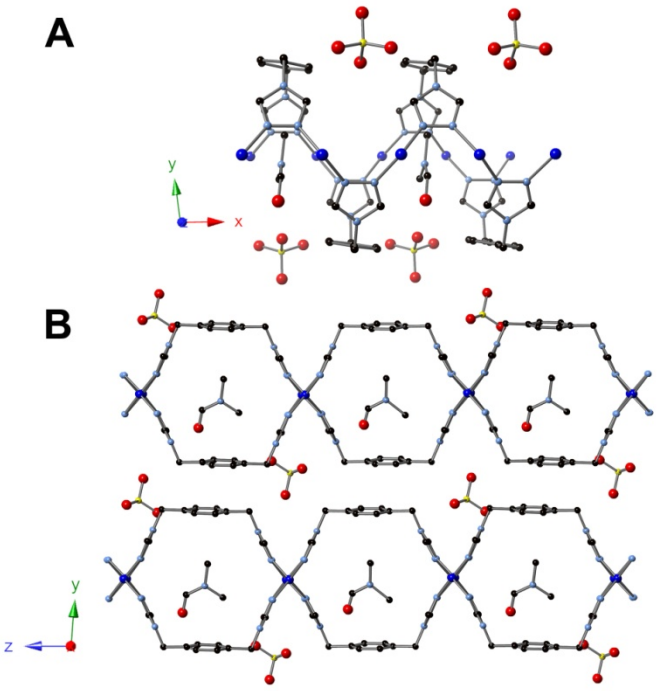


Figure 6.2. X-ray structure of $[Cu_2(\mathbf{2})_2(SO_4)] \cdot 2DMF \cdot 3H_2O$, **9**. (A) Crystal structure of **9** showing copper chains along the x-axis. (B) Crystal structure of **9** viewed orthogonal to the x-axis showing the fused-tube topology.

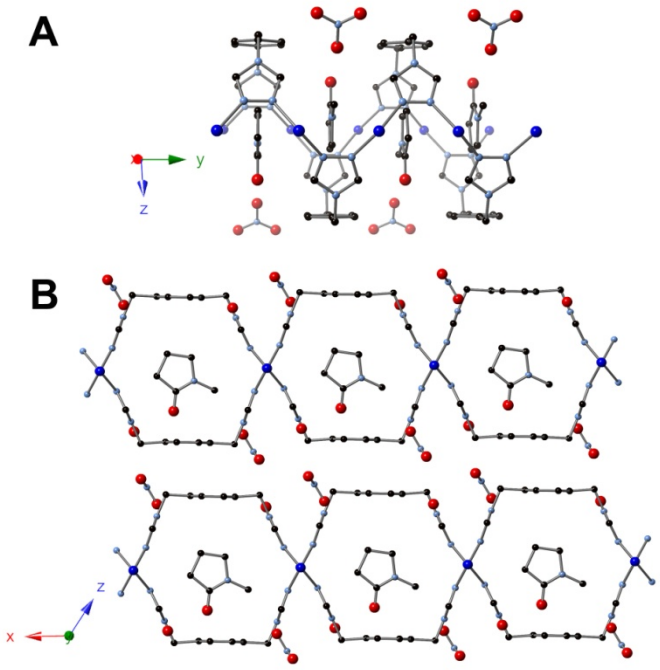


Figure 6.3. X-ray structure of [Cu(**2**)(NO_3)] • NMP • H_2O, **10**. (A) Crystal structure of **10** showing copper chains along the y-axis. (B) Crystal structure of **10** viewed orthogonal to the y-axis showing the fused-tube topology.

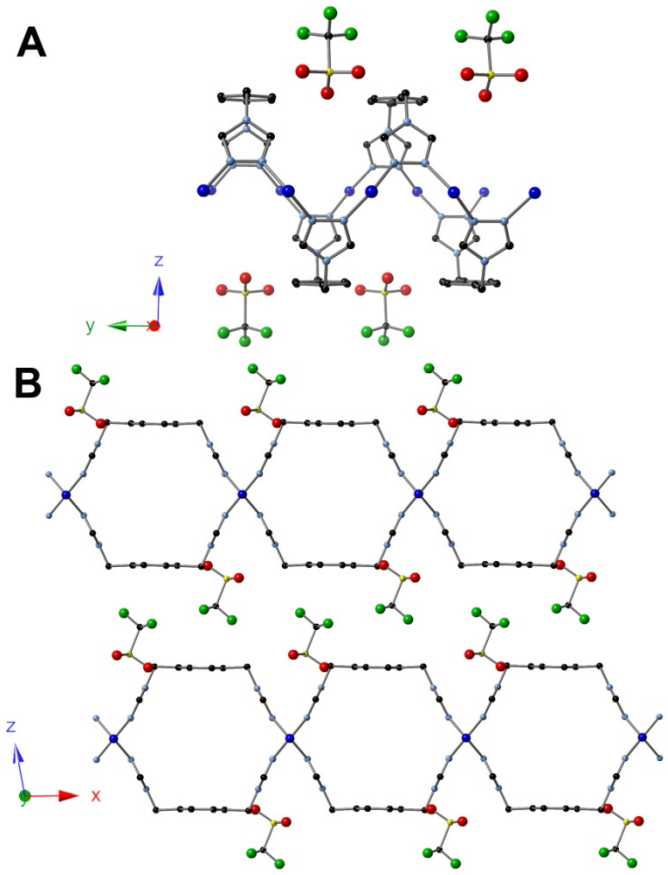


Figure 6.4. X-ray structure of [Cu(**2**)(SO_3CF_3)] • DMF, **11**. (A) Crystal structure of **11** showing copper chains along the y-axis. (B) Crystal structure of **11** viewed orthogonal to the y-axis showing the fused-tube topology.

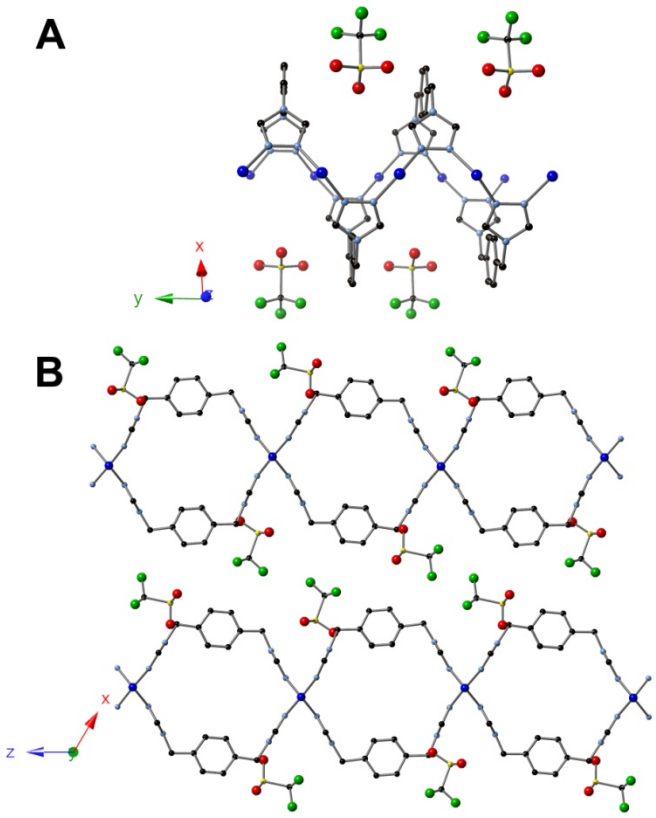


Figure 6.5. X-ray structure of [Cu(**2**)(SO_3CF_3)] • DMA, **12**. (A) Crystal structure of **12** showing copper chains along the y-axis. (B) Crystal structure of **12** viewed orthogonal to the y-axis showing the fused-tube topology.

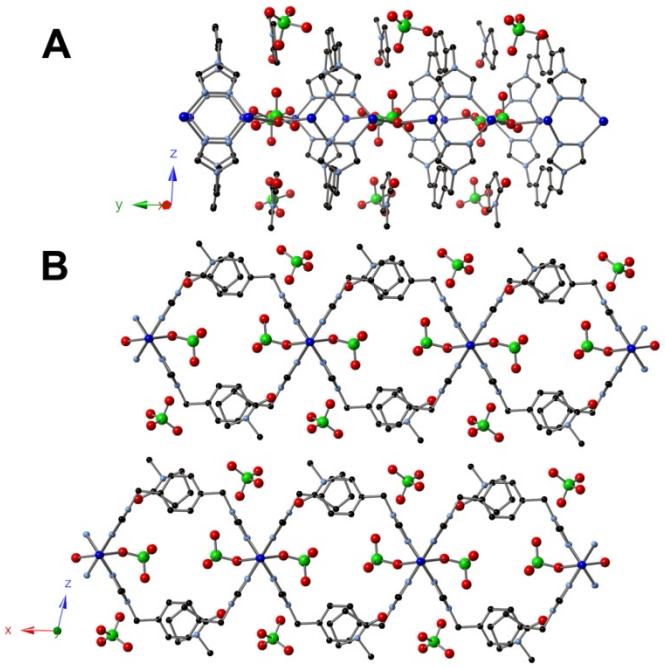


Figure 6.6. X-ray structure of [Cu(**2**)(ClO_4)$_2$] • NMP, **13**. (A) Crystal structure of **13** showing copper chains along the y-axis. (B) Crystal structure of **13** viewed orthogonal to the y-axis showing the fused-tube topology.

Table 6.1. Potentially porous MOFs.

#	Ligand	Metal	Formula	X-ray data file
14	**2**	$CuCl_2$	[Cu(**2**)$(Cl)_4$]	CM_Cl_blue_042912
15	**2**	$Cu(SO_3CF_3)_2$	[Cu(**2**)(SO_3CF_3)]	CM_3_277A5_060113
16	**4**	$Cu(ClO_4)_2$	[Cu(**4**)(ClO_4)]	CM_3_225D1_1512
17	**6**	$Cu(SO_4)$	[Cu_3(**6**)$_3(SO_4)_3$]	CM_3_163A4_9612
18	**7**	$Co(SO_4)$	[Co(**7**)(SO_4)]	CM_3_29B4rods5912

Table 6.2. Non-porous MOFs.

#	Ligand	Metal	Formula	X-ray data file
19	**1**	$Co(SO_4)$	$[Co_6(\mathbf{1})_3(SO_4)_5(OH)_2]$	CM_267B
20	**1**	$Cu(SO_4)$	$[Cu_3(\mathbf{1})_3(SO_4)_2(OH)(I)]$	CM_67C1KIversionofC2
21	**1**	$Cu(SO_4)$	$[Cu_3(\mathbf{1})_3(SO_4)_2(OH)(F)]$	CM_67A1KFversionofC2
22	**1**	$Cu(ClO_4)_2$	$[Cu_2(\mathbf{1})_2(OH)(ClO_4)_3]$	CM_3_267A5_051113
23	**1**	$Cu(SO_4)$	$[Cu4(\mathbf{1})_3(SO4)_2]$	CM_3_257D5norig050813
24	**1**	$Cu(SO_4)$	$[Cu_2(\mathbf{1})(SO_4)(H_2O)_2]$	CM_3_257D4_042413
25	**1**	$Cu(ClO_4)_2$	$[Cu(\mathbf{1})(ClO_4)]$	CM_3_257B4_042113
26	**1**	$CuBr_2$	$[Cu_4(\mathbf{1})(OCHO)_4(OH)_4]$	CM_3_41A451012
27	**1**	$CuBr_2$	$[Cu_2(\mathbf{1})(Br)_2]$	CM_3_41A4
28	**1**	$Ni(SO_4)$	$[Ni_6(\mathbf{1})(SO_4)_6]$	CM2119C1
29	**1**	$Cu(ClO_4)_2$	$[Cu_2(\mathbf{1})_2(ClO_4)_3(OH)]$	CM2165C1
30	**1**	$Cu(SO_4)$	$[Cu_3(\mathbf{1})_3(SO_4)_2(Br)(OH)]$	CM2207Btry2
31	**2**	$Cu(SO_4)$	$[Cu_2(\mathbf{2})_2(SO_4)]$	CM_SO4othercry
32	**2**	$Cu(SO_4)$	$[Cu_2(\mathbf{2})_3(SO_4)_2]$	CM_CuSO4tubeothercrystal
32	**2**	$Cu(NO_3)_2$	$[Cu_3(\mathbf{2})_2(NO_3)_2(OCHO)_2(OH)_2]$	CM_CuNO3semirigd
33	**2**	$CuBr_2$	$[Cu_4(\mathbf{2})_2(Br)_4(OH)_4]$	CM_CuBrNH3_92812
34	**2**	$Cu(ClO_4)_2$	$[Cu_4(\mathbf{2})_2(NMP)_4(ClO_4)_4(OH)_4]$	CM_139C5blue_112712
35	**2**	$Cu(ClO_4)_2$	$[Cu_2(\mathbf{2})(H_2O)_2(ClO_4)_2(OH)_2]$	CM_139b5blueredo
36	**2**	$Cu(SO_4)$	$[Cu_6(\mathbf{2})_4(SO_4)_5(OH)_2(H_2O)_2]$	CM_3_279B2_061413
37	**2**	$Cu(SO_4)$	$[Cu_8(\mathbf{2})_8(SO_4)_4]$	CM_3_257C4_042113
38	**2**	$Cd(SO_4)$	$[Cd_{12}(\mathbf{2})_8(SO_4)_9(OH)_6]$	CM_3_251A1_032813
39	**2**	$CdCl_2$	$[Cd(\mathbf{2})(Cl)_2]$	CM_3_249A2_032913
40	**2**	$Cd(SO_4)$	$[Cd_4(\mathbf{2})_4(SO_4)_4(H_2O)]$	CM_3_243A2redo_032913
41	**2**	$Cu(NO_3)_2$	$[Cu(\mathbf{2})(OCHO)_2]$	CM_3_237A2_020713
42	**2**	$Cu(ClO_4)_2$	$[Cu(\mathbf{2})(ClO_4)]$	CM_3_201B3_102212
43	**2**	$Cu(ClO_4)_2$	$[Cu_3(\mathbf{2})_6(ClO_4)_6]$	CM_3_201A1_101412
44	**2**	$Cu(ClO_4)_2$	$[Cu_2(\mathbf{2})_3(ClO_4)_2]$	CM_3_139B161912
45	**2**	$Cu(ClO_4)_2$	$[Cu_4(\mathbf{2})_3(OCHO)_4(O)_2]$	CM_3_139A3blue_111412
46	**2**	$CoCl_2$	$[Co_4(\mathbf{2})_4(OCCHO)_4]$	CM_3_105B2_91412
47	**2**	$Cu(SO_3CF_3)_2$	$[Cu_3(\mathbf{2})_5(SO_3CF_3)_6$	CM_3_35A2
48	**2**	$Cu(SO_3CF_3)_2$	$[Cu_2(\mathbf{2})(SO_3CF_3)_2(OH)_2]$	CM_3_35B2
49	**2**	$Mn(ClO_4)_2$	$[Mn_6(\mathbf{2})_8(ClO_4)_6]$	CM_3_15B1_6812
50	**2**	$Cu(ClO_4)_2$	$[Cu_2(\mathbf{2})(ClO_4)_2]$	CM3221A2
51	**3**	$Cd(SO_4)$	$[Cd(\mathbf{3})(SO_4)]$	CM_3_193B5_10212
52	**3**	$CuCl_2$	$[Cu_2(\mathbf{3})(Cl)_2]$	CM_3_189A5_10312
53	**4**	$Cu(SO_4)$	$[Cu_8(\mathbf{4})_8(SO_4)_4]$	CM_3_95A351212
54	**4**	$Cd(SO_4)$	$[Cd_6(\mathbf{4})_4(SO_4)_6(H_2O)_4]$	CM_3_245C3_032013lt
55	**4**	$Cu(ClO_4)_2$	$[Cu_4(\mathbf{4})_3(ClO_4)_4(NMP)_4]$	CM_3_225D5halflig_052113

Table 6.2. (continued)

#	Ligand	Metal	Formula	X-ray data file
56	**4**	$Cu(SO_4)$	$[Cu_2(\mathbf{4})_2(SO_4)]$	CM_3_177B4_92012
57	**5**	$Cu(SO_4)$	$[Cu_2(\mathbf{5})_2(SO_4)]$	CM_bpA2def
58	**5**	$Cu(SO_4)$	$[Cu_2(\mathbf{5})_3(SO_4)]$	CM_biphenylA2cuso4 dmfwater
59	**5**	$Cu(SO_4)$	$[Cu_6(\mathbf{5})_3(OAc)_2(SO_4)_6(HNMe_2)_2]$	CM_DMAA5redo52612
60	**5**	$Cu(ClO_4)_2$	$[Cu_2(\mathbf{5})_2(ClO_4)_2]$	CM_biphbpb3_030913
61	**5**	$Cu(ClO_4)_2$	$[Cu_5(\mathbf{5})_3(ClO_4)_2(OH)_3]$	CM_3_203C5_102012
62	**5**	$Cu(ClO_4)_2$	$[Cu_2(\mathbf{5})_2(ClO_4)_2]$	CM_3_203B3_102112
63	**5**	$Cu(SO_3CF_3)_2$	$[Cu(\mathbf{5})(SO_3CF_3)]$	CM_3_129A3_6512
64	**5**	$Cu(SO_4)$	$[Cu_2(\mathbf{5})3(SO_4)]$	CM_3_113A253112
65	**5**	$Cu(SO_4)$	$[Cu_2(\mathbf{5})3(SO_4)_2]$	CM_3_95A57712
66	**6**	$Cu(SO_4)$	$[Cu_4(\mathbf{6})_4(SO_4)_2]$	CM_3_163B5_9912
67	**6**	$Cu(SO_4)$	$[Cu_6(\mathbf{6})_3(SO_4)_3]$	CM_3_163A182912
68	**7**	$Co(SO_4)$	$[Co_4(\mathbf{7})(SO_4)_2(OH)_4(H_2O)_4]$	CM_3_29D5812

Conclusion

Employment of di-triazoles has led to the formation of additional MOFs whose structures have been presented. The ability for the ligand to undergo conformational changes lends itself to the formation of unique MOF topologies which have not been fully explored and are currently under investigation.

Experimental

The compound 1,2,4-triazole-1-propanenitrile,[23] **1**-**5**,[11c, 12] and **7**[61] were prepared as described previously (see Chapter 5 Experimental for synthesis of **3** and Chapter 4 Experimental for Isoreticular Synthesis for synthesis of **4**-**5**). All other reagents were purchased from commercial vendors and used without purification. ^1H and $^{13}C\{^1H\}$ NMR spectra were recorded at ambient temperature

on a Varian Mercury 300 MHz or a Varian VNMRS 500 MHz narrow-bore broadband system. ^{1}H and 13C NMR chemical shifts were referenced to the residual solvent. Solid ^{13}C CP MAS NMR samples were recorded on a Varian Inova 400 MHz spectrometer and referenced to an external adamantane sample. All mass spectrometry analyses were conducted at the Mass Spectrometry Center located in the Department of Chemistry at the University of Tennessee. The ESI/MS analyses were performed using a QSTAR Elite quadrupole time-of-flight (QTOF) mass spectrometer with an electrospray ionization source from AB Sciex (Concord, Ontario, Canada). Infrared spectra were collected on a Thermo Scientific Nicolet iS10 with a Smart iTR accessory for attenuated total reflectance. Thermogravametric analysis data were collected on a TA Instruments TGA Q50 under N_2. Carbon, hydrogen, and nitrogen analyses were obtained from Atlantic Microlab, Norcross, GA.

Synthesis of 4,4',4''-[benzene-1,3,5-triyltris(methylene)]tris-(1-(2-cyanoethyl)-1,2,4-triazolium) tribromide, 69. 1,3,5-tris(bromomethyl)benzene (4.00 g, 0.0112 mol) and 1,2,4-triazole-1-propanenitrile (4.11 g, 0.0336 mol) were added to a 50 mL round bottom flask and diluted with acetonitrile (15 mL). The reaction was heated to reflux until a white precipitate had formed after 1 h. The reaction was cooled to rt and diethyl ether (35 mL) was added to the reaction mixture, followed by drying under reduced pressure. The crude solid product was washed with acetonitrile (3 x 30 mL) and dried under reduced pressure to yield the pure product (7.40 g, 91.5% yield). ^{1}H NMR (DMSO-d_6, 300.1 MHz) δ

10.51 (s, 3H), 9.48 (s, 3H), 7.77 (s, 3H), 5.62 (s, 6H), 4.75 (t, *J* = 6.3 Hz, 6H), 3.28 (t, *J* = 6.3 Hz, 6H). $^{13}C\{^{1}H\}$ NMR (DMSO-d_6, 125.66 MHz): δ 144.86 , 143.52 , 134.73 , 130.58 , 117.69 , 50.05 , 47.27 , 17.28. IR (neat): 3408, 3100, 3012, 2968, 2255, 1836, 1610, 1577, 1523, 1451, 1409, 1368, 1342, 1317, 1280, 1229, 1175, 1148, 1067, 1046, 1023, 982, 920, 897, 783, 750, 697 cm^{-1}.

Synthesis of 4,4′,4''-(benzene-1,3,5-triyltris(methylene))tris(1,2,4-triazole), 6. Potassium hydroxide (0.671 g, 0.120 mol) and **69** (2.16 g, 0.00299 mol) were added to a 50 mL Erlenmeyer flask containing 20 mL of water. After stirring overnight, the product precipitated from solution as a white powder and was filtered and washed with tetrahydrofuran (3 x 50 mL). The pure product was dried under reduced pressure to yield 0.184 g (19.2 % yield). ^{1}H NMR (D_2O, 300.1 MHz): δ 8.45 (s, 6H), 7.17 (s, 3H), 5.30 (s, 6H). $^{13}C\{^{1}H\}$ NMR (DMSO-d_6, 125.66 MHz): δ 143.79 (t, *J* = 32.6 Hz), 137.05 , 127.27 , 48.14. IR (neat): 3102, 3033, 1609, 1532, 1468, 1454, 1384, 1363, 1330, 1292, 1213, 1180, 1166, 1079, 1071, 995, 971, 952, 941, 919, 871, 766, 738, 697, 677, 633 cm^{-1}.

Synthesis of $[Co(1)(SO_4)] \cdot [Co(H_2O)_6(SO_4)] \cdot 3H_2O$, 8. Cobalt(II) sulfate heptahydrate (0.0310 g, 0.110 mmol) and **1** (0.00419 g, 0.0221 mmol) were added to separate 4 mL scintillation vials and dissolved in 1 mL of water and 2 mL of a 1:1 water:ethanol mixture, respectively. The vials were heated to 85 °C for 30 min in an aluminum heating block, followed by mixing of the solutions and additional heating. After heating for 24 h, red needles formed and were analyzed.

Synthesis of $[Cu_2(2)_2(SO_4)] \cdot 2DMF \cdot 3H_2O$, 9. Copper(II) sulfate pentahydrate (0.00918 g, 0.0367 mmol), **2** (0.0177 g, 0.0735 mmol), and pyrazine (0.0147 g, 0.184 mmol) were added to separate 4 mL scintillation vials. Pyrazine and **2** were dissolved in 1 mL of DMF and mixed while copper sulfate was dissolved in 1 mL of water. Vials were heated to 85 °C for 30 min in an aluminum heating block, followed by mixing of the solutions and additional heating. After heating for 3 wks, colorless needles formed and were analyzed.

Synthesis of $[Cu(2)(NO_3)] \cdot NMP \cdot H_2O$, 10. Copper(II) nitrate trihydrate (0.0178 g, 0.735 mmol) and **2** (0.0177 g, 0.0735 mmol) were added to separate 4 mL scintillation vials and dissolved in 1 mL of water and 2 mL of DMF, respectively. The vials were heated to 85 °C for 30 min in an aluminum heating block, followed by mixing of the solutions and additional heating. After heating for 1 wk, colorless needles formed and were analyzed.

Synthesis of $[Cu(2)(SO_3CF_3)] \cdot DMF$, 11. Copper(II) triflate (0.0532 g, 0.147 mmol) and **2** (0.0177 g, 0.0735 mmol) were added to separate 4 mL scintillation vials and dissolved in 1 mL of water and 2 mL of DMF, respectively. The vials were heated to 85 °C for 30 min in an aluminum heating block, followed by mixing of the solutions and additional heating. After heating for 24 h, colorless needles formed and were analyzed.

Synthesis of $[Cu(2)(SO_3CF_3)] \cdot DMA$, 12. Copper(II) triflate (0.133 g, 0.368 mmol) and **2** (0.0177 g, 0.0735 mmol) were added to separate 4 mL scintillation vials and dissolved in 1 mL of water and 2 mL of DMA, respectively. The vials

were heated to 85 ℃ for 30 min in an aluminum heating block, followed by mixing of the solutions and additional heating. After heating for 1 wk, colorless needles formed and were analyzed.

Synthesis of [Cu(2)(ClO_4)$_2$] • NMP, 13. Copper(II) perchlorate hexahydrate (0.0545 g, 0.147 mmol) and **2** (0.0177 g, 0.0735 mmol) were added to separate 4 mL scintillation vials and dissolved in 1 mL of water and 2 mL of NMP, respectively. The vials were heated to 85 ℃ for 30 min in an aluminum heating block, followed by mixing of the solutions and additional heating. After heating for 24 h, blue needles formed and were analyzed.

X-ray Structure Determinations. Data was collected on a Bruker SMART APEXII three circle diffractometer equipped with a CCD area detector and operated at 1,800 W power (45 kV, 40 mA) to generate Mo Kα radiation (λ = 0.71073 Å). The incident X-ray beam was focused and monochromated using Bruker Excalibur focusing optics. Single crystals were mounted on nylon CryoLoops (Hampton Research) with Paratone-N (Hampton Research) and frozen at -100 ºC and -173 ºC, respectively. Initial scans of each specimen were taken to obtain preliminary unit cell parameters and to assess the mosaicity (i.e. breadth of spots between frames) of the crystal to select the required frame width for data collection. For all cases frame widths of 0.5º were judged to be appropriate and full hemispheres of data were collected using the *Bruker APEX2* software suite to carry out overlapping ϕ and ω scans at detector setting of 2θ = 28^o. Following data collection, reflections were sampled from all regions of the

Ewald sphere to re-determine unit cell parameters for data integration. Following exhaustive review of collected frames the resolution of the dataset was judged, and, if necessary, regions of the frames where no coherent scattering was observed were removed from consideration for data integration using the *Bruker SAINTplus* program.[26] Data was integrated using a narrow frame algorithm and was subsequently corrected for absorption. Absorption corrections were performed for both samples using the SADABS program.[26] Space group determination and tests for merohedral twinning were carried out using *XPREP*.[26] In all cases, the highest possible space group was chosen. Final models were refined anisotropically (with the exception of H atoms).

Chapter 7

Conclusion

The synthesis of breathing MOFs that possess multiple stable states as a function of guest is currently under intense investigation as their intrinsic flexibility allows for advantages in selective adsorption applications. A majority of breathing MOFs to date have stemmed from the isoreticular synthesis of a few known examples as there have been no methods to predict breathing behavior prior to MOF synthesis. The desire to synthesize breathing MOFs for their ability to control pore size as a function of pressure and concentration has led to a dire need for additional methods for the reticular synthesis of breathing MOFs.

To advance the synthesis of breathing MOFs, new methods to induce breathing must be examined. A major limit to the current synthesis of breathing MOFs is their "flexing" induced by changes at the metal-ligand interface which requires a certain coordination environment for breathing to occur. By moving the point of flexibility *away* from the rigid metal fragment, the synthesis of breathing MOFs will not be limited by the SBU obtained. One method to move the flexing point away from the rigid metal chains is to employ semi-rigid ligands during synthesis, allowing for breathing to occur solely on the ligand.

As semi-rigid ligands contain points of rotation, allowing for breathing to occur through judicious choice of ligand, an array of double-hinged di-1,2,4-triazoles with varying central moieties were synthesized. The subsequent employment of a multitude of di-triazoles has resulted in the formation of MOFs

with both new topologies and properties. The symmetric semi-rigid di-triazoles employed contain two points of rotation which allows for the possibility of multiple ligand conformations. The ability to undergo conformational changes has led to the synthesis of frameworks of multiple dimensionalities, of which three-dimensional frameworks were first examined.

Initially, two three-dimensional copper MOFs were synthesized from a semi-rigid di-triazole ligand containing a central butene moiety. These frameworks can be synthesized separately under identical conditions by only varying the time of the reaction. An alternative route to synthesize the thermodynamic product is to use the isolated kinetic product as a single source precursor, resulting in an irreversible transformation to yield a topologically distinct framework. The ability to alter framework topology as a function of reaction time and using MOFs as single source precursors expands the possibilities for MOF synthesis and may allow access to previously unattainable frameworks.

Through further exploration of reaction conditions with the butene-containing di-triazole, the introduction of bromide anions to a mixture of copper sulphate led to the formation of the three-dimensional copper MOF $[Cu_2(\mathbf{L})_2(SO_4)(Br)_2]\bullet xH_2O$. The MOF was found to reversibly change its framework structure as a function of solvation by repositioning the butene subunits of the di-triazole. Complete removal of interstitial solvent results in a loss of crystallinity but addition of water allows for recovery of the solvated forms.

Through a rotation of the ligand itself, the “kneecap” or point of flexibility in this breathing system was removed from the metal-ligand interface. Adsorption studies revealed the quantity of gases adsorbed increased for both CO_2 and CH_4 upon structural changes facilitated by addition of guest water. While adsorption values increased, the selectivity of CO_2 versus CH_4 adsorption did not increase.

Additional testing of di-triazoles beyond that of the central trans-butene moiety resulted in the formation of MOFs with different dimensionalities. Utilizing a di-triazole containing a central xylene moiety, a series of two-dimensional MOFs were synthesized due to the ligand adopting a *syn* conformation. Through the bridging of one-dimensional copper chains, a topology of fused 1D metal-organic nanotubes (MONTs) was synthesized. The frameworks undergo two different transformations in the solid state as a function of solvation: expansion or contraction of the layers or rotation of the central phenyl ring between fixed positions. Specifically, the 2D sheet layers expand or contract as a function of DMF concentration while DMA and NMP cause the phenyl ring to rotate perpendicular to the tube direction. Since the breathing mode of phenyl rotation is solely ligand based, solid state ^{13}C CP MAS NMR was employed to elucidate the switching mechanism between the parallel and perpendicular modes of the phenyl ring. Unlike PXRD, solid state ^{13}C CP MAS NMR could directly monitor phenyl rotation as a function of solvation, demonstrating that this is an effective approach for monitoring changes to a breathing framework that occur solely through “gate” switching of the ligand.

As the replacement of the central butene moiety with a phenyl moiety resulted in a preferred *syn* conformation of the ligand, additional di-triazoles with extended central aromatic structures were synthesized and tested. By extending the core of the ligand, a series of isoreticular frameworks was synthesized using di-triazoles containing phenyl, naphthyl, and biphenyl moieties to study the effect of central moiety on MOF pore size. In all cases, an identical topology was obtained in which the semi-rigid ligand adopts a *syn* conformation to bridge rigid metal fragments, leading again to the formation of 2D sheets. Solvent molecules lie within the voids of the frameworks while anions are located between the sheet layers. Increasing the central moiety from phenyl to biphenyl, the largest linker, resulted in an increase in the width of the pore by 4.5 Å. The height of the pores remains constant as only the central portion of the bridging ligand is varied. The preferred *syn* conformation by the di-triazoles has allowed for the first study of reticular synthesis in a non-rigid system.

The third dimensionality, 1D MONTS, was obtained through the use of di-triazoles which adopt a *syn* conformation, along with appropriate anion choice which provided a “cap” for the metal chains. Utilizing multiple di-triazoles led to the synthesis of a series of metal-organic nanotubes through the use of reticular design. The use of 1,2,4-triazoles has led to a generalized synthetic strategy in which the size of the tube can be adjusted through judicious ligand choice. Ligands containing central *m*-xylene, *p*-xylene, and naphthalene moieties were utilized and allowed for the first systematic study of gas adsorption in MONTs.

Adsorption studies allowed for a direct comparison of pore size on gas adsorption and showed that ligand choice has a large impact on both uptake and selectivity of CO_2 vs. CH_4.

As MOFs with varying dimensionalities and properties have been synthesized through the employment of semi-rigid di-triazoles, a multitude of reaction conditions were tested in addition to those previously mentioned. Through combinatorial synthesis, frameworks were synthesized which contain minor deviations to the aforementioned examples such as varying the anion. Although some frameworks synthesized contain only small differences, they may be of potential future interest. Other by-products of MOF synthesis have also been presented to show the vast array of topologies which are obtained from the possible configurations of the di-triazoles.

References

1. (a) Furukawa, H.; Cordova, K. E.; O'Keeffe, M.; Yaghi, O. M., The Chemistry and Applications of Metal-Organic Frameworks. *Science* **2013,** *341* (6149), 974; (b) Kitagawa, S.; Matsuda, R., Chemistry of coordination space of porous coordination polymers. *Coord. Chem. Rev.* **2007,** *251* (21-24), 2490-2509; (c) James, S. L., Metal-organic frameworks. *Chem. Soc. Rev.* **2003,** *32* (5), 276-288; (d) Meek, S. T.; Greathouse, J. A.; Allendorf, M. D., Metal-Organic Frameworks: A Rapidly Growing Class of Versatile Nanoporous Materials. *Adv. Mater.* **2011,** *23* (2), 249-267; (e) Mueller, U.; Schubert, M.; Teich, F.; Puetter, H.; Schierle-Arndt, K.; Pastre, J., Metal-organic frameworks-prospective industrial applications. *J. Mater. Chem.* **2006,** *16* (7), 626-636.

2. (a) Furukawa, H.; Kim, J.; Ockwig, N. W.; O'Keeffe, M.; Yaghi, O. M., Control of Vertex Geometry, Structure Dimensionality, Functionality, and Pore Metrics in the Reticular Synthesis of Crystalline Metal-Organic Frameworks and Polyhedra. *J. Am. Chem. Soc.* **2008,** *130* (35), 11650-11661; (b) Garibay, S. J.; Cohen, S. M., Isoreticular synthesis and modification of frameworks with the UiO-66 topology. *Chem. Commun.* **2010,** *46* (41), 7700-7702; (c) Deng, H.; Grunder, S.; Cordova, K. E.; Valente, C.; Furukawa, H.; Hmadeh, M.; Gandara, F.; Whalley, A. C.; Liu, Z.; Asahina, S.; Kazumori, H.; O'Keeffe, M.; Terasaki, O.; Stoddart, J. F.; Yaghi, O. M., Large-Pore Apertures in a Series of Metal-Organic Frameworks. *Science* **2012,** *336* (6084), 1018-1023; (d) Yaghi, O. M.; O'Keeffe, M.; Ockwig, N. W.; Chae, H. K.; Eddaoudi, M.; Kim, J., Reticular synthesis and the design of new materials. *Nature* **2003,** *423* (6941), 705-714.

3. (a) Yu, Y.; Ren, Y.; Shen, W.; Deng, H.; Gao, Z., Applications of metal-organic frameworks as stationary phases in chromatography. *TrAC, Trends Anal. Chem.* **2013,** *50*, 33-41; (b) Li, J.-R.; Ma, Y.-G.; McCarthy, M. C.; Sculley, J.; Yu, J.-M.; Jeong, H.-K.; Balbuena, P. B.; Zhou, H.-C., Carbon dioxide capture-related gas adsorption and separation in metal-organic frameworks. *Coord. Chem. Rev.* **2011,** *255*, 1791-1823; (c) Gascon, J.; Corma, A.; Kapteijn, F.; Llabres i. Xamena, F. X., Metal Organic Framework Catalysis: Quo vadis? *ACS Catal.* **2014,** *4* (2), 361-378; (d) Dhakshinamoorthy, A.; Opanasenko, M.; Cejka, J.; Garcia, H., Metal organic frameworks as heterogeneous catalysts for the production of fine chemicals. *Catal. Sci. Technol.* **2013,** *3* (10), 2509-2540; (e) Lee, J. Y.; Farha, O. K.; Roberts, J.; Scheidt, K. A.; Nguyen, S. B. T.; Hupp, J. T., Metal-organic framework materials as catalysts. *Chem. Soc. Rev.* **2009,** *38* (5), 1450-1459; (f) Kreno, L. E.; Leong, K.; Farha, O. K.; Allendorf, M.; Van, D. R. P.; Hupp, J. T., Metal-Organic Framework Materials as Chemical Sensors. *Chem. Rev.* **2012,** *112* (2), 1105-1125; (g) Chaemchuen, S.; Kabir, N. A.; Zhou, K.; Verpoort, F., Metal-organic frameworks for upgrading biogas via CO_2 adsorption to biogas green energy. *Chem. Soc. Rev.* **2013,** *42* (24), 9304-9332; (h) Li, J.-R.; Kuppler, R. J.; Zhou, H.-C., Selective gas adsorption and separation in metal-organic frameworks. *Chem. Soc. Rev.* **2009,** *38* (5), 1477-1504.

4. Wang, C.; Liu, D.; Lin, W., Metal-Organic Frameworks as A Tunable Platform for Designing Functional Molecular Materials. *J. Am. Chem. Soc.* **2013,** *135* (36), 13222-13234.

5. Perry, J. J. I. V.; Perman, J. A.; Zaworotko, M. J., Design and synthesis of metal-organic frameworks using metal-organic polyhedra as supermolecular building blocks. *Chem. Soc. Rev.* **2009,** *38* (5), 1400-1417.

6. (a) Kitagawa, S.; Kitaura, R.; Noro, S.-i., Functional porous coordination polymers. *Angew. Chem., Int. Ed.* **2004,** *43* (18), 2334-2375; (b) Férey, G.; Serre, C., Large breathing effects in three-dimensional porous hybrid matter: facts, analyses, rules and consequences. *Chem. Soc. Rev.* **2009,** *38*, 1380-1399; (c) Kitaura, R.; Fujimoto, K.; Noro, S.-i.; Kondo, M.; Kitagawa, S., A pillared-layer coordination polymer network displaying hysteretic sorption: $[Cu_2(pzdc)_2(dpyg)]_n$ (pzdc = pyrazine-2,3-dicarboxylate; dpyg = 1,2-di(4-pyridyl)glycol). *Angew. Chem., Int. Ed.* **2002,** *41*, 133-135; (d) Serre, C.; Millange, F.; Thouvenot, C.; Nogues, M.; Marsolier, G.; Loueer, D.; Férey, G., Very Large Breathing Effect in the First Nanoporous Chromium(III)-Based Solids: MIL-53 or CrIII(OH)·$\{O_2C\text{-}C_6H_4\text{-}CO_2\}$·$\{HO_2C\text{-}C_6H_4\text{-}CO_2H\}_x$·$H_2O_y$. *J. Am. Chem. Soc.* **2002,** *124*, 13519-13526.

7. (a) Sareeya, B.; Satoru, S.; Susumu, K., Chemistry and application of flexible porous coordination polymers. *Sci. Technol. Adv. Mater.* **2008,** *9* (1), 014108; (b) Kitagawa, S.; Uemura, K., Dynamic porous properties of coordination polymers inspired by hydrogen bonds. *Chem. Soc. Rev.* **2005,** *34* (2), 109-19; (c) Férey, G., Hybrid porous solids: past, present, future. *Chem. Soc. Rev.* **2008,** *37* (1), 191-214; (d) Horike, S.; Shimomura, S.; Kitagawa, S., Soft porous crystals.

Nat. Chem **2009,** *1* (9), 695-704; (e) Férey, G., Swelling Hybrid Solids. *Z. Anorg. Allg. Chem.* **2012,** *638* (12-13), 1897-1909.

8. Uemura, K.; Matsuda, R.; Kitagawa, S., Flexible microporous coordination polymers. *J. Solid State Chem.* **2005,** *178*, 2420-2429.

9. (a) Couck, S.; Denayer, J. F. M.; Baron, G. V.; Remy, T.; Gascon, J.; Kapteijn, F., An Amine-Functionalized MIL-53 Metal-Organic Framework with Large Separation Power for CO_2 and CH_4. *J. Am. Chem. Soc.* **2009,** *131*, 6326-6327; (b) Henke, S.; Schneemann, A.; Wuetscher, A.; Fischer, R. A., Directing the Breathing Behavior of Pillared-Layered Metal-Organic Frameworks via a Systematic Library of Functionalized Linkers Bearing Flexible Substituents. *J. Am. Chem. Soc.* **2012,** *134*, 9464-9474; (c) Loiseau, T.; Serre, C.; Huguenard, C.; Fink, G.; Taulelle, F.; Henry, M.; Bataille, T.; Férey, G., A rationale for the large breathing of the porous aluminum terephthalate (MIL-53) upon hydration. *Chem.--Eur. J.* **2004,** *10*, 1373-1382; (d) Dybtsev, D. N.; Chun, H.; Kim, K., Rigid and flexible: A highly porous metal-organic framework with unusual guest-dependent dynamic behavior. *Angew. Chem., Int. Ed.* **2004,** *43*, 5033-5036.

10. Murdock, C. R.; Hughes, B. C.; Lu, Z.; Jenkins, D. M., Approaches for synthesizing breathing MOFs by exploiting dimensional rigidity. *Coord. Chem. Rev.* **2014,** *258-259*, 119-136.

11. (a) Li, X.-L.; Liu, G.-Z.; Xin, L.-Y.; Wang, L.-Y., A novel metal-organic framework displaying reversibly shrinking and expanding pore modulation. *CrystEngComm* **2012,** *14* (18), 5757-5760; (b) Murdock, C. R.; Lu, Z.; Jenkins, D.

M., Effects of solvation on the framework of a breathing copper MOF employing a semirigid linker. *Inorg. Chem.* **2013,** *52* (4), 2182-7; (c) Murdock, C. R.; McNutt, N. W.; Keffer, D. J.; Jenkins, D. M., Rotating Phenyl Rings as a Guest-Dependent Switch in Two-Dimensional Metal-Organic Frameworks. *J. Am. Chem. Soc.* **2014,** *136* (2), 671-678.

12. Murdock, C. R.; Lu, Z.; Jenkins, D. M., Utilizing a copper MOF as a reagent in a solvent mediated reaction to form a topologically distinct MOF. *Dalton Trans.* **2012,** *41*, 7839-7841.

13. (a) Chae, H. K.; Siberio-Perez, D. Y.; Kim, J.; Go, Y. B.; Eddaoudi, M.; Matzger, A. J.; O'Keeffe, M.; Yaghi, O. M., A route to high surface area, porosity and inclusion of large molecules in crystals. *Nature* **2004,** *427* (6974), 523-527; (b) Dinca, M.; Long, J. R., Hydrogen storage in microporous metal-organic frameworks with exposed metal sites. *Angew. Chem., Int. Ed.* **2008,** *47* (36), 6766-6779; (c) Zhao, X.; Xiao, B.; Fletcher, A. J.; Thomas, K. M.; Bradshaw, D.; Rosseinsky, M. J., Hysteretic Adsorption and Desorption of Hydrogen by Nanoporous Metal-Organic Frameworks. *Science* **2004,** *306* (5698), 1012-1015; (d) Wang, C.; Zheng, M.; Lin, W., Asymmetric Catalysis with Chiral Porous Metal-Organic Frameworks: Critical Issues. *J. Phys. Chem. Lett.* **2011,** *2* (14), 1701-1709; (e) Férey, G.; Mellot-Draznieks, C.; Serre, C.; Millange, F.; Dutour, J.; Surble, S.; Margiolaki, I., A Chromium Terephthalate-Based Solid with Unusually Large Pore Volumes and Surface Area. *Science* **2005,** *309* (5743), 2040-2042.

14. (a) Zou, R.; Abdel-Fattah, A. I.; Xu, H.; Zhao, Y.; Hickmott, D. D., Storage and separation applications of nanoporous metal-organic frameworks. *CrystEngComm* **2010,** *12* (5), 1337-1353; (b) Doonan, C. J.; Morris, W.; Furukawa, H.; Yaghi, O. M., Isoreticular Metalation of Metal-Organic Frameworks. *J. Am. Chem. Soc.* **2009,** *131* (27), 9492-9493; (c) Bloch, E. D.; Britt, D.; Lee, C.; Doonan, C. J.; Uribe-Romo, F. J.; Furukawa, H.; Long, J. R.; Yaghi, O. M., Metal Insertion in a Microporous Metal-Organic Framework Lined with 2,2'-Bipyridine. *J. Am. Chem. Soc.* **2010,** *132* (41), 14382-14384; (d) Hong, D.-Y.; Hwang, Y. K.; Serre, C.; Férey, G.; Chang, J.-S., Porous chromium terephthalate MIL-101 with coordinatively unsaturated sites: surface functionalization, encapsulation, sorption and catalysis. *Adv. Funct. Mater.* **2009,** *19* (10), 1537-1552.

15. (a) Morris, W.; Doonan, C. J.; Furukawa, H.; Banerjee, R.; Yaghi, O. M., Crystals as Molecules: Postsynthesis Covalent Functionalization of Zeolitic Imidazolate Frameworks. *J. Am. Chem. Soc.* **2008,** *130* (38), 12626-12627; (b) Wang, Z.; Tanabe, K. K.; Cohen, S. M., Tuning Hydrogen Sorption Properties of Metal-Organic Frameworks by Postsynthetic Covalent Modification. *Chem. - Eur. J.* **2010,** *16* (1), 212-217 (c) Yang, S.; Martin, G. S. B.; Titman, J. J.; Blake, A. J.; Allan, D. R.; Champness, N. R.; Schroder, M., Pore with Gate: Enhancement of the Isosteric Heat of Adsorption of Dihydrogen via Postsynthetic Cation Exchange in Metal-Organic Frameworks. *Inorg. Chem.* **2011,** *50* (19), 9374-9384; (d) Morris, W.; Doonan, C. J.; Yaghi, O. M., Postsynthetic Modification of a

Metal-Organic Framework for Stabilization of a Hemiaminal and Ammonia Uptake. *Inorg. Chem.* **2011,** *50* (15), 6853-6855; (e) An, J.; Rosi, N. L., Tuning MOF CO_2 Adsorption Properties via Cation Exchange. *J. Am. Chem. Soc.* **2010,** *132* (16), 5578-5579.

16. (a) Wang, Z.; Cohen, S. M., Postsynthetic modification of metal-organic frameworks. *Chem. Soc. Rev.* **2009,** *38* (5), 1315-1329; (b) Tanabe, K. K.; Cohen, S. M., Postsynthetic modification of metal-organic frameworks-a progress report. *Chem. Soc. Rev.* **2011,** *40* (2), 498-519.

17. (a) Tanabe, K. K.; Wang, Z.; Cohen, S. M., Systematic Functionalization of a Metal-Organic Framework via a Postsynthetic Modification Approach. *J. Am. Chem. Soc.* **2008,** *130* (26), 8508-8517; (b) Song, Y.-F.; Cronin, L., Postsynthetic covalent modification of metal-organic framework (MOF) materials. *Angew. Chem., Int. Ed.* **2008,** *47* (25), 4635-4637; (c) Burnett, B. J.; Barron, P. M.; Hu, C.; Choe, W., Stepwise Synthesis of Metal-Organic Frameworks: Replacement of Structural Organic Linkers. *J. Am. Chem. Soc.* **2011,** *133* (26), 9984-9987; (d) Park, H. J.; Cheon, Y. E.; Suh, M. P., Post-synthetic reversible incorporation of organic linkers into porous metal-organic frameworks through single-crystal-to-single-crystal transformations and modification of gas sorption properties. *Chem. - Eur. J.* **2010,** *16* (38), 11662-11669, (e) Kim, M.; Cahill, J. F.; Su, Y.; Prather, K. A.; Cohen, S. M., Postsynthetic ligand exchange as a route to functionalization of metal-organic frameworks. *Chem. Sci.* **2012,** *3* (1), 126-130; (f) Gadzikwa, T.; Farha, O. K.; Malliakas, C. D.; Kanatzidis, M. G.; Hupp, J. T.; Nguyen, S. T.,

Selective Bifunctional Modification of a Non-catenated Metal-Organic Framework Material via "Click" Chemistry. *J. Am. Chem. Soc.* **2009,** *131* (38), 13613-13615.

18. (a) Chen, J.; Li, C.-P.; Shang, J.; Du, M., A 3-D metal-organic framework of CuII perchlorate and 2-(2-pyridyl)-5-(4-pyridyl)-1,3,4-oxadiazole showing the exclusive anion-exchange selectivity to benzoate. *Inorg. Chem. Commun.* **2012,** *15*, 172-175; (b) Fei, H.; Rogow, D. L.; Oliver, S. R. J., Reversible Anion Exchange and Catalytic Properties of Two Cationic Metal-Organic Frameworks Based on Cu(I) and Ag(I). *J. Am. Chem. Soc.* **2010,** *132* (20), 7202-7209; (c) Fu, J.; Li, H.; Mu, Y.; Hou, H.; Fan, Y., Reversible single crystal to single crystal transformation with anion exchange-induced weak Cu2+···I- interactions and modification of the structures and properties of MOFs. *Chem. Commun.* **2011,** *47* (18), 5271-5273; (d) Yang, Q.-Y.; Li, K.; Luo, J.; Pan, M.; Su, C.-Y., A simple topological identification method for highly (3,12)-connected 3D MOFs showing anion exchange and luminescent properties. *Chem. Commun.* **2011,** *47* (14), 4234-4236.

19. (a) Calderon-Casado, A.; Barandika, G.; Bazan, B.; Urtiaga, M.-K.; Vallcorba, O.; Rius, J.; Miravittles, C.; Arriortua, M.-I., Solid-state transformation of the MOF $[Ni_2(bipy)_{1.5}(PDC)_2(H_2O)_2]\cdot 3.5H_2O$. *CrystEngComm* **2011,** *13* (22), 6831-6838; (b) Ling, Y.; Zhang, L.; Li, J.; Du, M., A robust porous PtS-type Cu(II) metal-organic framework: single-crystal-to-single-crystal transformation with reversible guest intercalation accompanied by color change. *CrystEngComm* **2011,** *13* (3), 768-770; (c) Jiang, H.-L.; Tatsu, Y.; Lu, Z.-H.; Xu, Q., Non-, micro-,

and mesoporous metal-organic framework isomers: Reversible transformation, fluorescence sensing, and large molecule separation. *J. Am. Chem. Soc.* **2010,** *132* (16), 5586-5587; (d) Hauptvogel, I. M.; Biedermann, R.; Klein, N.; Senkovska, I.; Cadiau, A.; Wallacher, D.; Feyerherm, R.; Kaskel, S., Flexible and Hydrophobic Zn-Based Metal-Organic Framework. *Inorg. Chem.* **2011,** *50* (17), 8367-8374.

20. (a) Blake, A. J.; Champness, N. R.; Easun, T. L.; Allan, D. R.; Nowell, H.; George, M. W.; Jia, J.; Sun, X.-Z., Photoreactivity examined through incorporation in metal-organic frameworks. *Nat. Chem.* **2010,** *2* (8), 688-694; (b) Xie, M.-H.; Yang, X.-L.; Wu, C.-D., From 2D to 3D: A Single-Crystal-to-Single-Crystal Photochemical Framework Transformation and Phenylmethanol Oxidation Catalytic Activity. *Chem. - Eur. J.* **2011,** *17* (41), 11424-11427; (c) Modrow, A.; Zargarani, D.; Herges, R.; Stock, N., The first porous MOF with photoswitchable linker molecules. *Dalton Trans.* **2011,** *40* (16), 4217-4222; (d) Tanabe, K. K.; Allen, C. A.; Cohen, S. M., Photochemical activation of a Metal-Organic Framework to reveal functionality. *Angew. Chem., Int. Ed.* **2010,** *49* (50), 9730-9733; (e) Kaye, S. S.; Long, J. R., Matrix Isolation Chemistry in a Porous Metal-Organic Framework: Photochemical Substitutions of N_2 and H_2 in $Zn_4O[(\eta_6$-1,4-Benzenedicarboxylate)$Cr(CO)_3]_3$. *J. Am. Chem. Soc.* **2008,** *130* (3), 806-807; (f) Park, J.; Yuan, D.; Pham, K. T.; Li, J.-R.; Yakovenko, A.; Zhou, H.-C., Reversible Alteration of CO_2 Adsorption upon Photochemical or Thermal

Treatment in a Metal-Organic Framework. *J. Am. Chem. Soc.* **2012,** *134* (1), 99-102.

21. (a) Hanson, K.; Calin, N.; Bugaris, D.; Scancella, M.; Sevov, S. C., Reversible Repositioning of Zinc Atoms within Single Crystals of a Zinc Polycarboxylate with an Open-Framework Structure. *J. Am. Chem. Soc.* **2004,** *126* (34), 10502-10503; (b) Hu, S.; Zhang, J.-P.; Li, H.-X.; Tong, M.-L.; Chen, X.-M.; Kitagawa, S., A Dynamic Microporous Metal-Organic Framework with BCT Zeolite Topology: Construction, Structure, and Adsorption Behavior. *Cryst. Growth Des.* **2007,** *7* (11), 2286-2289.

22. (a) Mahata, P.; Prabu, M.; Natarajan, S., Role of Temperature and Time in the Formation of Infinite -M-O-M- Linkages and Isolated Clusters in MOFs: A Few Illustrative Examples. *Inorg. Chem.* **2008,** *47* (19), 8451-8463; (b) Forster, P. M.; Stock, N.; Cheetham, A. K., A high-throughput investigation of the role of pH, temperature, concentration, and time on the synthesis of hybrid inorganic-organic materials. *Angew. Chem., Int. Ed.* **2005,** *44* (46), 7608-7611.

23. Horváth, A., Michael Adducts in the Regioselective Synthesis of N-Substituted Azoles. *Synthesis* **1995,** *1995* (09), 1183-1189.

24. (a) Aromi, G.; Barrios, L. A.; Roubeau, O.; Gamez, P., Triazoles and tetrazoles: Prime ligands to generate remarkable coordination materials. *Coord. Chem. Rev.* **2011,** *255* (5-6), 485-546; (b) Liu, K.; Shi, W.; Cheng, P., The coordination chemistry of Zn(II), Cd(II) and Hg(II) complexes with 1,2,4-triazole derivatives. *Dalton Trans.* **2011,** *40* (34), 8475-8490.

25. Colson, J. W.; Woll, A. R.; Mukherjee, A.; Levendorf, M. P.; Spitler, E. L.; Shields, V. B.; Spencer, M. G.; Park, J.; Dichtel, W. R., Oriented 2D Covalent Organic Framework Thin Films on Single-Layer Graphene. *Science* **2011,** *332* (6026), 228-231.

26. Bruker *SAINT-Plus (Version 7.03)*, Bruker AXS Inc.: Madison, WI, 2004.

27. Spek, A. L., Single-crystal structure validation with the program PLATON. *J. Appl. Crystallogr.* **2003,** *36*, 7-13.

28. (a) Kitaura, R.; Seki, K.; Akiyama, G.; Kitagawa, S., Porous coordination-polymer crystals with gated channels specific for supercritical gases. *Angew. Chem., Int. Ed.* **2003,** *42*, 428-431; (b) Llewellyn, P. L.; Bourrrelly, S.; Serre, C.; Filinchuk, Y.; Férey, G., How hydration drastically improves adsorption selectivity for CO_2 over CH_4 in the flexible chromium terephthalate MIL-53. *Angew. Chem., Int. Ed.* **2006,** *45*, 7751-7754; (c) Chen, B.; Ma, S.; Zapata, F.; Fronczek, F. R.; Lobkovsky, E. B.; Zhou, H.-C., Rationally Designed Micropores within a Metal-Organic Framework for Selective Sorption of Gas Molecules. *Inorg. Chem.* **2007,** *46*, 1233-1236; (d) Yang, S.; Lin, X.; Lewis, W.; Suyetin, M.; Bichoutskaia, E.; Parker, J. E.; Tang, C. C.; Allan, D. R.; Rizkallah, P. J.; Hubberstey, P.; Champness, N. R.; Thomas, K. M.; Blake, A. J.; Schroeder, M., A partially inter-penetrated metal-organic framework for selective hysteretic sorption of carbon dioxide. *Nat. Mater.* **2012,** *11*, 710-716; (e) Chen, B.; Liang, C.; Yang, J.; Contreras, D. S.; Clancy, Y. L.; Lobkovsky, E. B.; Yaghi, O. M.; Dai, S., A microporous metal-organic framework for gas-chromatographic separation of

alkanes. *Angew. Chem., Int. Ed.* **2006,** *45*, 1390-1393; (f) Thallapally, P. K.; Tian, J.; Kishan, M. R.; Fernandez, C. A.; Dalgarno, S. J.; McGrail, P. B.; Warren, J. E.; Atwood, J. L., Flexible (Breathing) Interpenetrated Metal-Organic Frameworks for CO_2 Separation Applications. *J. Am. Chem. Soc.* **2008,** *130*, 16842-16843; (g) Demessence, A.; Long, J. R., Selective Gas Adsorption in the Flexible Metal-Organic Frameworks Cu(BDTri)L (L=DMF, DEF). *Chem.--Eur. J.* **2010,** *16*, 5902-5908; (h) Wuttke, S.; Bazin, P.; Vimont, A.; Serre, C.; Seo, Y.-K.; Hwang, Y. K.; Chang, J.-S.; Férey, G.; Daturi, M., Discovering the Active Sites for C3 Separation in MIL-100(Fe) by Using Operando IR Spectroscopy. *Chem.--Eur. J.* **2012,** *18*, 11959-11967; (i) Xiang, S.; He, Y.; Zhang, Z.; Wu, H.; Zhou, W.; Krishna, R.; Chen, B., Microporous metal-organic framework with potential for carbon dioxide capture at ambient conditions. *Nat. Commun.* **2012,** *3*, 954; (j) Han, S.; Huang, Y.; Watanabe, T.; Dai, Y.; Walton, K. S.; Nair, S.; Sholl, D. S.; Meredith, J. C., High-Throughput Screening of Metal-Organic Frameworks for CO_2 Separation. *ACS Comb. Sci.* **2012,** *14*, 263-267.

29. (a) El, O. R.; Carlin-Sinclair, A.; Guillou, N.; Walton, R. I.; Vermoortele, F.; Maes, M.; de, V. D.; Millange, F., Liquid-Phase Adsorption and Separation of Xylene Isomers by the Flexible Porous Metal-Organic Framework MIL-53(Fe). *Chem. Mater.* **2012,** *24*, 2781-2791; (b) Dan-Hardi, M.; Chevreau, H.; Devic, T.; Horcajada, P.; Maurin, G.; Férey, G.; Popov, D.; Riekel, C.; Wuttke, S.; Lavalley, J.-C.; Vimont, A.; Boudewijns, T.; de, V. D.; Serre, C., How Interpenetration

Ensures Rigidity and Permanent Porosity in a Highly Flexible Hybrid Solid. *Chem. Mater.* **2012,** *24*, 2486-2492.

30. (a) Horcajada, P.; Serre, C.; Maurin, G.; Ramsahye, N. A.; Balas, F.; Vallet-Regi, M.; Sebban, M.; Taulelle, F.; Férey, G., Flexible porous metal-organic frameworks for a controlled drug delivery. *J. Am. Chem. Soc.* **2008,** *130*, 6774-80; (b) Della, R. J.; Liu, D.; Lin, W., Nanoscale Metal-Organic Frameworks for Biomedical Imaging and Drug Delivery. *Acc. Chem. Res.* **2011,** *44*, 957-968; (c) Taylor-Pashow, K. M. L.; Della, R. J.; Xie, Z.; Tran, S.; Lin, W., Postsynthetic Modifications of Iron-Carboxylate Nanoscale Metal-Organic Frameworks for Imaging and Drug Delivery. *J. Am. Chem. Soc.* **2009,** *131*, 14261-14263; (d) Huxford, R. C.; Della, R. J.; Lin, W., Metal-organic frameworks as potential drug carriers. *Curr. Opin. Chem. Biol.* **2010,** *14*, 262-8.

31. (a) Alberti, G.; Giontella, E.; Murcia-Mascaros, S., Mechanism of the Formation of Organic Derivatives of γ-Zirconium Phosphate by Topotactic Reactions with Phosphonic Acids in Water and Water-Acetone Media. *Inorg. Chem.* **1997,** *36*, 2844-2849; (b) Alberti, G.; Murcia-Mascaros, S.; Vivani, R., Pillared Derivatives of γ-Zirconium Phosphate Containing Nonrigid Alkyl Chain Pillars. *J. Am. Chem. Soc.* **1998,** *120*, 9291-9295.

32. (a) Chen, B.; Ma, S.; Zapata, F.; Lobkovsky, E. B.; Yang, J., Hydrogen Adsorption in an Interpenetrated Dynamic Metal-Organic Framework. *Inorg. Chem.* **2006,** *45*, 5718-5720; (b) Uribe-Romo, F. J.; Hunt, J. R.; Furukawa, H.;

Kloeck, C.; O'Keeffe, M.; Yaghi, O. M., A Crystalline Imine-Linked 3-D Porous Covalent Organic Framework. *J. Am. Chem. Soc.* **2009,** *131*, 4570-4571.

33. Férey, G.; Mellot-Draznieks, C.; Serre, C.; Millange, F.; Dutour, J.; Surble, S.; Margiolaki, I., A Chromium Terephthalate-Based Solid with Unusually Large Pore Volumes and Surface Area. *Science* **2005,** *309*, 2040-2042.

34. (a) Serre, C.; Millange, F.; Surble, S.; Férey, G., A route to the synthesis of trivalent transition-metal porous carboxylates with trimeric secondary building units. *Angew. Chem., Int. Ed.* **2004,** *43*, 6286-6289; (b) Surble, S.; Serre, C.; Mellot-Draznieks, C.; Millange, F.; Férey, G., A new isoreticular class of metal-organic-frameworks with the MIL-88 topology. *Chem. Commun.* **2006**, 284-286; (c) Serre, C.; Mellot-Draznieks, C.; Surble, S.; Audebrand, N.; Filinchuk, Y.; Férey, G., Role of Solvent-Host Interactions That Lead to Very Large Swelling of Hybrid Frameworks. *Science* **2007,** *315*, 1828-1831; (d) Horcajada, P.; Salles, F.; Wuttke, S.; Devic, T.; Heurtaux, D.; Maurin, G.; Vimont, A.; Daturi, M.; David, O.; Magnier, E.; Stock, N.; Filinchuk, Y.; Popov, D.; Riekel, C.; Férey, G.; Serre, C., How Linker's Modification Controls Swelling Properties of Highly Flexible Iron(III) Dicarboxylates MIL-88. *J. Am. Chem. Soc.* **2011,** *133*, 17839-17847; (e) Serre, C.; Surble, S.; Mellot-Draznieks, C.; Filinchuk, Y.; Férey, G., Evidence of flexibility in the nanoporous iron(iii) carboxylate MIL-89. *Dalton Trans.* **2008**, 5462-5464; (f) Mellot-Draznieks, C.; Serre, C.; Surble, S.; Audebrand, N.; Férey, G., Very Large Swelling in Hybrid Frameworks: A Combined Computational and Powder Diffraction Study. *J. Am. Chem. Soc.* **2005,** *127*, 16273-16278; (g)

Alaerts, L.; Maes, M.; Giebeler, L.; Jacobs, P. A.; Martens, J. A.; Denayer, J. F. M.; Kirschhock, C. E. A.; De, V. D. E., Selective Adsorption and Separation of ortho-Substituted Alkylaromatics with the Microporous Aluminum Terephthalate MIL-53. *J. Am. Chem. Soc.* **2008,** *130*, 14170-14178; (h) Finsy, V.; Kirschhock, C. E. A.; Vedts, G.; Maes, M.; Alaerts, L.; De, V. D. E.; Baron, G. V.; Denayer, J. F. M., Framework Breathing in the Vapour-Phase Adsorption and Separation of Xylene Isomers with the Metal-Organic Framework MIL-53. *Chem.--Eur. J.* **2009,** *15*, 7724-7731; (i) Salles, F.; Bourrelly, S.; Jobic, H.; Devic, T.; Guillerm, V.; Llewellyn, P.; Serre, C.; Férey, G.; Maurin, G., Molecular Insight into the Adsorption and Diffusion of Water in the Versatile Hydrophilic/Hydrophobic Flexible MIL-53(Cr) MOF. *J. Phys. Chem. C* **2011,** *115*, 10764-10776.

35. Férey, G., Some suggested perspectives for multifunctional hybrid porous solids. *Dalton Trans.* **2009**, 4400-4415.

36. (a) Choi, H. J.; Dinca, M.; Long, J. R., Broadly Hysteretic H_2 Adsorption in the Microporous Metal-Organic Framework Co(1,4-benzenedipyrazolate). *J. Am. Chem. Soc.* **2008,** *130*, 7848-7850; (b) Salles, F.; Maurin, G.; Serre, C.; Llewellyn, P. L.; Knofel, C.; Choi, H. J.; Filinchuk, Y.; Oliviero, L.; Vimont, A.; Long, J. R.; Férey, G., Multistep N_2 Breathing in the Metal-Organic Framework Co(1,4-benzenedipyrazolate). *J. Am. Chem. Soc.* **2010,** *132*, 13782-13788.

37. (a) Yun, S. K.; Pinnavaia, T. J., Water Content and Particle Texture of Synthetic Hydrotalcite-like Layered Double Hydroxides. *Chem. Mater.* **1995,** *7*, 348-54; (b) Qian, K.; Fang, G.; Wang, S., A novel core-shell molecularly

imprinted polymer based on metal-organic frameworks as a matrix. *Chem. Commun.* **2011,** *47*, 10118-10120; (c) Abid, H. R.; Tian, H.; Ang, H.-M.; Tade, M. O.; Buckley, C. E.; Wang, S., Nanosize Zr-metal organic framework (UiO-66) for hydrogen and carbon dioxide storage. *Chem. Eng. J.* **2012,** *187*, 415-420.

38. (a) Yazaydin, A. O.; Benin, A. I.; Faheem, S. A.; Jakubczak, P.; Low, J. J.; Willis, R. R.; Snurr, R. Q., Enhanced CO_2 Adsorption in Metal-Organic Frameworks via Occupation of Open-Metal Sites by Coordinated Water Molecules. *Chem. Mater.* **2009,** *21*, 1425-1430; (b) Jiang, J., Charged soc metal-organic framework for high-efficacy H_2 adsorption and syngas purification: Atomistic simulation study. *AIChE J.* **2009,** *55*, 2422-2432; (c) Liu, B.; Smit, B., Molecular Simulation Studies of Separation of CO_2/N_2, CO_2/CH_4, and CH_4/N_2 by ZIFs. *J. Phys. Chem. C* **2010,** *114*, 8515-8522; (d) Liu, J.; Wang, Y.; Benin, A. I.; Jakubczak, P.; Willis, R. R.; Le, V. M. D., CO_2/H_2O Adsorption Equilibrium and Rates on Metal-Organic Frameworks: HKUST-1 and Ni/DOBDC. *Langmuir* **2010,** *26*, 14301-14307; (e) Soubeyrand-Lenoir, E.; Vagner, C.; Yoon, J. W.; Bazin, P.; Ragon, F.; Hwang, Y. K.; Serre, C.; Chang, J.-S.; Llewellyn, P. L., How Water Fosters a Remarkable 5-Fold Increase in Low-Pressure CO_2 Uptake within Mesoporous MIL-100(Fe). *J. Am. Chem. Soc.* **2012,** *134*, 10174-10181.

39. (a) Uemura, K.; Matsuda, R.; Kitagawa, S., Flexible microporous coordination polymers. *Journal of Solid State Chemistry* **2005,** *178* (8), 2420-2429; (b) Férey, G.; Serre, C., Large breathing effects in three-dimensional porous hybrid matter: facts, analyses, rules and consequences. *Chem Soc Rev*

2009, *38* (5), 1380-99; (c) Kole, G. K.; Vittal, J. J., Solid-state reactivity and structural transformations involving coordination polymers. *Chemical Society reviews* **2013,** *42* (4), 1755-75; (d) Férey, G., Some suggested perspectives for multifunctional hybrid porous solids. *Dalton Trans.* **2009,** (23), 4400-15.

40. Dhotel, A.; Chen, Z.; Delbreilh, L.; Youssef, B.; Saiter, J. M.; Tan, L., Molecular motions in functional self-assembled nanostructures. *Int. J. Mol. Sci.* **2013,** *14* (2), 2303-33.

41. Khan, N. A.; Hasan, Z.; Jhung, S. H., Adsorptive removal of hazardous materials using metal-organic frameworks (MOFs): a review. *J. Hazard. Mater.* **2013,** *244-245* (0), 444-56.

42. Kitaura, R.; Seki, K.; Akiyama, G.; Kitagawa, S., Porous Coordination-Polymer Crystals with Gated Channels Specific for Supercritical Gases. *Angew. Chem., Int. Ed.* **2003,** *42* (4), 428-431.

43. Fletcher, A. J.; Thomas, K. M.; Rosseinsky, M. J., Flexibility in metal-organic framework materials: Impact on sorption properties. *J. Solid State Chem.* **2005,** *178* (8), 2491-2510.

44. (a) Husain, A.; Ellwart, M.; Bourne, S. A.; Ohrstrom, L.; Oliver, C. L., Single-Crystal-to-Single-Crystal Transformation of a Novel 2-Fold Interpenetrated Cadmium-Organic Framework with Trimesate and 1,2-Bis(4-pyridyl)ethane into the Thermally Desolvated Form Which Exhibits Liquid and Gas Sorption Properties. *Cryst Growth Des* **2013,** *13* (4), 1526-1534; (b) Park, I.-H.; Lee, S. S.; Vittal, J. J., Guest-Triggered Supramolecular Isomerism in a Pillared-Layer

Structure with Unusual Isomers of Paddle-Wheel Secondary Building Units by Reversible Single-Crystal-to-Single-Crystal Transformation. *Chem. – Eur. J.* **2013,** *19* (8), 2695-2702.

45. (a) Horike, S.; Matsuda, R.; Tanaka, D.; Matsubara, S.; Mizuno, M.; Endo, K.; Kitagawa, S., Dynamic motion of building blocks in porous coordination polymers. *Angew. Chem.* **2006,** *45* (43), 7226-30; (b) Gould, S. L.; Tranchemontagne, D.; Yaghi, O. M.; Garcia-Garibay, M. A., Amphidynamic character of crystalline MOF-5: rotational dynamics of terephthalate phenylenes in a free-volume, sterically unhindered environment. *J. Am. Chem. Soc.* **2008,** *130* (11), 3246-7; (c) Winston, E. B.; Lowell, P. J.; Vacek, J.; Chocholousova, J.; Michl, J.; Price, J. C., Dipolar molecular rotors in the metal-organic framework crystal IRMOF-2. *Phys. Chem. Chem. Phys.* **2008,** *10* (34), 5188-91.

46. Seo, J.; Matsuda, R.; Sakamoto, H.; Bonneau, C.; Kitagawa, S., A pillared-layer coordination polymer with a rotatable pillar acting as a molecular gate for guest molecules. *J. Am. Chem. Soc.* **2009,** *131* (35), 12792-800.

47. Yang, W.; Davies, A. J.; Lin, X.; Suyetin, M.; Matsuda, R.; Blake, A. J.; Wilson, C.; Lewis, W.; Parker, J. E.; Tang, C. C.; George, M. W.; Hubberstey, P.; Kitagawa, S.; Sakamoto, H.; Bichoutskaia, E.; Champness, N. R.; Yang, S.; Schroder, M., Selective CO_2 uptake and inverse CO_2/C_2H_2 selectivity in a dynamic bifunctional metal-organic framework. *Chem. Sci.* **2012,** *3* (10), 2993-2999.

48. Murdock, C. R.; Lu, Z.; Jenkins, D. M., Utilizing a copper MOF as a reagent in a solvent mediated reaction to form a topologically distinct MOF. *Dalton Trans.* **2012,** *41* (26), 7839-41.

49. Coronado, E.; Gimenez-Marques, M.; Minguez Espallargas, G., Combination of magnetic susceptibility and electron paramagnetic resonance to monitor the 1D to 2D solid state transformation in flexible metal-organic frameworks of Co(II) and Zn(II) with 1,4-bis(triazol-1-ylmethyl)benzene. *Inorg. Chem.* **2012,** *51* (7), 4403-10.

50. (a) Kanoh, H.; Kondo, A.; Noguchi, H.; Kajiro, H.; Tohdoh, A.; Hattori, Y.; Xu, W. C.; Inoue, M.; Sugiura, T.; Morita, K.; Tanaka, H.; Ohba, T.; Kaneko, K., Elastic layer-structured metal organic frameworks (ELMs). *J. Colloid Interface Sci.* **2009,** *334* (1), 1-7; (b) Kajiro, H.; Kondo, A.; Kaneko, K.; Kanoh, H., Flexible two-dimensional square-grid coordination polymers: structures and functions. *Int. J. Mol. Sci.* **2010,** *11* (10), 3803-45.

51. (a) Hong, M.; Zhao, Y.; Su, W.; Cao, R.; Fujita, M.; Zhou, Z.; Chan, A. S., A Silver(I) Coordination Polymer Chain Containing Nanosized Tubes with Anionic and Solvent Molecule Guests. *Angew. Chem.* **2000,** *39* (14), 2468-2470; (b) Dong, Y. B.; Jiang, Y. Y.; Li, J.; Ma, J. P.; Liu, F. L.; Tang, B.; Huang, R. Q.; Batten, S. R., Temperature-dependent synthesis of metal-organic frameworks based on a flexible tetradentate ligand with bidirectional coordination donors. *J. Am. Chem. Soc.* **2007,** *129* (15), 4520-1; (c) Ren, S.-B.; Yang, X.-L.; Zhang, J.; Li, Y.-Z.; Zheng, Y.-X.; Du, H.-B.; You, X.-Z., An infinite photoluminescent

coordination nanotube [CuSCN(L)][middle dot](DMF)$_{0.5}$. *CrystEngComm* **2009,** *11* (2), 246-248; (d) Thanasekaran, P.; Luo, T. T.; Lee, C. H.; Lu, K. L., A journey in search of single-walled metal-organic nanotubes. *J. Mater. Chem.* **2011,** *21* (35), 13140-13149.

52. Dybtsev, D. N.; Chun, H.; Kim, K., Rigid and flexible: a highly porous metal-organic framework with unusual guest-dependent dynamic behavior. *Angew. Chem.* **2004,** *43* (38), 5033-6.

53. (a) Hoffmann, H.; Debowski, M.; Müller, P.; Paasch, S.; Senkovska, I.; Kaskel, S.; Brunner, E., Solid-State NMR Spectroscopy of Metal–Organic Framework Compounds (MOFs). *Materials* **2012,** *5* (12), 2537-2572; (b) Sutrisno, A.; Huang, Y., Solid-state NMR: a powerful tool for characterization of metal-organic frameworks. *Solid State Nucl. Mag.* **2013,** *49-50* (0), 1-11.

54. (a) Rabone, J.; Yue, Y.-F.; Chong, S. Y.; Stylianou, K. C.; Bacsa, J.; Bradshaw, D.; Darling, G. R.; Berry, N. G.; Khimyak, Y. Z.; Ganin, A. Y.; Wiper, P.; Claridge, J. B.; Rosseinsky, M. J., An Adaptable Peptide-Based Porous Material. *Science* **2010,** *329* (5995), 1053-1057; (b) Stylianou, K. C.; Rabone, J.; Chong, S. Y.; Heck, R.; Armstrong, J.; Wiper, P. V.; Jelfs, K. E.; Zlatogorsky, S.; Bacsa, J.; McLennan, A. G.; Ireland, C. P.; Khimyak, Y. Z.; Thomas, K. M.; Bradshaw, D.; Rosseinsky, M. J., Dimensionality Transformation through Paddlewheel Reconfiguration in a Flexible and Porous Zn-Based Metal–Organic Framework. *J. Am. Chem. Soc.* **2012,** *134* (50), 20466-20478; (c) Lee, E. Y.; Jang, S. Y.; Suh, M. P., Multifunctionality and Crystal Dynamics of a Highly

Stable, Porous Metal–Organic Framework [$Zn_4O(NTB)_2$]. *J. Am. Chem. Soc.* **2005,** *127* (17), 6374-6381.

55. (a) Herm, Z. R.; Bloch, E. D.; Long, J. R., Hydrocarbon Separations in Metal-Organic Frameworks. *Chem. Mater.* **2014,** *26* (1), 323-338; (b) Yan, Y.; Yang, S.; Blake, A. J.; Schroder, M., Studies on Metal-Organic Frameworks of Cu(II) with Isophthalate Linkers for Hydrogen Storage. *Acc. Chem. Res.* **2014,** *47* (2), 296-307.

56. Devic, T.; David, O.; Valls, M.; Marrot, J.; Couty, F.; Férey, G., An Illustration of the Limit of the Metal Organic Framework's Isoreticular Principle Using a Semirigid Tritopic Linker Obtained by "Click" Chemistry. *J. Am. Chem. Soc.* **2007,** *129* (42), 12614-12615.

57. (a) Sgobba, V.; Guldi, D. M., Carbon nanotubes-electronic/electrochemical properties and application for nanoelectronics and photonics. *Chem. Soc. Rev.* **2009,** *38* (1), 165-184; (b) Baughman, R. H.; Zakhidov, A. A.; de Heer, W. A., Carbon nanotubes-the route toward applications. *Science* **2002,** *297* (5582), 787-792.

58. (a) Otsubo, K.; Wakabayashi, Y.; Ohara, J.; Yamamoto, S.; Matsuzaki, H.; Okamoto, H.; Nitta, K.; Uruga, T.; Kitagawa, H., Bottom-up realization of a porous metal-organic nanotubular assembly. *Nat. Mater.* **2011,** *10* (4), 291-295; (b) Unruh, D. K.; Gojdas, K.; Libo, A.; Forbes, T. Z., Development of Metal-Organic Nanotubes Exhibiting Low-Temperature, Reversible Exchange of Confined Ice Channels. *J. Am. Chem. Soc.* **2013,** *135* (20), 7398-7401; (c) Ju, P.; Jiang, L.;

Lu, T.-B., An unprecedented dynamic porous metal-organic framework assembled from fivefold interlocked closed nanotubes with selective gas adsorption behaviors. *Chem. Commun.* **2013,** *49* (18), 1820-1822; (d) Dai, F.; He, H.; Sun, D., A Metal-Organic Nanotube Exhibiting Reversible Adsorption of $(H_2O)_{12}$ Cluster. *J. Am. Chem. Soc.* **2008,** *130* (43), 14064-14065; (e) Lu, Z.-Z.; Zhang, R.; Li, Y.-Z.; Guo, Z.-J.; Zheng, H.-G., Solvatochromic Behavior of a Nanotubular Metal-Organic Framework for Sensing Small Molecules. *J. Am. Chem. Soc.* **2011,** *133* (12), 4172-4174.

59. (a) Luo, T.-T.; Wu, H.-C.; Jao, Y.-C.; Huang, S.-M.; Tseng, T.-W.; Wen, Y.-S.; Lee, G.-H.; Peng, S.-M.; Lu, K.-L., Self-Assembled Arrays of Single-Walled Metal-Organic Nanotubes. *Angew. Chem., Int. Ed.* **2009,** *48* (50), 9461-9464; (b) He, H.; Collins, D.; Dai, F.; Zhao, X.; Zhang, G.; Ma, H.; Sun, D., Construction of Metal-Organic Frameworks with 1D Chain, 2D Grid, and 3D Porous Framework Based on a Flexible Imidazole Ligand and Rigid Benzenedicarboxylates. *Cryst. Growth Des.* **2010,** *10* (2), 895-902.

60. Wu, G.; Bai, J.; Jiang, Y.; Li, G.; Huang, J.; Li, Y.; Anson, C. E.; Powell, A. K.; Qiu, S., Rolling Up the Sheet: Constructing Metal-Organic Lamellae and Nanotubes from a $[\{Mn_3(propanediolato)_2\}(dicyanamide)_2]_n$ Honeycomb Skeleton. *J. Am. Chem. Soc.* **2013,** *135* (49), 18276-18279.

61. Naik, A. D.; Marchand-Brynaert, J.; Garcia, Y., A simplified approach to N- and N,N'-linked 1,2,4-triazoles by transamination. *Synthesis* **2008,** (1), 149-154.

VITA

Christopher Ray Murdock was born on January 25, 1987 in Ft. Worth, TX to Gary Murdock and Daphne Markham. After moving to Sturgis, Kentucky and graduating from Union County High School, he stayed close to home and attended Kentucky Wesleyan College. During college, he initially started as a pre-medicine major but, after two summers of undergraduate research, decided to change paths and pursue a degree in chemistry. After graduating magna cum laude in 2009 with a bachelors of science, he arrived two weeks after graduation to start his graduate degree early at the University of Tennessee - Knoxville. During his time in the PhD program at UTK, Chris published multiple papers, attended three national ACS conferences, and attained multiple awards for his accomplishments.